

Muhammad Khalid Hassan Loane

**Contractor renormalization group
method: applications to strongly
correlated systems**

DOCTORAL THESIS

For obtaining the academic degree of
Doktor der technischen Wissenschaften

Doctoral Programme of Technical Sciences
Technical Physics



Graz University of Technology

Graz University of Technology

Supervisor:

Univ.-Prof. Dr.rer.nat. Enrico Arrigoni
Institute of Theoretical and Computational Physics

Graz, February 2013

Deutsche Fassung:

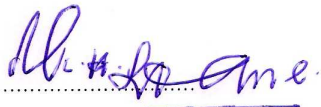
Beschluss der Curricula-Kommission für Bachelor-, Master- und Diplomstudien vom 10.11.2008

Genehmigung des Senates am 1.12.2008

EIDESSTATTLICHE ERKLÄRUNG

Ich erkläre an Eides statt, dass ich die vorliegende Arbeit selbstständig verfasst, andere als die angegebenen Quellen/Hilfsmittel nicht benutzt, und die den benutzten Quellen wörtlich und inhaltlich entnommene Stellen als solche kenntlich gemacht habe.

am. 19.01.2013



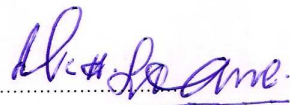
(Unterschrift)

Englische Fassung:

STATUTORY DECLARATION

I declare that I have authored this thesis independently, that I have not used other than the declared sources / resources, and that I have explicitly marked all material which has been quoted either literally or by content from the used sources.

date 19.01.2013



(signature)

Acknowledgements

I consider myself lucky and privileged to work in the group of professor Enrico Arrigoni. Due to his constant support, I was able to work in the numerical correlated system. He was very patient with me during the course of my studies and gave his suggestions during the research and computational work. I have learned a lot from my professor, which will be part of me for any of the future endeavours. I also thank him for providing me remote access of computational resources. This helped me a lot during the work.

I have interactions with all other group members, which enriched my experience of working in the scientific community. Among the people who shared their academic and social life with me were Dr. Liviu Chioncel and Dr. Xiancong Lu. Dr. Liviu was trained in showing the positive and visionary side of things out of any kind problems. Dr. Lu. was available to discuss new things, as he enjoyed learning new things. Both of them left the institute at different times, but I think the time spent with them was well worth. I also want to thank Dr. Markus Aichhorn, who always gave his valuable time for academic as well as language related problems. I thank all my colleagues at the university for brightening up my stay at the university. They gave me the experience of knowing the thinking style of people of different cultures, from different part of world (The people working at itcp, graz can be viewed of having an International flavour). There are many common things in this scientific community.

For computational matters, I want to thank Mr, Andreas Hirczy. Whenever I done something to my computer, he fixed it. Whenever software mentions a missing library or some other problems, he gives instructions to fix these things in no time. Unless there is some power failure, there were no problems in successful running of machines.

I also want to thank the funding agency, Higher Education Commission, Pakistan. They were instrumental for me to be able to do my work comfortably. I also thank my employer for their support and understanding during the research work. This gave me enough confidence to complete my work.

It would not have been possible to undertake this endeavour without the support of my parents with all their means. From my childhood, they made available every possible resources in their capacity for me. They are the main architects to materialise my dreams. I also want to thank my brother who took the financial responsibilities during my absence.

I also want to thank the graz-community, who gave me the feeling of being at home (not in the virtual sense), while I was away from my own home. I was also impressed by graz administration, which never required a second visit for any work.

I thank all the factors responsible for my trainings of applying the scientific approach to any problems. The beautiful world of renormalization is also very fascinating. Whatever will be the future missions, my learning will always be there as a guiding factor.

Abstract

In this thesis, the contractor renormalization group method (CORE) is applied to investigate the critical phenomena in strongly correlated systems. The numerical implementation of the CORE algorithm, which forms the basis of the simulations done in this work, is also discussed. Another aspect of the study is to simulate strongly-correlated systems using different parameters for the CORE simulations to find an optimal combination for the given computational resources.

The quantum phase transition in $(1+1)$ -transverse Ising model is the first system explored by CORE simulations. The renormalization flow of the input parameters h/J_x is specific to the CORE simulations as there is an evolution of renormalized parameters which were not present in the input hamiltonian. Finite size scalings were used to find the critical exponent approximations for the magnetization as 0.12 ± 0.01 , and that of the correlation length as 1 ± 0.01 compared to the exact results of 0.125 and 1 respectively. The dynamical critical exponent approximation is found to be 1 ± 0.1 by multiple iterations CORE algorithm close to the exact result 1.

The critical behaviour of the gapless regime of the spin-1/2 XXZ-antiferromagnetic chain is also investigated with the application of an external transverse field. The critical exponent approximations by CORE simulations are in very good match with those found by field-theoretical studies.

The J_1 - J_2 Heisenberg model is also investigated for the renormalization flow of the competing interactions J_2/J_1 . The critical coupling is found to be at 0.240 ± 0.001 showing an error of 0.5% with that of the exact results.

The critical behaviour of the alternating Heisenberg chain (AHC) is also simulated by CORE algorithm for the lattice size of 324 sites. The critical behaviour of energy density and singlet-triplet gap comply with the Cross-Fisher power laws in the alternations range from 0.008 to 0.1. The bulk limit critical exponent approximation of the energy density found by CORE range-2 simulations is even closer to the field theoretical results. The approximation for the critical exponents of the energy density and the gap at CORE range-3 simulations are found to be 1.46 and 0.82, which have a difference of 1% and 9% respectively, from that of the DMRG-extrapolated results for infinite limit.

The frustrations is also added to the alternation model to find its effects on the critical behaviour. With the increasing frustrations, the deviation of the critical behaviour from that of the power laws decreases. At the critical frustration 0.2411, the deviation between the critical behaviour and the power law vanish so the logarithmic corrections are no more needed. According to the CORE range-3 simulations, the approximation for the critical exponents of the energy density decreases from 1.43 to 1.26, while that of singlet-triplet gap from 0.81 to 0.70 for the increasing frustrations from 0.05 to 0.2411. When compared to the DMRG-extrapolated results for infinite behaviour, these approximate results show a variation of error from 1% to 5% and from 5% to 9% for the energy density and that of the gap respectively. It is also seen that the accuracy achieved by taking single blocks of big sizes in the first CORE iteration can be maintained even if the single block size is reduced in the subsequent CORE iterations.

Kurzfassung

In dieser Arbeit wird das Contractor-Renormalisation-Group-Verfahren (CORE) angewandt, um die kritische Phänomene in stark korrelierten Systemen zu untersuchen. Die numerische Umsetzung des CORE-Algorithmus, mittels dessen die Simulationen in dieser Arbeit durchgeführt wurden, wird diskutiert. Ein weiterer Aspekt der Studie ist es, effiziente Parameter für die CORE-Simulationen zu finden, um die Berechnung von Eigenschaften stark-korrelierter Systeme an die gegebenen Rechenressourcen optimal anpassen zu können.

Der Quanten-Phasenübergang im $(1+1)$ -transversalen Ising-Modell ist das erste Problem, das mittels CORE Simulationen untersucht wird. Der Renormierungsfluss der Input-Parameter h/J_x ist spezifisch für die CORE-Simulationen, da es auch Flüsse von Parametern gibt, die nicht Teil des ursprünglichen Hamiltonians waren. Finite-Size Skalierungen wurden verwendet, um die kritischen Exponenten der Magnetisierung zu 0.12 ± 0.01 und der Korrelationslänge zu 1.0 ± 0.1 zu bestimmen, im Vergleich mit den exakten Resultaten 0.125 bzw. 1.0 . Der dynamische kritische Exponent wurde durch mehrere Iterationen des CORE-Algorithmus zu 1.0 ± 0.1 bestimmt, in Übereinstimmung mit dem exakten Resultat 1.0 .

Das kritische Verhalten im Regime ohne Anregungslücke der Spin-1/2 XXZ-antiferromagnetische Kette wurde auch unter dem Einfluss eines externen transversalen Feldes untersucht. Die berechneten kritischen Exponenten sind in perfekter Übereinstimmung mit jenen aus feldtheoretischen Studien.

Der Renormierungsgruppenfluss der konkurrierenden Wechselwirkungen J_2/J_1 wurde auch für die J_1 - J_2 Heisenberg-Kette untersucht. Die kritische Kuppelung wurde bei 0.240 ± 0.001 gefunden, was eine 0.5% Fehler zum exakten Wert bedeutet.

Das kritische Verhalten der alternierenden Heisenberg-Kette (AHC) wurde auch mittels des CORE-Algorithmus auf Gittern mit 324 Gitterstellen simuliert. Der Wert der Energiedichte und der Singulett-Triplett Anregungslücke in der Nähe des kritischen Punktes folgt den Cross-Fisher Potenzgesetzen, für Alternierungsparameter zwischen 0.008 und 0.1. Der kritische Exponent für die Energiedichte bei Range-2 ist näher an den theoretischen Ergebnissen. Die kritischen Exponenten für die Energiedichte und die Anregungslücke wurden in Range-3 Simulationen berechnet, was 1.46 im ersten bzw. 0.82 im zweiten Fall lieferte. Das bedeutet eine Fehler von 1% bzw. 9% zu Resultaten von DMRG, extrapoliert zum thermodynamischen Limes.

Auch der Effekt von Frustration auf das kritische Verhalten wird untersucht. Mit zunehmender Frustration wird das kritische Verhalten durch Potenzgesetze immer besser beschrieben. Am kritischen Punkt 0.2411 verschwindet die Abweichung vom Potenzgesetz, und logarithmische Korrekturen sind nicht mehr notwendig. Unsere CORE range-3 Simulation zeigt, dass mit zunehmender Frustration von 0.05 bis 0.2411 der kritische Exponent für die Energiedichte von 1.43 auf 1.26 sinkt, während der Exponent der Singulett-Triplett Anregungslücke von 0.81 auf 0.70 sinkt. Verglichen mit den DMRG Resultaten zeigen unsere Daten eine Abweichung zwischen 1% und 5% für die Energiedichte, bzw. zwischen 5% und 9% für die Anregungslücke. Es konnte auch gezeigt werden, dass die Genauigkeit der CORE Rechnungen mit grossen Blöcken in der

ersten Iteration aufrecht erhalten werden kann, selbst wenn die Blockgrößen in den weiteren Iterationen reduziert werden.

Contents

| | | |
|----------|--|-----------|
| 1 | Renormalization Group Theory (RGT) and Phase Transitions | 1 |
| 1.1 | Kadanoff Scaling Picture of Lattice Geometry | 1 |
| 1.2 | Real Space Renormalization Methods | 3 |
| 1.2.1 | Naive Real Space Renormalization Group (RSRG) | 3 |
| 1.2.2 | Density Matrix Renormalization Group (DMRG) | 4 |
| 1.2.3 | The Contractor Renormalization Method (CORE) | 5 |
| 1.3 | Phase Transitions and Critical Exponents | 6 |
| 1.3.1 | Phase Transitions | 6 |
| 1.3.2 | The Order Parameter | 7 |
| 1.3.3 | Correlation Length | 7 |
| 1.3.4 | Critical Exponents | 7 |
| 1.3.5 | Universality | 8 |
| 1.4 | Finite Size Scaling | 8 |
| 1.5 | Plan of Work | 9 |
| 2 | CONTRACTOR RENORMALIZATION (CONCEPT & IMPLEMENTATION) | 11 |
| 2.1 | CORE Approximation: Basic Idea | 11 |
| 2.2 | CORE Algorithm: Implementation Concepts | 14 |
| 2.3 | CORE Algorithm : Numerical Implementation | 16 |
| 2.3.1 | CORE Algorithm: Inputs | 17 |
| 2.3.2 | CORE Algorithm: The Structure | 19 |
| 2.3.3 | CORE Algorithm : The Loop | 20 |
| 2.4 | Finite Cluster Method | 22 |
| 2.5 | Conclusion | 23 |
| 3 | Ising Model in Transverse Magnetic Field | 25 |
| 3.1 | Ising Model in Transverse Field (<i>ITF</i>) | 25 |
| 3.2 | Phase Transitions and Critical Properties of the $(1 + 1)$ Ising Model | 26 |
| 3.3 | Renormalization Flow of Parameters of the Ising Model | 27 |
| 3.3.1 | Extraction of Parameters from range-2 simulations | 28 |
| 3.3.2 | Extraction of Parameters from range-3 calculations | 29 |
| 3.4 | Evaluation of the Renormalized Magnetization Operator in $(1 + 1)$ Ising Model | 32 |
| 3.5 | Critical Exponents using the CORE Algorithm | 34 |
| 3.6 | Critical Exponents Using Finite Size Scaling | 35 |
| 3.6.1 | CORE Algorithm and Finite Size Scaling | 35 |
| 3.6.2 | Critical Exponent of the Correlation Length ν | 38 |
| 3.6.3 | Critical Exponent of Magnetization β | 40 |

| | | |
|----------|---|-----------|
| 3.7 | Dynamical Critical Exponent z | 40 |
| 3.8 | Conclusion | 42 |
| 4 | Critical Exponent (Energy Gap) of XXZ Model in Transverse Field | 44 |
| 4.1 | Phase Diagram of the XXZ-model | 44 |
| 4.2 | Critical Exponent of the Energy Gap With Applied Transverse Field | 45 |
| 4.3 | Evaluation of the Energy Gap Critical Exponent | 46 |
| 4.4 | Evaluation of the Critical Exponent of the Gap λ | 47 |
| 4.4.1 | Evaluation of the ϕ -Exponent | 47 |
| 4.4.2 | Evaluation of the α -Exponent | 47 |
| 4.5 | Numerical Perspective : CORE simulations | 48 |
| 4.6 | scheme 1: Gap Exponent at ($\Delta = 0.5$) | 48 |
| 4.6.1 | Scheme 1: Evaluation of the ϕ -Exponent at ($\Delta = 0.5$) | 49 |
| 4.6.2 | Scheme 1: Evaluation of the α -Exponent at ($\Delta = 0.5$) | 51 |
| 4.6.3 | Scheme 1: Evaluation of the Gap-Exponent λ at ($\Delta = 0.5$) | 51 |
| 4.7 | scheme 2: Gap Exponent at ($\Delta = 0.5$) | 52 |
| 4.7.1 | scheme 2: Evaluation of the ϕ -Exponent at ($\Delta = 0.5$) | 52 |
| 4.7.2 | scheme 2: Evaluation of the α -Exponent at ($\Delta = 0.5$) | 53 |
| 4.7.3 | Scheme 2: Evaluation of the Gap-Exponent λ at ($\Delta = 0.5$) | 54 |
| 4.8 | Gap Exponents using CORE simulations For Different Anisotropy Parameters | 55 |
| 4.8.1 | Evaluation of ϕ -exponent For Different Anisotropy Parameters | 55 |
| 4.8.2 | Evaluation of α -Exponent For Different Anisotropy Parameters | 58 |
| 4.8.3 | Validity of ϕ -exponent and α -exponent For Different Anisotropy Parameters | 60 |
| 4.9 | Conclusion | 62 |
| 5 | Alternating spin-$\frac{1}{2}$ Heisenberg Chains (AHC) | 63 |
| 5.1 | Alternating Heisenberg Chain (AHC) | 63 |
| 5.2 | Application of CORE to the Alternating Heisenberg Model | 65 |
| 5.3 | CORE Simulations for AHC at Range-2 | 67 |
| 5.3.1 | Critical Exponent for the Energy Stabilization at Range-2 | 68 |
| 5.3.2 | Critical Exponent for the Gap for (AHC) at Range-2 | 69 |
| 5.4 | CORE Simulations For (AHC) at Range-3 | 70 |
| 5.4.1 | Critical Exponent for the Energy Stabilization at Range-3 | 72 |
| 5.4.2 | Critical Exponent for the Gap for (AHC) at Range-3 | 73 |
| 5.5 | CORE Simulations For (AHC) at Range-3, Bigger iterated single Blocks | 74 |
| 5.5.1 | Critical Exponent for the Energy Stabilization for (AHC) at Range-3 (Bigger Blocks) | 75 |
| 5.5.2 | Critical Exponent for the Singlet-Triplet Gap for (AHC) at Range-3 (Bigger Blocks) | 75 |
| 5.6 | Renormalization Flow of the alternation Parameter δ , couplings J | 77 |
| 5.7 | Conclusion | 78 |
| 6 | Heisenberg spin-$\frac{1}{2}$ Chain with Alternations and Frustrations | 80 |
| 6.1 | Renormalization Flow of parameters J_2 and J_1 | 82 |
| 6.1.1 | Renormalization Flow of competing interactions $\frac{J_2}{J_1}$ using CORE Simulations | 82 |
| 6.1.2 | Critical Coupling (at bulk limit) | 84 |
| 6.2 | Critical Exponents for Spin- $\frac{1}{2}$ Heisenberg model (Alternations and Frustrations) | 85 |
| 6.3 | CORE Simulations at range-2 for (AHC) with Frustration | 86 |

| | | |
|----------|--|------------|
| 6.4 | CORE Simulations at range-3 for AHC with Frustration | 88 |
| 6.4.1 | Critical Exponent of the Energy Stabilization at Range-3 | 88 |
| 6.4.2 | Critical Exponent of the Gap at Range-3 | 91 |
| 6.4.3 | Critical Exponents with CORE range-3 : tabulated results | 92 |
| 6.5 | Conclusion | 94 |
| A | Energy Re-Scaling for Renormalized Hamiltonians | 97 |
| A.1 | CORE Iterations: Shifting and Re-Scaling | 97 |
| A.2 | Energy Spectrum Re-Scaling for h_r | 98 |
| A.3 | Shifting the hamiltonian contributions h_r | 98 |
| A.4 | Nullifying Shifting and re-Scaling | 98 |
| A.4.1 | Nullifying Shifting and re-Scaling for h_1 | 99 |
| A.4.2 | Nullifying Shifting and re-Scaling for h_2 | 99 |
| A.4.3 | Nullifying Shifting and re-Scaling for h_3 | 100 |
| A.5 | Shifting re-Scaling for Different Lattice Geometries | 101 |
| A.6 | Conclusion | 101 |
| B | CORE algorithm with Degenerate models | 102 |
| B.1 | Spin- $\frac{1}{2}$ Basis states for three site single block | 102 |
| B.2 | Conserve-Sz Super Block Range-2 | 103 |
| B.3 | Conserve-Sz Super Block Range-3 | 103 |

List of Figures

| | | |
|------|---|----|
| 1.1 | Renormalization of the 1-dimensional lattice | 2 |
| 1.2 | Schematic diagram of the truncation procedure in Naive Real Space Renormalization Method | 4 |
| 1.3 | schematic diagram of the iterations of naive real space renormalization method. | 4 |
| 1.4 | schematic diagram showing the truncation difference between the Naive RSRG and the CORE method. | 6 |
| 3.1 | phase diagram of spin- $\frac{1}{2}$ (1 + 1)-dimensional Ising model | 26 |
| 3.2 | Evolution of the renormalized parameter ratio $\frac{h}{J_x}$ with CORE simulations at range-2. | 28 |
| 3.3 | Evolution of the renormalized parameter ratio $\frac{h}{J_x}$ with CORE simulations at range-2. | 29 |
| 3.4 | Evolution of $\frac{h}{J_x}$ with CORE renormalization transformation iterations at range-3. | 30 |
| 3.5 | Evolution of $\frac{h}{J_x}$ with CORE renormalization transformation iterations at range-3. | 30 |
| 3.6 | Evolution of $\frac{h}{J_x}$ with CORE renormalization transformation iterations at range-3. | 31 |
| 3.7 | Evolution of J_y and J_z with CORE renormalization transformation iterations. | 31 |
| 3.8 | Evolution of J_y and J_z with CORE renormalization transformation iterations close to the critical point | 32 |
| 3.9 | Plots of magnetization of (1+1)-Ising model for various starting parameters | 32 |
| 3.10 | Plots of magnetization of (1+1)-Ising model for various starting parameters | 33 |
| 3.11 | Evolution of $\frac{h}{J_x}$ with CORE renormalization transformation iterations at range-3. | 33 |
| 3.12 | Average Magnetization for different site lattices in relation to the starting parameter $\frac{h}{J_x}$ using only the first CORE iteration. | 36 |
| 3.13 | Plots of magnetization of (1+1)-Ising model for various starting parameters using CORE 2^{nd} and 3^{rd} iteration. | 36 |
| 3.14 | The crossing of the scaling parameter $mL^{\frac{1}{8}}$, in relation to the starting parameter $\frac{h}{J_x}$ for the 1^{st} CORE iteration. | 37 |
| 3.15 | Plots of the scaling parameter $mL^{\frac{1}{8}}$, in relation to the starting parameter $\frac{h}{J_x}$ using the 2^{nd} and 3^{rd} CORE iteration. | 38 |
| 3.16 | the best collapse on the universal curve gives the critical exponents of $\nu = 1$ for the CORE 1^{st} -iteration | 39 |
| 3.17 | The collapse on the universal curve for the critical exponents of correlation length $\nu = 1$ for the CORE 2^{nd} - and 3^{rd} -iteration | 39 |
| 3.18 | Dynamical gap critical exponent z at starting parameter $\frac{h}{J_x} = 1$ against the renormalization steps | 41 |
| 4.1 | Scheme 1: CORE simulations and finite size scaling at $\Delta = 0.5$ and $h = 0.001$ | 49 |

| | | |
|------|--|----|
| 4.2 | Scheme 1: CORE simulations and finite size scaling at $\Delta = 0.5$ and $h = 0.001$. . . | 49 |
| 4.3 | Scheme 1: CORE simulations and finite size scaling at $\Delta = 0.5$ and $h = 0.001$. . . | 50 |
| 4.4 | Scheme 1: CORE simulations and finite size scaling at $\Delta = 0.5$ and $h = 0.001$. . . | 50 |
| 4.5 | Scheme 1: CORE simulations and finite size scaling at $\Delta = 0.5$ and $L = 6$ | 51 |
| 4.6 | scheme 1: Plot for gap ratio $K(L, h)$ versus the scaling function $L^\phi h^\alpha$ using CORE simulations. | 52 |
| 4.7 | Scheme 2: CORE simulations and finite size scaling at $\Delta = 0.5$ and $h = 0.001$. . . | 53 |
| 4.8 | Scheme 2: CORE simulations and finite size scaling at $\Delta = 0.5$ and $L = 36$ | 53 |
| 4.9 | scheme 2: Plot for gap ratio $K(L, h)$ versus the scaling function $L^\phi h^\alpha$ using CORE simulations at $\Delta = 0.5$ | 54 |
| 4.10 | CORE simulations and finite size scaling at $\Delta = 0.7$ and $h = 0.001$ | 55 |
| 4.11 | CORE simulations and finite size scaling at $\Delta = 0.7$ and $h = 0.001$ | 56 |
| 4.12 | CORE simulations and finite size scaling at $\Delta = 0.7$ and $h = 0.001$ | 56 |
| 4.13 | CORE simulations and finite size scaling at $\Delta = 0.7$ and $h = 0.001$ | 56 |
| 4.14 | Scheme 2: CORE simulations and finite size scaling at $\Delta = 0.7$ and $L = 24$ | 58 |
| 4.15 | CORE simulations and finite size scaling at $\Delta = 0.7$ | 58 |
| 4.16 | CORE simulations and finite size scaling at $\Delta = 0.7$ | 59 |
| 4.17 | CORE simulations for the gap plotted against the scaling function $L^\phi h^\alpha$ at $\Delta = 0.7$ | 60 |
| 4.18 | Each anisotropy have its particular ϕ - and α -exponent given by tables (4.3) and (4.4) respectively. | 61 |
| 4.19 | Each anisotropy have its particular ϕ - and α -exponent given by tables (4.3) and (4.4) respectively. | 61 |
| 5.1 | log-log plot of Energy Stabilization with alternation parameters. Hamiltonians are made from CORE 1 st and 2 nd iterations. Single block of 1 st iteration consist of 8 sites, while subsequent iterations single blocks consist of 4 renormalized sites. | 68 |
| 5.2 | log-log plot of Energy Stabilization with alternation parameter. CORE simulations are done at range-2. | 69 |
| 5.3 | log-log plot for singlet-triplet gap with alternation parameters using CORE 1 st and 2 nd iteration at range-2. | 70 |
| 5.4 | log-log plot of Energy Stabilization with alternation parameters. Hamiltonians are made from CORE 4 th and 5 th iterations at range-3. | 72 |
| 5.5 | Energy stabilization for (AHC) with CORE simulations at range-3. | 73 |
| 5.6 | log-log plot of singlet-triplet gap with alternation parameters using CORE 3 rd and 4 th -iterations at range-3. | 73 |
| 5.7 | singlet-triplet gap with CORE simulations at range-3. | 74 |
| 5.8 | log-log plot of Energy Stabilization with alternation parameters. Hamiltonians are made from CORE 2 nd and 3 rd iterations at range-3 with bigger blocks. . . . | 75 |
| 5.9 | log-log plot of singlet-triplet gap with alternation parameters. Hamiltonians are made from CORE 2 nd and 3 rd iterations at range-3 with bigger blocks. | 76 |
| 5.10 | Renormalization flow of coupling J and alternation parameter δ | 77 |
| 6.1 | Renormalization Flow of parameter $\frac{J_2^I}{J_1^I}$ with respect to starting ratio $\frac{J_2^S}{J_1^S}$ | 83 |
| 6.2 | Renormalization Flow of parameter $\frac{J_1^I}{J_1^I}$ with respect to starting ratio $\frac{J_2^S}{J_1^S}$ | 83 |
| 6.3 | Renormalization Flow of parameter $\frac{J_2^I}{J_1^I}$ with respect to starting ratio $\frac{J_2^S}{J_1^S}$ | 84 |
| 6.4 | CORE simulations with five sites per single block. Renormalized hamiltonians are made taking $\{8, 10, 12\}$ renormalized sites after 3 rd CORE iteration. | 85 |

LIST OF FIGURES

| | | |
|------|---|-----|
| 6.5 | Renormalization Flow of parameter $\frac{J_2^I}{J_1^I}$ with respect to starting ratio $\frac{J_2^s}{J_1^s}$ | 85 |
| 6.6 | log-log plot of Energy Stabilization with alternation parameters. Hamiltonians are made from CORE 3 rd and 4 th iteration at range-3. The frustration is 0.2411 | 89 |
| 6.7 | log-log plot of Energy Stabilization with alternation parameters. Hamiltonians are made from CORE 3 rd and 4 th iterations at range-3. | 90 |
| 6.8 | log-log plot of Energy Stabilization with alternation parameters. The CORE simulations are done at range-3, Hamiltonians are made from CORE 3 rd and 4 th iterations. | 90 |
| 6.9 | log-log plot for singlet-triplet gap with alternation parameters using CORE 3 rd and 4 th iteration. The frustration is 0.2411 | 91 |
| 6.10 | log-log plot for singlet-triplet gap with alternations. | 91 |
| 6.11 | log-log plot for singlet-triplet gap with alternations. | 92 |
| A.1 | Renormalized site after 1 st , 2 nd and 3 rd -Iteration represented by blue, green and red blocks respectively | 99 |
| A.2 | After 1 st , 2 nd and 3 rd -Iteration, interaction between two renormalized blocks is shown by arrows | 100 |
| A.3 | Arrows show missing range-3 contributions due to shifting scaling for 1 st -three CORE iterations | 101 |

List of Tables

| | | |
|------|---|-----|
| 3.1 | critical exponents of different universality classes | 27 |
| 4.1 | critical exponents of the gap for anisotropy parameters ($-1 < \Delta \leq 1$). | 45 |
| 4.2 | ϕ -exponents for the best overlap between the CORE simulations and equation (4.14) for anisotropy ($\Delta = 0.5$) | 52 |
| 4.3 | ϕ -exponent for different anisotropy parameters | 57 |
| 4.4 | α -exponent for different anisotropy parameters | 59 |
| 4.5 | ϕ - and α -exponent by CORE and Modified Lanczos | 61 |
| 4.6 | gap-exponents by different Methods | 62 |
| 5.1 | critical exponents by CORE simulations at range-2 | 70 |
| 5.2 | critical exponents with increasing lattice sizes with CORE simulations at range-3. | 74 |
| 5.3 | critical exponents of energy stabilization and gap by CORE simulations at range-3 with bigger blocks | 76 |
| 6.1 | The bulk energy density of (AHC) with Frustration with CORE algorithm at range-2 and range-3 | 81 |
| 6.2 | critical exponents by CORE simulations at Range-2 with Frustrations=0.05 | 87 |
| 6.3 | critical exponents by CORE simulations at Range-2 with Frustrations=0.1 | 87 |
| 6.4 | critical exponents by CORE simulations at Range-2 with Frustrations 0.15 | 87 |
| 6.5 | critical exponents by CORE simulations at Range-2 with Frustrations=0.2 | 88 |
| 6.6 | critical exponents by CORE simulations at Range-2 with Frustrations=0.2411 | 88 |
| 6.7 | Critical Exponents of energy stabilization and gap at range-3 with frustration 0.05 | 92 |
| 6.8 | Critical Exponents of energy stabilization and gap at range-3 with frustration 0.1 | 93 |
| 6.9 | Critical Exponents of energy stabilization and gap at range-3 with frustration 0.15 | 93 |
| 6.10 | Critical Exponents of energy stabilization and gap at range-3 with frustration 0.2 | 93 |
| 6.11 | Critical Exponents of energy stabilization and gap at range-3 with frustration 0.2411 | 94 |
| 6.12 | coefficient and critical exponents for the power law describing the energy stabilization and singlet-triplet gap corresponding to different frustrations. These are found by CORE simulations at range-2. | 95 |
| 6.13 | coefficient and critical exponents for the power law describing the energy stabilization and singlet-triplet gap corresponding to different frustrations. These are found by CORE simulations at range-3. | 95 |
| B.1 | Conserve- Sz with Sz quantum number zero for range-2 super block | 103 |
| B.2 | Conserve- Sz for Sz quantum number $-\frac{1}{2}$ for range-3 super block | 103 |

Chapter 1

Renormalization Group Theory (RGT) and Phase Transitions

When a system is studied on the microscopic scale, the starting point is usually the microscopic hamiltonian, describing the major energies of the system. But the macroscopic properties of the systems are source of its interaction with the “real world”. Some of these macroscopic properties are non-trivial such as magnetism, high temperature superconductivity etc. The non-trivial phenomena occurring on the macroscopic scale has its basis in the phenomena occurring on the microscopic scale. Until the early 1970s, the macroscopic properties of the systems were studied by solving the hamiltonians analytically at the thermodynamic limits. The other method was to simulate a small system, then extrapolating the results to the thermodynamic limits [32]. This technique works very well, but not close to the critical point where the correlation length becomes infinite. Kadanoff published a paper in 1966 [2], arguing that close to the phase transition a system displays long range fluctuations. So one needs to solve the hamiltonian for large length scales. Kadanoff introduced the concept of scaling by mapping a lattice system onto itself by reduction of states [1]. This maps a quantum model to the infinite lattice with sufficient reduction of states, so that the resultant hamiltonian can be applied a solution more easily. Kadanoff scaling picture have the important features which served as basics for Wilson and others, who provided a more quantitative realization of the full renormalization group [3]. The renormalization group analysis was able to form a bridge between theoretical and the experimental studies of the critical phenomena.

1.1 Kadanoff Scaling Picture of Lattice Geometry

“Real Space Renormalization” is applicable to the systems based on the regular lattice structure called “discrete lattice symmetry”. For a 1-dimensional lattice, a sketch of the Kadanoff scaling picture can be described by figure (1.1).

A renormalization group transformation is applied to this lattice, replacing a group of two microscopic lattice sites with a new single site. In this way, the original lattice is transformed into new lattice, represented by small square blocks as shown in the figure (1.1b). These blocks are viewed as new renormalized sites of the new renormalized lattice after the first renormalization group transformation (RGT).

The scaling factor is defined as the factor by which the renormalized lattice is to be reduced to make it similar to the original microscopic lattice. The scaling factor of this transformation is

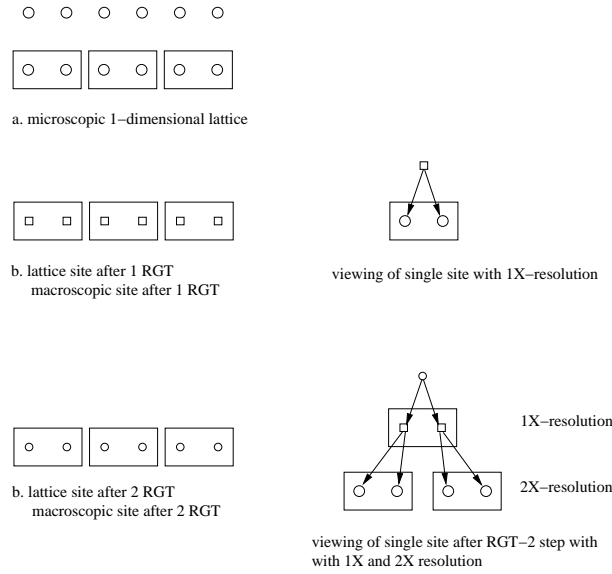


Figure 1.1: Renormalization of the 1-dimensional lattice

2. In the last step for the renormalization of the lattice, one has to scale down the renormalized lattice by the scaling factor so that it becomes self similar with the original microscopic lattice [32]. During the renormalization of the lattice, it is very important to document the important parameters e.g., iteration numbers, scaling factors etc, so that the equivalent microscopic sites can be calculated at any of the real space RGT-step. This will also help determine the site averaged quantities, like magnetic moment, susceptibility etc.

If more than one renormalization group transformations (RGT) are required, then the same procedure is repeated for the previous renormalized lattice.

In terms of our observational frame (or experimental scale), all the non-trivial phenomena has its roots embedded in the microscopic scale. The dynamics of the observational frame may be called as “renormalized” dynamics, while the dynamics of the microscopic scale may be called as “fundamental” dynamics.

The renormalized dynamics can be explained by Ising model. This model has only two fundamental parameters at the microscopic scale, the coupling strength between the neighbouring spins J (trying to align the system) and the external field h (trying to destroy the order). The strength of these two parameters $\{J, h\}$ on the fundamental scale is transformed by renormalization group transformation (RGT) to the observational scale $\{J', h'\}$, where these parameters becomes relevant or irrelevant depending if either of these elements is boosted or diminished[4, 5]. If one can specify the new parameters with the new observational frame, then each new renormalization transformation iteration can be regarded as the moving the observational frame, until one reaches at the point, that a further movement of the observational frame makes no difference, as the quantities of interest are already converged. This method of analysis is called the Renormalization Group Transformation (RGT).

So for reaching the fix point, the observational scale is moved with the increasing renormalization group transformations (RGT), until there will be no more change in the renormalized parameters.

1.2 Real Space Renormalization Methods

There has been great effort to study different quantum systems using the renormalization group transformation. Therefore many methods and their variants have been developed for working on the renormalization group transformations. To get an overview of working with renormalization group transformations (RGT), one can study a few of the methods based on this method. The main purpose of this overview is to get the understanding how these methods work for the lattice hamiltonians, taking results to the thermodynamic limit.

The first of these methods is called “Naive Real Space Renormalization Group” gives an insight of the working of the renormalization group transformation. It is not much accurate but one can study it as to understand the main features of the scaling algorithm. The major assumption of this method is that the ground state of the renormalized lattice is to a good approximation composed of the ground state of the constituting blocks of the previous lattice. However this approximation is not valid in all the cases, thereby prompting a thought that renormalization group methods are only the approximate procedures.

The second method to be studied is an improvement on the naive RSRG, which is called the Density Matrix Renormalization Group (DMRG). It has successfully applied to the quantum systems in one dimension using small computational resources.

The third method will be the Contractor Renormalization group method (CORE) and will be studied in detail. This method is also used for the simulations in this work.

1.2.1 Naive Real Space Renormalization Group (RSRG)

For a more detailed description of this method see [6, 7] and for a recent discussion, please look at [9]. The generic algorithm for the naive renormalization group methods works as follows.

1. The first step is to renormalize the lattice. The transformation is done with scaling parameter b , making single blocks of b sites. The hamiltonian is written for the single block denoted by H_0 and for the interblock denoted by V_0 .
2. The single block hamiltonian H_0 is diagonalized to get full energy spectrum of N eigen states. This spectrum is get sorted. A finite subset M , having the lowest eigen values of this spectrum is selected, where N is the total number of states of the single block. These lowest eigenstates M will form the low energy eigenspace of the cluster hamiltonian. This subspace is called retained sub-space.
3. Project the block hamiltonian H_0 on this truncated sub-space, making new hamiltonian $H_{0,trunc}$. This renormalized hamiltonian $H_{0,trunc}$ will give the same states for the new renormalized sites. Figure (1.2) shows a schematic diagram for this procedure.
4. The inter-block subspace will be the product sub-space of the retained states of two neighbouring blocks. The inter-block hamiltonian V_0 is applied to this product space and the low energy renormalized inter-block hamiltonian $V_{0,trunc}$ is found in the same way.
5. In this way, after the application of the renormalization group transformation, the blocks of the microscopic sites become new renormalized sites. The low energy retained states of the microscopic blocks become the states of the new renormalized sites. The low energy inter-block hamiltonian $V_{0,trunc}$ will become the renormalized inter-site(new renormalized site) hamiltonian.
6. This procedure can be iterated to find the renormalized hamiltonians corresponding to bigger microscopic sites, represented by $H_{i,trunc}$ and inter-block renormalized hamiltonians

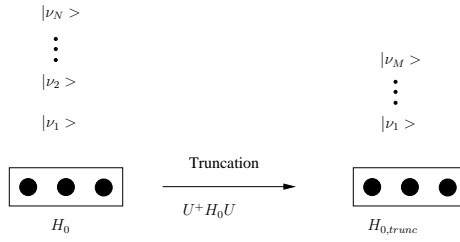


Figure 1.2: Schematic diagram of the truncation procedure in Naive Real Space Renormalization Method

$V_{i, trunc}$, where i is the iteration count of the renormalization group transformation. The process for obtaining the renormalized hamiltonians is explained in the figure (1.3). With the increasing iterations, there will be more error incorporated in the hamiltonian.

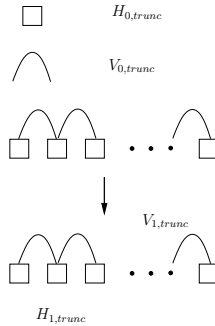


Figure 1.3: schematic diagram of the iterations of naive real space renormalization method.

7. One can go to any number of renormalization group transformations finding $H_{i, trunc}$ and $V_{i, trunc}$ to simulate the results at the thermodynamic limit, but practically after only a few iterations the accumulated errors crosses the tolerance limits.

The major drawback of this algorithm is to throw away the higher excited states without taking care of their contributions to the ground state. For this reason this method is not accurate enough for finding the results at the thermodynamic limits.

1.2.2 Density Matrix Renormalization Group (DMRG)

There are two major problems with the naive RSRG. The first is the enlargement of the clusters with the blocks that were not previously connected with the rest of the system. The other problem is with the cut-off scale. The cut-off scale is based on the energies of hamiltonian. It means that the high energy spectrum of the hamiltonian is not contributing when the size of the system increases. To overcome these problems, density matrix renormalization group method was suggested [10, 11, 12].

The method is kind of iterative method and is based on the truncation of the Hilbert space used to represent the Hamiltonian in a controlled way, keeping the most probable eigenstates.

This technique was introduced by S.R.White in 1992 and give improved results. Afterwards it become a the major tool to study the quantum systems at thermodynamics limits.

Here a small finite system becomes a bigger lattice system by iteratively incorporation of new sites. At each iteration, the most relevant eigenstates are retained according to their density-matrix weight. These eigenstates are used for spanning the target states [51]. A generic algorithm for one dimensional system using Density Matrix Renormalization Group (DMRG) method can be described as follows.

The algorithm can be started by taking a cluster containing only a single site and retain M states $|sm_1\rangle \cdots |sm_M\rangle$ of the cluster. Add a site to this cluster, N being the dimension of this new site with basis vectors $|sn_1\rangle \cdots |sn_N\rangle$. So the basis of this new cluster is the tensor product of the contributing states. The basis for the new cluster runs from 1 to $M \times N$. A supercluster will be made by combining two already formed clusters. In the next step one finds the ground state and some the lowest energy states of this super cluster. The best way of finding this ground state is by using the Lanczos method. These are called the target states. This target state or the ground state of the super block can be expanded in terms basis states of the contributing clusters. The density matrix of the left cluster can be evaluated by taking the trace over right cluster in the ground state within the super cluster. Eigenstates of density matrix form a complete basis for subsystem block. Eigenvalues give the weight of a state and the m eigenstates corresponding to highest eigenvalues are kept. In this way, the states with the largest weight in the expansion of the target state are retained. The procedure is repeated until we find a convergence to the thermodynamic limit.

It is numerically feasible and accurate for low dimension systems. It is however limited by the dimensionality or range of interactions and becomes computationally expensive for higher dimensions. For example, if m states are required for obtaining results in 1-dimensional, then for d -dimensions m^d states are necessary to obtain comparable results. The DMRG method has its limitations with convergence issues and very large number of states required for dealing with complicated systems [18].

There is another technique that instead working on the ground and few excited states, gives information in the form of operators at each iteration step of Wilson-Kadanoff scaling theory. This is called the Contractor renormalization method and will be applied to strongly co-related quantum spin models in this work.

1.2.3 The Contractor Renormalization Method (CORE)

The contractor renormalization (CORE) group method, working on the Kadanoff-Wilson real space transformation principle for lattice systems was introduced by Colin J. Morningstar and M. Weinstein in 1994 [16]. It also truncates the higher energy states but incorporate their effects on the renormalized hamiltonians. The exact diagonalization of these low energy renormalized hamiltonians give ground state and the lowest excited states, keeping the influence of the truncated higher excited states as shown in the figure (1.4). This task is accomplished by diagonalizing the super block range- r (block consisting of r - single blocks). The exact eigenstates of the super block are projected onto the tensor product states formed from the retained states of single blocks constituting the range- r super block.

Thus the renormalized hamiltonian calculated by CORE retains the influence of the higher excited states, in contrast to naive RSRG, where the higher states are discarded along with their influence, incorporating errors in the effective hamiltonian.

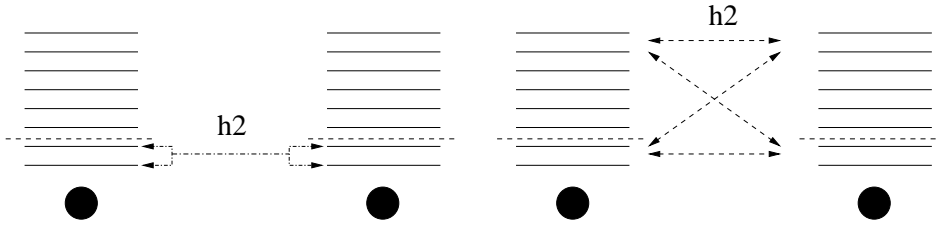


Figure 1.4: schematic diagram showing the truncation difference between the Naive RSRG and the CORE method.

1.3 Phase Transitions and Critical Exponents

The main purpose of the real space renormalization group methods is their applications to the systems of infinite extent e.g., to study the critical phenomena. Therefore one can give a short introduction of these phenomenas.

1.3.1 Phase Transitions

In the real world the matter exists in different macroscopic phases in thermodynamic equilibrium. These phases of matter are controlled by thermodynamic variables such as temperature, external magnetic field etc. By changing one or more than one thermodynamic variables, the matter can be transformed from one phase to another. The example of phase transition from daily life are liquid solid (water) and in some scientific analysis ferromagnetism-paramagnetism (Fe, Ni), antiferromagnetism-paramagnetism $RnMnF_2$, La_2CuO_4 etc.

Phase transition occur in the parametric space of the thermodynamic variables, where the free energy of the system becomes non-analytic. Such a behaviour generally comes from the interactions in the thermodynamic limit ($N \rightarrow \infty$). In a finite system, the partition function is always analytic, so non-analyticity is not the property of the finite systems [14]. The non-analytic behaviour comes due to interactions of infinite number of particles (thermodynamic limit). Macroscopic systems are generally contain multiple of $\sim 10^{23}$ number of particles and states, so they can be viewed as systems close to the thermodynamic limit.

Phase Transitions may show a abrupt (discontinuous) or gradual (continuous) behaviour. In case of the abrupt change of phase, the phase change has taken place at well defined values of thermodynamic variables. These well defined parameters determine the phase boundary of the thermodynamic system [14]. The discontinuous phase transition has a discontinuity in the first derivative of the free energy with respect to the tuning parameter. These types of systems do not show critical (long range) behaviour so they are not topic of discussion on critical phenomena. The second order phase transitions show a discontinuity in the second derivative of the free energy with respect to the tuning parameter, showing the critical behaviour and is a subject of discussion in this work.

In a classical system, the phase transition are brought about by the thermal fluctuations. These thermal fluctuation are freezed at the temperature $T = 0$. So the classical system freezes to fluctuationless ground state at $T = 0$ [32]. In quantum systems, however, there are fluctuations even at $T = 0$ driven by Heisenberg uncertainty principle. These fluctuations in the ground state can be the source of phase transitions at $T = 0$, which are called quantum phase transitions. One can try to apply CORE algorithm to these types of phase transitions.

The 2^{nd} -order phase transitions can be characterized by a quantity called order parameter.

It is a quantity indeterminate at the critical point.

1.3.2 The Order Parameter

For a quantitative analysis of the continuous phase transition, a quantity called the order parameter is to be identified for that phase transition. It is a quantity, whose expectation value (average) is zero on one side of phase transition and remains finite on the other side of the phase transition. The order parameter may not be unique for the system under consideration. There is no general scheme for defining the order parameter. Each of the model showing the phase transition is to be investigated individually for finding its order parameter. For example, magnetization can be taken as order parameter for a system showing a phase transition from ferromagnetic phase to paramagnetic phase, Density difference $|\rho_{fluid}(T) - \rho_{gas}(T)|$ for fluid-gas phase transition and string order parameter characterizing the haldane phase in quantum ladders.

1.3.3 Correlation Length

The theory of phase transition and critical phenomena depend on the fluctuations on the thermodynamic scale and the most important parameter in this regard is the Correlation length ξ . It can be defined in terms of the average length of the fluctuations of the order parameter. It means that order parameter remains constant after approaching this length. So at the length scale greater than the correlation length, the system is thought of to be frozen in terms of fluctuations and the system is iterated to one of the two fixed points, depending on the history of the parameters. After reaching the correlation length, the renormalized parameters remains constant even if one is iterating the system with more renormalization group transformations to reach still greater length scales. In the continuous phase transitions, at the critical point, the fluctuations occur at all the length scales. It means that correlation length diverges at the critical point ($\xi \rightarrow \infty$). It means the system remains invariant under kadanoff block transformation.

At the critical point, in the thermodynamic limit, the correlation length diverges according to the power law

$$\xi \sim |t|^{-\nu} \tag{1.1}$$

where t is the reduced critical parameter and ν is the critical exponent of the correlation length. The ν remains same if one is approaching the critical from any of the phases $t \rightarrow 0^+$ and $t \rightarrow 0^-$, but the pre-factors are generally different. The ratios of the pre-factors are called amplitude ratios and are generally universal.

1.3.4 Critical Exponents

In continuous phase transitions, several of the thermodynamics quantities diverge at or near the critical point showing the power-law behaviour. The exponents of these power laws are called critical exponents, characterizing the phase transition of these thermodynamics quantities. The critical exponents are not independent of each other. They fulfill several in-equalities [32].

For illustration of the critical exponents, consider a hamiltonian $H(\lambda)$, whose phase transition is due to the dimensionless controlling parameter (λ). Generally speaking, in many cases of quantum systems showing the phase transitions, as the controlling parameter approaches the critical point ($\lambda \rightarrow \lambda_c$), the long range fluctuations above the ground state vanishes. The gap (Δ) between the ground state and first excited state can be considered such a fluctuation. In most of the cases as the controlling parameter (λ) approaches its critical value (λ_c), the gap Δ vanishes according to the power law

$$\Delta \propto |\lambda - \lambda_c|^{z\nu} \quad (1.2)$$

where z and ν are the critical exponents. The critical exponents are universal in nature and do not depend on the microscopic details of the system.

In addition to the characteristic energy scales (gap), there is a correlation length ξ of the continuous phase transitions also diverging at the critical point as

$$\xi^{-1} \propto |\lambda - \lambda_c|^\nu \quad (1.3)$$

where ξ is the characteristic length (correlation length), ν is the critical exponent of the correlation length. From the last two equations, it can be seen that the characteristic energy scale (gap) vanishes obeying the power law with $-z$ as power (critical exponent) on the correlation length.

$$\Delta \propto \xi^{-z} \quad (1.4)$$

The critical exponents of the several phase transitions will be studied by using the CORE simulations. This will test the CORE algorithm to its limits bringing forward its virtues and disadvantages from calculating critical exponents of several different thermodynamics quantities.

1.3.5 Universality

If completely different system behave qualitatively in a similar way on large length scales, then they are said to have same universality class. Generally, the universality class of the system depends on few of its characteristics like

- dimensions of the system
- interactions
- symmetries of the hamiltonians
- dimensionality of order parameter

The critical exponents of the same universality class systems are also similar. Due to this property, one can use simplified systems to compute the critical exponents that are also valid for more complicated systems of the same universality class.

1.4 Finite Size Scaling

Finite Size Scaling is a standard technique used to study the phase transitions in quantum systems. In 2^{nd} -order phase transitions, the correlation length diverges at the critical point. Therefore the length of the lattice L becomes a relevant quantity near the critical point. The thermodynamic quantities (gap, magnetization etc) can be written in the form of scaling functions incorporating the lattice length L .

With the help of finite size scaling method, the relevant thermodynamics quantities are measured at varying lattice sizes for studying their effects. So for implementation of finite size scaling method, one takes a sequence of finite lattices. These finite lattices are solved exactly by using various methods like lanczos, CORE etc. Then the various thermodynamics quantities of interest are calculated as a function of the lattice length L . The finite lattice sizes are not small enough that conventional computation methods like exact diagonalization can be

employed on mediocre computational resources. The methods like modified lanczos, density matrix renormalization group (DMRG) are already used for finding the critical exponents using the finite size scaling methods. In this work finite size scaling will be used along with the CORE algorithm to study phase transitions, finding the critical exponents.

The use of finite size scaling method with CORE algorithm shows the applicability of the CORE method to wide range of problems. Although the CORE algorithm is devised to study the critical phenomena, i.e., the large lattice sizes where the infinite lattice behaviour sets in, it is equally well capable of finding the lattice hamiltonians of small or mediocre size lattice systems. The finite size scaling becomes a necessity for some of the phase transitions. For example, if there is a level crossing, while simulating a quantum system at a certain CORE iteration, there will be no credible results at and beyond this CORE iteration, and so one is unable to go for the infinite lattice behaviour. The CORE iterations before the level crossings becomes the only credible data to be worked on.

The other advantage of using CORE with finite size scalings lies in its implementation with far less computational resources. The CORE algorithm is designed to work for critical phenomena. It means many CORE iterations will be needed to study critical phenomena. But with each increasing iteration, there will be a CORE approximation and numerical error incorporated in the results. A meaningful iteration process will involve shifting and scaling as explained in appendix (A). While using finite size scaling, one generally need mediocre lattice sizes, so there will be very little of the accumulated errors due to small number of CORE iterations. Shifting, scaling may still be needed as during simulations, it was seen it gives more accurate results after each of the CORE iteration.

1.5 Plan of Work

In this work, the CORE approximation [16, 17] is studied and its numerical implementation is done in a generalized way. The advantage of writing a generalized CORE program makes the choice of single block lattice sizes and number of states to be retained more flexible. Then the numerical implementation of the CORE algorithm is done for upto the range-3. The code is written in such a way that one can switch between range-2 and range-3 so that a comparison can be made between their results. Obviously range-3 results are better. But some models, computationally more expensive at range-3 will be dealt with range-2. The calculations at range-2 can make use of bigger block sizes while remaining in the same computational resources so that one can go for the lattice sizes which can describe infinite lattice behaviour. The generalized nature of algorithm implementation also allowed to change the single block lattice sizes and the retained states between the CORE iterations. This makes more complex problems to be solved by CORE algorithm while remaining within the mediocre computational resources.

The numerical implementation of the CORE algorithm for the various correlated models will be studied. The various issues in the numerical implementation along with their solutions will also be studied.

The chapter-2 discusses the CORE approximation along with its numerical implementation. It lays down the basis of the program, that is written for implementation of the CORE simulations.

In chapter-3, the $(1 + 1)$ -Ising model will be discussed using both the CORE range-2 and range-3 simulations. The simulations will be done with the increasing CORE iterations. The phase transition and the renormalization flow of controlling parameters will be discussed. Then critical exponents of the ferromagnetic-paramagnetic phase transition will also be simulated. The results from the range-3 simulations are found to be better than that of the range-2 simulations,

confirming the already established results. So for the rest of work range-3 simulations will be implemented where the computational resources allowed to do so.

In chapter-4, the gap exponent of the XXZ-model with the application of the external field will be discussed. The XXZ-model is gapless in the range of $(-1 < \Delta < 1)$. With the application of the external field the gap opens up. The gap-exponent of this phase transition is studied with CORE simulations range-3. The CORE simulation for the XXZ-model will be done with two types of range-3 simulations. In the first type of range-3 simulations, a smaller block of two sites will be taken while there will be three retained states. In the second type of range-3 simulations, a bigger block of three sites will be taken, while there will be two retained states. The results of the second scheme will be quite good, confirming the claim of the author [16] that the results will be somewhat robust with respect to truncation of states.

In chapter-5, critical exponents of spin- $\frac{1}{2}$ antiferromagnetic Heisenberg chain with alternations will be studied. Here the CORE simulations will be done for both range-2 and range-3. Then again, two different schemes for range-3 simulations are adopted. Here range-2 and range-3 schemes are adopted based on the computational resources. While using range-3 simulations, some aspects of convergence cannot be studied with considerable accuracy. For that aspect (large lattice sizes), one has to switch to range-2 simulations.

In chapter-6, critical exponents of spin- $\frac{1}{2}$ antiferromagnetic Heisenberg chain along with the alternations and frustrations will be studied. These simulations are done with respect to results found in the last chapter. The behaviour of the critical exponents in the frustration span from 0.05 to 0.2411 will be studied. The results found are in accordance with different numerical studies.

At the end, various issues concerning the implementation of the CORE algorithm will be discussed in appendices. Appendix A, gives the concept of shifting and scaling which are necessary, if there are many iterations of the CORE algorithm to be implemented. The scaling and shifting parameters also give important information in this regard.

Appendix B, give a concept of implementing CORE algorithm for conserve- Sz quantum number. This technique is not used for the simulations in this work, but has potential for the systems, where the contributing states according to some theorem are always of some specific Sz -quantum number.

From now on, the journey to the study and implementation of the CORE algorithm will be getting started.

Chapter 2

CONtractor RENormalization (Concept & Implementation)

Many problems in physics, from particle physics to quantum computing can only be solved through solutions by numerical methods. The physics of strongly correlated systems is one of the such problems [18]. The analytic solutions are not always the feasible option. So one has to switch to numerical methods in these situations. In strongly correlated systems, the conventional techniques are also not an option. This is because even for a modest size systems, enormous computational resources are required, and then extrapolation is needed for studying the behaviour at the thermodynamics limits. There will be inaccuracies, if the finite size systems with small lattice sizes are extrapolated to the systems having infinite volume. Density Matrix Renormalization group (DMRG) is one of the techniques, successful in one dimension, while for the multi-dimensional systems, its requirements on computational resources increase rapidly.

A technique was introduced by the Morningstar and Weinstein [16, 17] in 1994 called the Contractor Renormalization (CORE) Group Method. This technique was a good improvement from the existing renormalization group methods. In contrast to the naive renormalization group methods and their variants, the contractor renormalization group method transforms the original microscopic hamiltonian to a entirely different hamiltonian introducing the new renormalized sites and the new interactions depending on the blocking scheme and range- r contributions respectively. It gives information about the low energy spectrum. It is based on contraction and expansion methods, which can be improved at the cost of more computational resources, but even with the mediocre computational resources, it gives good results. Before going into details of the numerical implementations, the basic idea behind the CONtractor RENormalization (CORE) group method should be discussed.

2.1 CORE Approximation: Basic Idea

The Contractor Renormalization method has improved the accuracy of the renormalization group methods, while using the same computational resources. The Contractor renormalization (CORE) is a systematic and non-perturbative technique using the Kadanoff-Wilson real-space renormalization group ideas, incorporating the real space renormalization transformations to study the low energy effective hamiltonians also called renormalized hamiltonians.

CORE is able to find the renormalized hamiltonians and renormalized operators of interest by iterating the CORE renormalization transformations, which represents the increasing system

sizes on the equivalent microscopic lattice, but with thinned number of states. The CORE method can also be used both by extrapolation and Kadanoff-Wilson renormalization ideas. For extrapolation, generally only a single CORE iteration is done, while to see the renormalization flow of parameters based on Kadanoff-Wilson method, multiple CORE renormalization iterations have to be done. Due to capability of the CORE method to go for multiple iterations, the CORE technique can be used to study the critical phenomena, where the correlation length is infinite.

For calculating the low energy hamiltonian, one starts with the variational ansatz. The variational ansatz employs an operator, the so called contractor e^{-tH} , which is applied to the trial state $|\Phi\rangle = \sum_{i=1}^n a_i |\phi_i\rangle$.

$$\begin{aligned} e^{-tH} |\Phi\rangle &= \sum_i e^{-tH} a_i |\phi_i\rangle \\ &= \sum_i a_i e^{-t\epsilon_i} |\epsilon_i\rangle \end{aligned} \quad (2.1)$$

Here the index i runs for all the eigenstates of the hamiltonian H . In the limit $t \rightarrow \infty$, the contractor operator contracts the normalized variational trial state $|\Phi\rangle$ to the lowest eigenstate $|\epsilon_0\rangle$ of the hamiltonian H . If there is a non-vanishing overlap between the trial state $|\Phi\rangle$ and the lowest energy eigen state (ground state) $|\epsilon_0\rangle$ of the hamiltonian H , then the expectation value of the hamiltonian H in the limit $t \rightarrow \infty$ becomes $|\epsilon_0\rangle$, i.e., the ground state of the hamiltonian.

This can be written as

$$\langle E(t) \rangle = \frac{\langle \Phi | e^{-tH} H e^{-tH} | \Phi \rangle}{\langle \Phi | e^{-2tH} | \Phi \rangle} \xrightarrow{t \rightarrow \infty} \epsilon_0 \quad (2.2)$$

$$|\epsilon_0\rangle = \lim_{t \rightarrow \infty} \frac{e^{-tH/2} |\Phi\rangle}{\sqrt{\langle \Phi | e^{-tH} | \Phi \rangle}} \quad (2.3)$$

The contractor operator e^{-tH} is not exactly computable and the same is true for its expectation value.

To proceed forward, a new operator $T(t)$ is to be constructed, which closely resembles to the contractor operator e^{-tH} for t in the span of $(0 < t < t_{max})$. The new operator $T(t)$ is also supposed to be an easily computable operator. To find such an operator $T(t)$, the hamiltonian H can be re-written in terms of computable parts $H = H_1 + H_2$. So the contractor can be expressed in terms of computable parts e^{-tH_1} and e^{-tH_2} as a symmetric product [19]

$$e^{-tH} = e^{-tH_1/2} e^{-tH_2/2} e^{C_3(t)} e^{-tH_2/2} e^{-tH_1/2} \quad (2.4)$$

The $e^{C_3(t)}$ is the sum of the terms of the order t^3 or higher. This term can be approximated with any of the operator which fulfills the symmetries of the hamiltonian H . The simplest of the approximations will be the replacement of the $e^{C_3(t)}$ with an identity operator. Another approximation is to retain low order terms in $e^{C_3(t)}$. Then the exponential of these operators can be written as the symmetric product of exactly computable terms. Other types of approximations can also be used. The upper boundary of the expectation value for the given contractor can be thought of

$$\langle E_T(t) \rangle = \frac{\langle \Phi | T(t) H T(t) | \Phi \rangle}{\langle \Phi | T(t)^2 | \Phi \rangle} \quad (2.5)$$

To get the ground state energy, one has to minimize the $E_T(t)$ with respect to t and any of the parameters in the trial state $|\Phi\rangle = \sum_{i=1}^n a_i |\phi_i\rangle$.

For this purpose, the best trial state $|\Phi\rangle$ can be calculated by varying the coefficients a_i in the expansion, so that minimization of the energy is achieved. Equivalently it can be achieved by solving the eigen value problem [16]

$$\det \left([[T(t)HT(t)]] - \lambda [[T(t)^2]] \right) = 0 \quad (2.6)$$

where $[[\dots]]$ denotes the subspace spanned by the tensor product of the retained states. If P is the projection operator of the retained states, then it can be given as

$$P = \sum_{j=1}^n |\nu_j\rangle \langle \nu_j| \quad (2.7)$$

Any operator can be projected on this sub-space by

$$[[O]] = POP^+ \quad (2.8)$$

This equation can be transformed into an equation where one can see the mapping of the original hamiltonian into an transformed renormalized hamiltonian [16]

$$H_{ren}^1(t) = [[T(t)^2]]^{-\frac{1}{2}} [[T(t)HT(t)]] [[T(t)^2]]^{-\frac{1}{2}} \quad (2.9)$$

The above equation (2.9) shows the major improvement of the CORE method over the naive RSRG. In the naive RSRG, $[[H]]$ is found at each iterating step, which do not retain the effect of higher excited states. But in CORE one has renormalized hamiltonian H_{ren} after each renormalization group transformation. It is a new hamiltonian which retains the effect of the dropped states. It can also been seen that at $t = 0$ limit, CORE hamiltonian transform into naive RSRG. So the effects of higher dropped states are incorporated into the low energy renormalized hamiltonian.

After the first run of the CORE Algorithm, one can go on iterating using the renormalized hamiltonians at each of the iteration step, generating the sequence of renormalized hamiltonians, which can be written as

$$H_{ren}^{n+1} = [[T^n(t)^2]]^{-\frac{1}{2}} [[T^n(t)H_{eff}^n(t_n^*)T^n(t)]] [[T^n(t)^2]]^{-\frac{1}{2}} \quad (2.10)$$

with

$$T^n(t) \simeq e^{-t(H_{eff}^n(t_n^*))} \quad (2.11)$$

where $(*)$ denotes the contractor applied to renormalized hamiltonian from previous CORE iteration.

Any extensive operator of interest for the system can be evaluated using the same transformation as done for the hamiltonian. A series of iterated renormalized operators $O_{eff}^n(t_n^*)$ along with the renormalized hamiltonians can also be found out. The renormalized operators can also be written as

$$O_{ren}^{n+1} = [[T^n(t)^2]]^{-\frac{1}{2}} [[T^n(t)O_{eff}^n(t_n^*)T^n(t)]] [[T^n(t)^2]]^{-\frac{1}{2}} \quad (2.12)$$

As the CORE iterations are proceeded, the states of the renormalized hamiltonians are thinned due to the truncation process and ultimately one gets a renormalized hamiltonian at a higher iteration with such a small dimension that it can easily be diagonalized on small or mediocre computational resources.

It is not clear how to form the contractor $T(t)$ or to find the operator $[[T(t)]]^{-\frac{1}{2}}$ as $t \rightarrow \infty$. There is an equivalent result used to calculate equation (2.10). For using that result, two quantities are needed to be calculated [17]. This will be discussed in the next section.

The first of this quantity is the unitary triangulation matrix S of the dimension $M^r \times M^r$. It is the overlap matrix of the tensor product states of the constituent blocks of the super-block range- r with a new basis. The new basis is such that the states of the super-block range- r has a finite overlap with only one specific exact eigenstate of the super-block range- r . The second quantity is the contraction remnant. These are the remnant states $|\tau_\beta\rangle$ of the super-block range- r in the retained subspace P (2.7).

Having found these two quantities, the renormalized hamiltonian of the super-block range- r is given by

$$H_{ren} = S^+ H_\tau S \quad (2.13)$$

where the super-block range- r hamiltonian in the ortho-normalized contraction remnant states is given by

$$H_\tau = \text{Diag}(\tau_0, \dots, \tau_{M^r}) \quad (2.14)$$

For obtaining the super block range- r , this alternate approach will be followed instead of finding the contractor operators.

2.2 CORE Algorithm: Implementation Concepts

In the spirit of renormalization group transformation, consider a sub-lattice G consisting of r -connected individual blocks $B_1, B_2, B_3, \dots, B_r$, called super block range- r . The hamiltonian of the superblock range- r can be denoted by $H(G)$. A few of the lattice sites are selected to make an individual block. The criteria for selecting the number of individual lattice sites for the individual blocks depends on multiple factors specific to individual problem. It depends on the range- r of the CORE simulations as with the increasing range- r , the bigger blocks need more computational resources. It also depends on the number of retained states (fulfilling the degeneracy requirements). Then there are other reasons which will be discussed during the simulations.

After selecting the individual blocks, each consisting of L lattice sites, each having n states, a single block will be diagonalized finding its eigenvalues and eigenstates. There will be n^L eigen vectors for a single individual block. The lowest M eigenvectors of each block will be kept. The choice of M will depend on the available computational resources, degeneracy and the desired accuracy (more retained states giving more accuracy).

Hence the projector for the super block range- r , which project M retained states of the r -constituent connected blocks in terms of the tensor product states

$$P = P_1 \otimes P_2 \otimes \dots \otimes P_r \quad (2.15)$$

It can be written explicitly as

$$P = \sum_{m_1=1}^M |\nu_{m_1}\rangle \langle \nu_{m_1}| \otimes \sum_{m_2=1}^M |\nu_{m_2}\rangle \langle \nu_{m_2}| \otimes \dots \otimes \sum_{m_r=1}^M |\nu_{m_r}\rangle \langle \nu_{m_r}| \quad (2.16)$$

If $|\omega_\alpha(G)\rangle$ is the tensor product of all the retained states of the r -constituting blocks of the super block range- r , Then equation (2.16) can be written as

$$P = \sum_{\alpha=1}^{M^R} |\omega_{\alpha}(G)\rangle \langle \omega_{\alpha}(G)| \quad (2.17)$$

The tensor product states $|\omega_{\alpha}(G)\rangle$ of the constituent blocks are expanded in terms of the exact eigenstates $|\epsilon_{\beta}(G)\rangle$ of the super block range- r hamiltonian, consisting of the whole sublattice of r -connected blocks.

$$|\omega_{\alpha}(G)\rangle = \sum_{\beta=1}^{M^R} c_{\alpha\beta} |\epsilon_{\beta}(G)\rangle \quad (2.18)$$

applying the contractor to these resultant states,

$$e^{-tH(G)} |\omega_{\alpha}(G)\rangle = \sum_{\beta=1}^{M^R} c_{\alpha\beta} e^{-t\epsilon_{\beta}(G)} |\epsilon_{\beta}(G)\rangle \quad (2.19)$$

The limit $t \rightarrow \infty$ is applied in order to get the ground state. On applying this limit, any state which has a non-zero overlap with the exact ground state of the super block range- r hamiltonian $|\epsilon_{\circ}\rangle$ will contract into the ground state, thus causing numerical problems to calculate $T(t)$, so the CORE algorithm can not proceeding in this way.

Fortunately, there is a solution for such a problem, which also have the virtue that there is no need to explicitly calculating the contractor e^{-tH} . To persue this approach, a change of basis for the tensor product states of the super block range- r is done

$$|\varrho_{\gamma}(G)\rangle = \sum_{\alpha=1}^{M^R} d_{\gamma\alpha} |\omega_{\alpha}(G)\rangle \quad (2.20)$$

The projector of the tensor product state (2.17) for individual blocks in the new basis can also be written as

$$P = \sum_{\gamma}^{M^R} |\varrho_{\gamma}(G)\rangle \langle \varrho_{\gamma}(G)| \quad (2.21)$$

The main feature of this new basis relies in its overlap properties with the exact eigenstates of the superblock range- r hamiltonian $H(G)$, where the new basis $|\varrho_{\gamma}(G)\rangle$ have the following overlap properties with respect to the exact eigenstate $|\epsilon_{\beta}(G)\rangle$ of the super block range- r hamiltonian

$$\langle \varrho_{\gamma}(G) | \epsilon_{\beta}(G) \rangle \neq 0 \quad (2.22)$$

$$\langle \varrho_{\gamma}(G) | \epsilon_{\beta}(G) \rangle = 0; \text{ for } \gamma > \beta \quad (2.23)$$

Each state of this new basis $|\varrho_{\gamma}(G)\rangle$ will contract to a different eigenstate of the super block hamiltonian $|\epsilon_{\beta}(G)\rangle$ as $t \rightarrow \infty$ condition is applied. The property of the new basis $|\varrho_{\gamma}(G)\rangle$ makes it to contracts onto a different eigenstate $|\epsilon_{\beta}(G)\rangle$ of the superblock hamiltonian as shown from the following table

$$\begin{array}{ccc}
 |\varrho_{M^r}\rangle & \xrightarrow{t \rightarrow \infty} & |\epsilon_{M^r}\rangle \\
 \vdots & \vdots & \vdots \\
 \vdots & \vdots & \vdots \\
 \vdots & \vdots & \vdots \\
 |\varrho_2\rangle & \xrightarrow{t \rightarrow \infty} & |\epsilon_2\rangle \\
 |\varrho_1\rangle & \xrightarrow{t \rightarrow \infty} & |\epsilon_1\rangle \\
 |\varrho_o\rangle & \xrightarrow{t \rightarrow \infty} & |\epsilon_o\rangle
 \end{array}$$

With the introduction of the new basis, the major difficulties in applying $t \rightarrow \infty$ is removed. Considering the equation (2.6), the eigen value problem can be started as

$$[[T(t)HT(t)]|\varrho\rangle = \lambda [[T(t)^2]|\varrho\rangle \quad (2.24)$$

operating the above equation with $\langle \varrho |$

$$\langle \varrho | [[T(t)HT(t)]|\varrho\rangle = \lambda \langle \varrho | [[T(t)^2]|\varrho\rangle \quad (2.25)$$

The projection to the new basis of M^R retained states can be explicitly written down

$$\frac{\sum_{m,n}^{M^R} \langle \varrho | \varrho_m(G) \rangle \langle \varrho_m | T(t)HT(t) | \varrho_n \rangle \langle \varrho_n | \varrho \rangle}{\sum_{p,q}^{M^R} \langle \varrho | \varrho_p(G) \rangle \langle \varrho_p | T(t)^2 | \varrho_q \rangle \langle \varrho_q | \varrho \rangle} = \lambda \quad (2.26)$$

The renormalized hamiltonian has the expectation value λ as given in the above equation. The renormalized hamiltonian in the subspace called contraction remnant $|\varrho\rangle$ can be simplified to yield the following result

$$H_{ren}^r = \sum_n^{M^r} |\varrho_n\rangle \epsilon_n \langle \varrho_n | \quad (2.27)$$

Finding these contraction remnant states $|\varrho_n\rangle$ numerically, having the same low energy eigen values as that of the lowest eigen states of the original hamiltonian on the full subspace, the renormalized hamiltonian can be found.

The same contraction remnant in the retained sub-space can be used to find the renormalized operator O_{ren} of any given operator of interest.

$$O_{ren}^r = \sum_{m,n}^{M^r} |\varrho_m\rangle o_{mn} \langle \varrho_n | \quad (2.28)$$

In the next section, algorithmic steps will be given to find numerically the renormalized hamiltonian and operators.

2.3 CORE Algorithm : Numerical Implementation

From the on-going discussion, it has been established that from the computational point of view, there are two main tasks need to be accomplished to find the renormalized hamiltonian H_{ren} of the super block range- r .

The first is the change of basis of the tensor product states $|\omega_\alpha(G)\rangle$ of the retained states from each of the constituent block of the super block range- r . The new basis $|\varrho_\alpha\rangle$ has the property that it contracts into unique eigenstate of the super block range- r hamiltonian $H(G)$. This will be accomplished by finding the triangulation matrix $S(G)_{\alpha\beta} = \langle \varrho_\alpha(G) | \omega_\beta(G) \rangle$.

The second requirement is to find the contraction remnant. The contraction remnant is the M^r lowest lying eigenstates of the super block $H(G)$ but with the property that their projection on the tensor product states is non-vanishing and these states are linearly independent. So after having found the triangulation matrix $S(G)$ and the contraction remnant, the evaluation of the low energy renormalized hamiltonian is straight forward.

The major steps for achieving this task can be accomplished as follows.

2.3.1 CORE Algorithm: Inputs

One can discuss the quantities that should be computed only once for each of the CORE iteration before going into the loop of the CORE algorithm for that simulation.

Diagonalizing Single Block

In the first step, one has to find the eigen values and the eigen vectors of the single block hamiltonian. Generally the single block hamiltonian is of small manageable dimensions, so one can apply exact diagonalization e.g., LAPACK routines finding all the eigen values and eigen vectors, otherwise there is no problem if one is using some specialized routine e.g., Arnoldi method for computing some of the lowest eigen values and eigen vectors. The main point is that there should be enough eigen values so that the degeneracy of the retained states should be properly checked on the sorted data of eigen values with the corresponding eigen vectors.

Truncation of the Energy Spectrum

To proceed with the CORE algorithm, truncation is done to the energy spectrum of the single block hamiltonian. The degeneracy is respected during the truncation process, otherwise it will effect the symmetries of the input hamiltonian. Either the degeneracy is fully retained or fully truncated.

Another consideration is the number of the retained states. While retaining more states will make the renormalized hamiltonians more precise, but it will also increases the dimensions of the renormalized hamiltonians, needing more computational resources. The dimensions of the hamiltonian with M retained states and L sites is M^L . With the retaining of more states, it amounts to the bigger matrices needing large memory resources. So the truncation of states is done based on multiple factors, like, degeneracy of the problem, accuracy needed for the problem and the computational resources available.

Range-1 contribution to Renormalized Hamiltonian

A projector is made from the retained states of the single block

$$P = \sum_{j=1}^n |\omega_j\rangle \langle \omega_j| \quad (2.29)$$

The range-1 hamiltonian contribution to renormalized hamiltonian can be trivially calculated as

$$h_1 = PH_jP \quad (2.30)$$

The range-1 operator contribution to renormalized operator of interest ‘ O ’ can be calculated by

$$h_1 = PO_jP \quad (2.31)$$

Diagonalizing Super Block Range- r

The next task in the implementation of the CORE algorithm is to diagonalize the hamiltonian of super block range- r . The super block range- r consists of r -connected single blocks and can be viewed as consisting of equivalent number of sites of r -connected single blocks. Like in the single block hamiltonians, only a few low energy eigen states of the super block range- r are needed. The exact diagonalization can be done for finding the entire energy spectrum, if the super block range- r is small enough. The other choice will be to find only a few lowest eigen states by lanczos or any other method. Arnoldi routines are recommended if only 20% or less eigen vectors are needed. This condition is generally fulfilled by super block range- r but not by the constituting single block.

It is also to be noted that using Arnoldi or any other routine to find the lowest energy spectrum is not sometimes straight forward. For example if the Arnoldi routine is giving the lowest eigen value by magnitude, then the plus or minus signs of the eigen values is not known. In such situations, hamiltonian matrix can be shifted by its largest eigenvalue in magnitude, also found by Arnoldi’s method added by some arbitrary value. It ensures the resultant hamiltonian matrix has a positive energy spectrum. The lowest energy spectrum of the original hamiltonian matrix can be found by shifting back the eigen values of this hamiltonian.

Degeneracy ‘ D ’ of the super block range- r

Taking the sorted eigenvalues of the super block range- r hamiltonian, a degeneracy list “ D ” can be made based on its eigen-values. The degeneracy list is made starting from the first eigen value and its degeneracy till the degeneracies of all the computed eigen values are mentioned. For non-degenerate eigen values the degeneracy is “ $D = 1$ ”.

Tensor Product States of Super Block range- r

The super-block range- r is made from r constituent blocks, each having M retained states. The tensor product of the retained states of all the constituent blocks are the tensor product states of the super block range- r . There will be M^r tensor product states.

Construction of the Overlap matrix Q (super-block Range- r)

The tensor product states of the super-block range- r $|\omega(G)\rangle$ are calculated from the retained states of the constituting single block. The super block range- r hamiltonian must have its unique eigenstates $|\epsilon_\beta(G)\rangle$. The scalar product of each of the tensor product state with that of the exact eigenstates of the super block range- r hamiltonian is calculated in matrix form as

$$Q(G) = \langle \omega_\alpha(G) | \epsilon_\beta(G) \rangle \quad (2.32)$$

The matrix $Q(G)$ is made in such a way that the exact eigenstates of the super block range- r hamiltonian are along the columns of the matrix starting from the lowest energy eigen state in the ascending order while the tensor product states are along the rows of the matrix $Q(G)$ with no specific order. If the total eigen states of the single block hamiltonian is N , and there are M retained states in a constituting single block, then the dimensions of the matrix $Q(G)$ will be $M^r \times N^r$, where r is the range of the simulations. If the super block range- r has big dimensions

(~ 500 or more) and only a few lowest eigen states ‘ S ’ are computed then the dimensions of the $Q(G)$ matrix is $M^r \times S^r$. The first column of the matrix $Q(G)$ is filled by taking the scalar product of the lowest eigenstate of the super block hamiltonian with that of each of the tensor product state. For the second column, the scalar product of the first excited eigen state with that of each of the tensor product state and so on.

In this way, each column of the matrix $Q(G)$ is the projection of one of the exact eigenstates of the super block range- r with all of the tensor product states. This matrix is one of the input ingredient of the CORE algorithm. Since the tensor product states are being expanded in terms of the eigenstates of the super-block range- r , if some of the eigenstate of the superblock do not exist in the expansion of the tensor product state, then the scalar product between these two states will be zero and the matrix $Q(G)$ will have a zero column for that eigenstate of the hamiltonian. In this case, this eigen-state are dropped and the loop of the CORE algorithm is proceeded with the remaining of the eigen states.

2.3.2 CORE Algorithm: The Structure

Having the pre-requisites, the loops for finding the contraction remnant and change of basis matrix $S(G)$ can be started. Before starting the loop of the CORE algorithm for a generalized system, one can define some of the variables to be used in the CORE algorithm.

1. The first variable to be defined is u . It is the number of contraction remnant states evaluated in the current loop. It is generally equal to the current degeneracy of the contributing eigen-state of the super block range- u . For non-degenerate contributing eigenstate $u = 1$.
2. The second variable to be defined is p . It is the total number of contraction remnant states evaluated including that of the current loop. Actually p works as a memory variable. It tracks the number of evaluated contraction remnant states and points to the position where the contraction remnant is to be added. So it starts with $p = 0$. After each loop, the variable p is incremented as

$$p \leftarrow p + u \tag{2.33}$$

3. The third variable to be defined is q . It is the current contributing eigen state of the super block range- r hamiltonian. It also acts as the memory element, indicating the current number of eigen vectors of the super block range- r hamiltonian, which have to be acted upon.

If there is a non-degenerate eigen state, it will either be contributing or not contributing. In case of contributing state of the super-block range- r hamiltonian, there will be one or more non-zero overlaps with any of the tensor product states. Therefore the corresponding column entries of the matrix Q has one or more non-zero entries. For the non-contributing eigen state, all overlaps with tensor product states vanish and all the corresponding column entries of the matrix Q are zero. In this case, one has to discard the state and move on to the next state, but still has to increment the variable q , so that it points to the correct state. The variable q may be written as

$$q \leftarrow q + u \tag{2.34}$$

where u is the contributing or non-contributing eigen state of the super block range- r . The lowest of the eigen vector of the super block range- r hamiltonian is enumerated as zero, therefore the variable q can also be initialized by zero $q = 0$.

4. Another variable to be defined is $m = M^r$, where r is the range of the superblock. The contraction remnant contains M^r ortho-normalized states. In each loop of the CORE algorithm, u contraction remnant states will be formed, so for each loop of the CORE algorithm, the quantity m is decremented as

$$m \leftarrow m - u \quad (2.35)$$

5. A unity matrix $S(G)$ with the dimensions $M^r \times M^r$ is defined, where M is the number of retained states of a single block and r is the range of the CORE simulations.

2.3.3 CORE Algorithm : The Loop

After defining all the variables and quantities for the implementation of the CORE algorithm, the process of finding the renormalized hamiltonian for super-block range- r can be started. The programming loop in the CORE algorithm accomplishes two tasks, a change of basis which takes the tensor product state of the retained states for super block range- r hamiltonian to the states, where each state has non-vanishing overlap with only one state of the super-block range- r hamiltonian. The other task is to find the contraction remnant which has the non-vanishing overlap with the tensor product states but are linearly independent of each other.

The procedure can be followed as [17]

1. A matrix called ‘ C ’ is formed from the overlap matrix $Q(G)$ according to the degeneracy list of the super-block range- r hamiltonian. Starting from the lowest (or current) eigenstate of the hamiltonian, with degeneracy ‘ D ’, the first ‘ D ’ columns of the overlap matrix $Q(G)$ are selected as matrix ‘ C ’. For a non-degenerate eigen state, $D = 1$, so only the first column is selected as matrix ‘ C ’. It should be noted that for the columns of matrix $Q(G)$ selected, there should be a non-vanishing overlap between the tensor-product states and exact eigenstates of the super-block range- r hamiltonian. In case matrix ‘ C ’ containing all zeros, these ‘ D ’ columns from matrix $Q(G)$ are truncated. Then matrix ‘ C ’ is checked for the next eigen-value and its degeneracy with remaining of the matrix $Q(G)$ of the super-block range- r hamiltonian. For degeneracy ‘ D ’, the contributing states are $|\epsilon_q\rangle, \dots, |\epsilon_{q+D-1}\rangle(G)$.
2. After the matrix C is formed, the orthonormal bases for the nullspace and range of matrix ‘ C ’ are found by performing singular matrix decomposition (SVD) on matrix C , the result will be

$$C = U\Sigma V^\dagger \quad (2.36)$$

where U is the $m \times m$ unitary matrix, V is a $D \times D$ unitary matrix, and Σ is an $m \times D$ matrix of the form

$$\Sigma = \begin{bmatrix} \Delta_{u \times u} & 0_{u \times (D-u)} \\ 0_{(m-u) \times u} & 0_{(m-u) \times (D-u)} \end{bmatrix} \quad (2.37)$$

$\Delta = \text{diag}(\sigma_1, \dots, \sigma_u)$ where the elements σ_j are real and satisfy $\sigma_1 \geq \sigma_2 \geq \dots \sigma_u > 0$ and $u \leq \min(m, D)$ is the rank of matrix C .

3. calculate $Q(G) = U^\dagger Q(G)$, then trim the first D columns (which have already been used in forming matrix C) and the first r rows, which are the number of contraction remnant states calculated in this loop. This makes our new current matrix $Q(G)$, which will be used

in the consequent loops. The current matrix $Q(G)$ will now have the dimensions $(m - u) \times (N^r - q - D)$, if super block range- r is diagonalized for the entire energy spectrum or $(m - r) \times (S^r - q - D)$, if only a smaller group of lowest eigenstates is calculated.

4. A matrix R is formed consisting of

$$R = \begin{bmatrix} 1_{p \times p} & 0_{p \times m} \\ 0_{m \times p} & 0_{m \times m} \end{bmatrix} \quad (2.38)$$

and calculate $S(G) = RS(G)$

5. The current contraction remnant can be formed by

$$|\tau_{p+s-1}(G)\rangle = \sum_{s'=1}^D V_{s's} |\epsilon_{p+s-1}(G)\rangle \quad (2.39)$$

with corresponding degenerate eigenvalues $\tau_{p+s-1} = \epsilon_q(G)$, for $s = 1 \cdots u$. update each variable $p \rightarrow p + u$, $q \rightarrow q + D$ and $m \rightarrow m - u$.

6. This loop will be repeated until M^r remnant eigenstates which are the orthogonal eigen vectors in the retained sub-space P are formed, so the condition on the loop can be set at $p = M^r$

At the end, there will be a contraction remnant and change of basis matrix $S(G)$. The target is to find the renormalized super block range- r hamiltonian in the contraction remnant sub-space. These matrices can be formed as

$$H_\tau(G)_{\alpha\beta} = \langle \tau_\alpha(G) | H_\tau(G) | \tau_\beta(G) \rangle = \delta_{\alpha\beta} \tau_\alpha(G) \quad (2.40)$$

Any operator matrix in the contraction remnant space is given by

$$O_\tau(G)_{\alpha\beta} = \langle \tau_\alpha(G) | O_\tau(G) | \tau_\beta(G) \rangle \quad (2.41)$$

The renormalized operator of the super block range- r is given by using the result in equation (2.13).

$$H_{ren}(G) = S^+(G) H_\tau(G) S(G) \quad (2.42)$$

$$O_{ren}(G) = S^+(G) O_\tau(G) S(G) \quad (2.43)$$

In this way, the renormalized hamiltonians and operators for the super block range- r are found by CORE algorithm. The renormalized hamiltonians of even bigger lattices than that of super-block range- r is needed. For this purpose finite cluster method will be used.

The basic idea works as follows. After finding the single block range-1 contributions, the interaction hamiltonian between the r -connected blocks is to be found. As the renormalized hamiltonian is an extensive quantity, all the contributions from the super block range- r hamiltonian are subtracted except the needed one.

2.4 Finite Cluster Method

For an extensive quantity, the finite cluster method expresses this quantity in infinite volume in terms of finite-volume contribution, e.g., hamiltonian (energy) of the system. Consider an idea of finite cluster method applied to the lattice hamiltonian. First a sub-lattice consisting of block of microscopic lattice sites are made. Then one can make the sub-lattices of successively increasing sizes by connecting the sublattices made in the previous step called super sub-lattice range- r , where $r = 1, 2, 3, \dots, \infty$. The contribution of each of the super sub-lattice range- r is evaluated. Thus the effective hamiltonian of the super sub-lattice (very large lattice up to ∞) can be made by adding up the contributions by all the range- r sub-lattices of the finite volume.

Considering a sub-lattice of r -connected blocks (B_1, \dots, B_r) , one can write the basic idea as

$$H_{tot} = \sum_{i=-\infty}^{\infty} \sum_{r=1}^{\infty} h_r(B_i, \dots, B_{i+r-1}) \quad (2.44)$$

where H_{tot} is the total energy of the infinite lattice as calculated by the Finite Cluster Method. Finite Cluster Method (FCM) is described in detail with applications in the references [20, 21, 22, 23]. Therefore one can use finite cluster method (FCM) to compute the renormalized hamiltonian H_r approximately and nonperturbatively to the desired accuracy i.e., range of the calculation r .

The renormalized hamiltonians by the CORE method are also extensive in nature. In the CORE method, the effects of the truncated states are incorporated to the hamiltonian operator, so the finite cluster method (FCM) can also be applied in relation to the CORE [17].

In the CORE algorithm perspective, the finite volume contribution upto the range- ∞ is not needed since the energy is converged for as low as for the range-2 contributions. The CORE algorithm is added by finite cluster method after each of the CORE iteration finding the range- r contributions. In this work, the contributions upto range-3 will be calculated.

1. First, compute the CORE renormalized hamiltonian for the single block of the sub-lattice. This renormalized hamiltonian can be denoted as

$$H_{ren}(B_i) = h_1(B_i) \quad (2.45)$$

This is called the range-1 term for the cluster expansion after the CORE renormalized transformation iteration.

2. In the next step, the CORE renormalized hamiltonian for the super block range-2, consisting of two connected blocks denoted by $H_{ren}(B_i, B_{i+1})$ is calculated. This renormalized hamiltonian $H_{ren}(B_i, B_{i+1})$ contains all the contributions to the cluster expansion upto the range-2. So

$$H_{ren}(B_i, B_{i+1}) = h_1(B_i) + h_1(B_{i+1}) + h_2(B_i, B_{i+1}) \quad (2.46)$$

The range-2 contribution $h_2(B_i, B_{i+1})$ is to be calculated from equation (2.46).

3. The range-3 contribution to the CORE renormalized hamiltonian can be calculated by finding the CORE renormalized hamiltonian of the super block range-3 consisting of three connected blocks of the sub-lattice $H_{ren}(B_i, B_{i+1}, B_{i+2})$. This renormalized hamiltonian contains all the contributions to the cluster expansion upto the range-3. So writing this explicitly

$$\begin{aligned}
H_{ren}(B_i, B_{i+1}) = & h_1(B_i) + h_1(B_{i+1}) + h_1(B_{i+2}) \\
& + h_2(B_i, B_{i+1}) + h_2(B_{i+1}, B_{i+2}) \\
& + h_3(B_i, B_{i+1}, B_{i+2})
\end{aligned} \tag{2.47}$$

Since the range-1 and range-2 contributions $h_1(B_i)$ and $h_2(B_i, B_{i+1})$ are already calculated so the range-3 contribution $h_3(B_i, B_{i+1}, B_{i+2})$ can be found from the equation (2.47).

After finding the range-1, range-2 and range-3 contribution as $h_1(B_i)$, $h_2(B_i, B_{i+1})$ and $h_3(B_{i+1}, B_{i+1}, B_{i+2})$, one can use equation (2.44) to find the renormalized hamiltonian for the renormalized lattice after any of the CORE iteration. It is to be noted that the finite cluster method can also be applied to any extensive operator ‘ O ’ in the same way to find the renormalized operator O_{ren} .

2.5 Conclusion

CORE is an important addition to the hamiltonian based techniques working on the Kadanoff-Wilson real-space renormalization group transformation. The is a non-perturbative method based on the cluster expansion and contraction techniques. It has many advantages over other real space renormalization methods. It has no fermion sign problem, therefore it is equally applicable to fermion and boson problems. The energy densities are also very easy to adjust with a simple addition of chemical potential in the hamiltonians. The original states in the microscopic lattice can be mapped onto very different states depending on the retained states. However the new renormalized hamiltonian incorporate the same low energy physics. The increasing CORE iterations give the renormalized hamiltonians with sufficiently thinned states for the renormalized sites.

The CORE applies the scaling from the Kadanoff-Wilson renormalization group to the Hamiltonian systems. In this method, a renormalized hamiltonian is found that acts on truncated basis set exactly producing the low energy states. This method has long range hamiltonian contributions which vanish fairly fast. These two virtues, to be able to truncate the subspace quite significantly and having kept only a few term in the long range interactions make this algorithm successful with a mediocre computational systems. The CORE algorithm can be described for a 1-dimensional lattice in a nutshell as follows:

First a single block of the lattice with index j is chosen. This simple block is exactly diagonalized, and a truncation is done for the eigen-states of this block keeping some of the lowest energy states that do not violate the degeneracy of the problem. A projector P_{r1} is made from the retained states of the single block and is used to find the range-1 contributions to the renormalized hamiltonian $h_1 = P_{r1}H_jP_{r1}$.

Then range- r term is calculated considering r -connected blocks forming super block range- r . A Hilbert space of the tensor product states of the retained states of r -connected blocks is made. The full hamiltonian of the connected blocks is also diagonalized for some of its low energy eigenstates. The eigen-states of the full hamiltonian are projected on the tensor product states and Gram-Schmidt orthonormalized in order to get a new basis of M^r states. Some of the exact eigenstates of super-block range- r have a vanishing projection with tensor product states or vanish during the orthonormalization procedure, therefore they are discarded. Therefore the full super-block range- r hamiltonian is diagonalized for more than M^r states to compensate for those lost states.

The super-block range- r renormalized hamiltonian can then be written as

$$H_{ren} = \sum_{n=1}^{M^r} \epsilon_n |\varrho_n\rangle\langle\varrho_n| \quad (2.48)$$

The range- r connected contributions h_r are found by subtracting all other contributions. The renormalized hamiltonian for any number of renormalized sites is given by

$$H_{ren} = \sum_{\langle i \rangle} h_i + \sum_{\langle ij \rangle} h_{ij} + \sum_{\langle ijk \rangle} h_{ijk} + \dots \quad (2.49)$$

It can be viewed as the transformation that transforms the microscopic hamiltonian H_o on the microscopic lattice to renormalized hamiltonian H_{ren} on coarser renormalized lattice . To extract the low energy physics, the CORE algorithm is applied repeatedly, starting from the microscopic hamiltonian, then using the renormalized hamiltonian after each of the CORE iterations, i.e., $H_1 = CRGT(H_o)$, $H_2 = CRGT(H_1)$, $H_3 = CRGT(H_2)$, \dots . Here CRGT stands for CORE renormalization group transformation. This iterated flow of hamiltonians using the CORE algorithm reaches a fix point, characterized by $CRGT(H^*) = H^*$. Thus the iterations by CORE transformations gives a sequence of renormalized hamiltonians, each with truncated subspace, but with the increasing equivalent microscopic sites. The result is in the very few states of the renormalized hamiltonian at the critical point resulting in the renormalized hamiltonian which is easy to exactly diagonalize.

The renormalized hamiltonian for sufficiently big lattice sizes can be found by iterating with the CORE algorithm to find the critical behaviour in accordance with the Kadanoff theory of the renormalization group. If CORE iterations is restricted to only 1st-iteration due to any reason like level-crossing then extrapolation or some other method like finite size scalings can be used with renormalized hamiltonians by CORE to find the critical behaviour.

In this way, the CORE method can be used numerically to study the critical behaviour and phase transitions.

Chapter 3

Ising Model in Transverse Magnetic Field

Ising Model with Transverse Magnetic Field, also called $(1 + 1)$ -dimensional Ising model, is the simplest of the models that shows the quantum phase transition at the zero temperature ($T = 0$) [28]. At ($T = 0$), the thermal fluctuations are frozen (vanish) and the only fluctuations possible will be that of the quantum fluctuations [32]. The external field is responsible for these fluctuations, bringing the quantum phase transition. In this chapter, the phase transition of the Ising model will be investigated using the CORE algorithm.

3.1 Ising Model in Transverse Field (*ITF*)

The hamiltonian of the spin- $\frac{1}{2}$, $(1 + 1)$ -dimensional, Ising model is given by

$$H = - \sum_{i=1}^{L-1} J \sigma_i^x \cdot \sigma_{i+1}^x - h \sum_{i=1}^L \sigma_i^z \quad (3.1)$$

where L is the number of lattice sites in the 1-dimensional chain. J is the nearest neighbour coupling between the spins in the x-direction. σ^x and σ^z are the Pauli matrices corresponding to the x-component and z-component of the spin- $\frac{1}{2}$ operators at site i . Because of $[\sigma^x, \sigma^z] \neq 0$ there are quantum fluctuations controlled by the parameter ratio $\frac{h}{J}$ [24].

There are several reasons that make spin- $\frac{1}{2}$, $(1 + 1)$ -dimensional, Ising model suitable to be investigated with CORE algorithm [17]. The most important reason is the phase transition, controlled by the parameter $\frac{h}{J}$. When there is no externally applied field $h = 0$, the Ising model is symmetric with two possible orientations of the Ising Spin corresponding to the two eigenvalues of $\sigma_j^x = +1, -1$ and the ground state of the Ising model will be two-fold degenerate. Introducing an externally applied transverse magnetic field changes this situation as it tries to break this symmetry. When $\frac{h}{J} > \left(\frac{h}{J}\right)_c$, the ground state of the system becomes unique [33].

This phase transition can be studied requiring multiple CORE iterations for each of the starting ratios h/J_x , giving renormalized hamiltonians for the renormalized lattices. The order parameter of this phase transition is the magnetization operator [17]. This allows to use the another capability of the CORE algorithm finding the renormalized operator with each of the CORE renormalized transformation iteration.

3.2 Phase Transitions and Critical Properties of the (1 + 1) Ising Model

The hamiltonian in equation (3.1) contains two terms J and h . If there is no external field, the spin will align ferromagnetically. So at $h = 0$, the system is in the ferromagnetic ground state. Similarly if $J = 0$, the system will be in a paramagnetic state. The ferromagnetic and paramagnetic states can be seen from another point of view. If one start from the ferromagnetic state $h = 0$, then start to increase the externally applied field h gradually. This results in the reduction of the magnetic order, induced by J term. This magnetic order will not completely vanish for some arbitrary small value of external magnetic field. Similarly if one starts from $J = 0$, the initial ground state of the system will be paramagnetic. Now spin interaction J is increased gradually, the paramagnetic ground state will not be destroyed completely for a small increase in the spin interaction energy. So there will two regimes based on the ground states. In the first regime $J \gg h$, the ground state of the Ising hamiltonian will be ferromagnetic whereas in the other regime $h \gg J$, the ground state of the Ising hamiltonian will be paramagnetic. These are the two quantitatively different ground states depending on the ratio of the input parameters $\frac{h}{J}$. So there will be quantum phase transition at some value of the parameters ratio $\frac{h}{J}$, called the critical coupling point $(\frac{h}{J})_c$ of this phase transition [35].

The two different phases in the transverse Ising model are characterized by the magnetization in their ground states. Therefore the best order parameter in this case will be the magnetization in the x-direction $M = \frac{1}{L} \sum_{i=1}^L \sigma_i^x$ [17]. The magnetization will have a finite value in the ferromagnetic phase while it will vanish in the paramagnetic regime. The CORE algorithm is able to determine the system properties at or near the critical point, characterized by infinite correlation length, simulating properties like magnetization, excitation gap etc. The behaviour of these properties can be determined by the evaluation of their respective critical exponents, which in turn give information about the universality class of the system.

The schematic phase diagram for the transverse Ising model is shown in the figure (3.1). The critical point characterizes the zero temperature phase transition from the ferromagnetic state to paramagnetic state. This unstable critical point also called the fix point occurs at some critical value $(\frac{h}{J})_c$.

If one starts at some of the single parameter $\frac{h}{J} \ll (\frac{h}{J})_c$, the system will become more and more ordered after each iteration, and goes towards the trivial fix point $\frac{h}{J} = 0$. On the other hand if one starts at some point $\frac{h}{J} \gg (\frac{h}{J})_c$, the system will become more and more disordered after each iteration and goes towards the other trivial fix point $\frac{h}{J} = \infty$ [35]. Only if one starts on exactly on the unstable critical fix point, the system remains on that point throughout the renormalization transformations. This is in analogy with the unstable equilibrium in classical mechanics that this point is also called as unstable fix point.

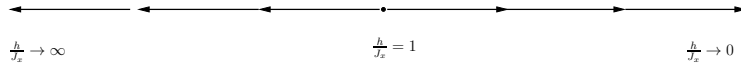


Figure 3.1: phase diagram of spin- $\frac{1}{2}$ (1 + 1)-dimensional Ising model

There is one-to-one correspondence between phase transition Ising model of the dimension “d” and that of the classical Ising model of the dimension “d+1” [34], so the critical exponents of the transverse Ising model in one dimension are the same as that of the classical Ising model in 2-dimensions analytically solved by Onsager [25] as given in the table (3.1).

There will be two methods to find the critical point of the phase transition with CORE

| Universality Class | Critical Exponents | | | | | | |
|--------------------|--------------------|---------------|---------------|----------|-------|---------------|-----|
| Classical Models | α | β | γ | δ | ν | η | z |
| Ising (2d) | 0 | $\frac{1}{8}$ | $\frac{7}{4}$ | 15 | 1 | $\frac{1}{4}$ | 1 |
| Ising (3d) | 0.10 | 0.33 | 1.24 | 4.8 | 0.63 | 0.04 | 1 |
| Heisenberg(2d) | -0.12 | 0.36 | 1.39 | 4.8 | 0.71 | 0.04 | 1 |

Table 3.1: critical exponents of different universality classes

algorithm undertaken in this chapter. The first method is based on extraction of renormalized parameters after each of the CORE iterations. In the second method, the order parameter of this phase transition, magnetization, will be used to find the critical point of this phase transition.

3.3 Renormalization Flow of Parameters of the Ising Model

The renormalized effective hamiltonian as obtained by CORE algorithm can be written as [17]

$$\hat{H}_{ren} = -J_x \hat{\sigma}_1^x \hat{\sigma}_2^x - J_y \hat{\sigma}_1^y \hat{\sigma}_2^y - J_z \hat{\sigma}_1^z \hat{\sigma}_2^z - h (\hat{\sigma}_1^z + \hat{\sigma}_2^z) + C \quad (3.2)$$

The equation (3.2) may contain some of the new terms (parameters J_y, J_z) fulfilling the symmetry requirements of the original model plus a constant [17]. This shows the difference between CORE and the naive renormalization group transformation. There will be no additional parameters in the renormalized hamiltonian found by naive RSRG except for those found in the original model. But in case of the renormalized hamiltonians as found by CORE, the additional parameters come into play describing the more complete picture at the increasing lattice lengths.

One can find the renormalized parameters h and J_x by simple manipulation of equation (3.2) [37]

$$-J_x = \frac{1}{Tr(\sigma^{xx} \sigma^{xx})} Tr(\sigma^{xx} H_{ren}) \quad (3.3)$$

$$-h = \frac{1}{Tr(\sigma_{tot}^z \sigma_{tot}^z)} Tr(\sigma_{tot}^z H_{ren}) \quad (3.4)$$

One can denote J as J_x , which distinguish J_x from the other renormalized parameters, like $\{J_y, J_z\}$.

This is in contrast to the unstable fix point, where the starting parameters do not change with the increasing CORE iterations. So for finding the fix point by the CORE algorithm, the evolution of $\frac{h}{J_x}$ is still important. This ratio can be obtained by finding the evolution of the individual parameters like h and J_x .

The equations (3.3,3.4) for the renormalized parameters are obtained, for the case, in which the renormalized hamiltonian keeps the form of the original hamiltonian. It means that after each of the CORE transformation iteration, a single renormalized site have the same number of states as that of the microscopic site of the starting hamiltonian. This is achieved by retaining the same number of lowest eigen vectors in the single block hamiltonian, as that of the number of states in the original microscopic site of the lattice [36]. It means that in the case of Ising model, one has to keep two states per single block at each new CORE renormalization transformation iterations. This results in the renormalized lattice low energy hamiltonian that is of the same form as that of the original hamiltonian.

Away from the critical point, the controlling parameter $\frac{h}{J_x}$ will keep on changing after each of the CORE renormalization transformation iteration until the system reaches to one of its fix point. At the critical point there will be no change on the controlling parameter $\frac{h}{J_x}$ with the increasing CORE renormalization transformations.

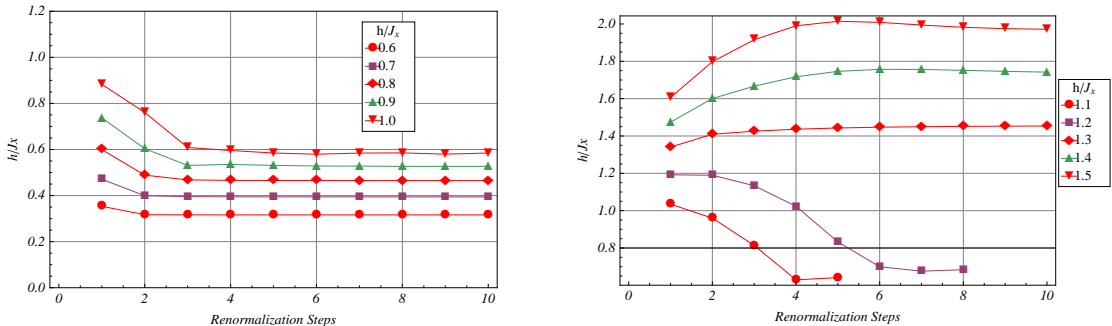
In order to illustrate the parameters going to one of the fix points by the CORE algorithm, one can take a small sub-lattice single block to illustrate the flow of parameters to one of the fix points, otherwise in the case of big sub-lattice single blocks taken with the CORE algorithm, the parameter will be flowing too fast to one of its fix points so that one can only plot for only a few CORE renormalization transformation iterations before the parameters flow to one of its the fix point.

3.3.1 Extraction of Parameters from range-2 simulations

For capturing of the renormalization flow of parameters from the renormalized Ising hamiltonian, one can implement CORE algorithm with two site single blocks with two retained states at range-2. The CORE renormalized hamiltonians are simulated for the first ten CORE renormalized transformation iterations. The renormalized hamiltonian, after each of the CORE renormalized transformation will be made of two renormalized sites. In case of CORE range-2 simulations, the CORE approximation errors will have a major contribution in each of the iteration. Due to the nature of the system going to one of its two trivial fix points depending on the starting ratio of the controlling parameter $\frac{h}{J_x}$, the critical point can be determined from these curves.

The plot (3.2a) show that the renormalized ratio h/J_x is attracted towards the trivial fix point $h/J_x = 0$. After reaching the trivial fix point $h/J_x = 0$, there will be no further change in the ratio h/J_x with the increasing CORE iterations. It should be noted that for the first ten CORE transformation iterations, the renormalized hamiltonian corresponds to the microscopic sites $\{4, 8, 16, 32, 64, 128, 256, 512, 1024, 2048\}$, starting to show the behaviour at the thermodynamics limit.

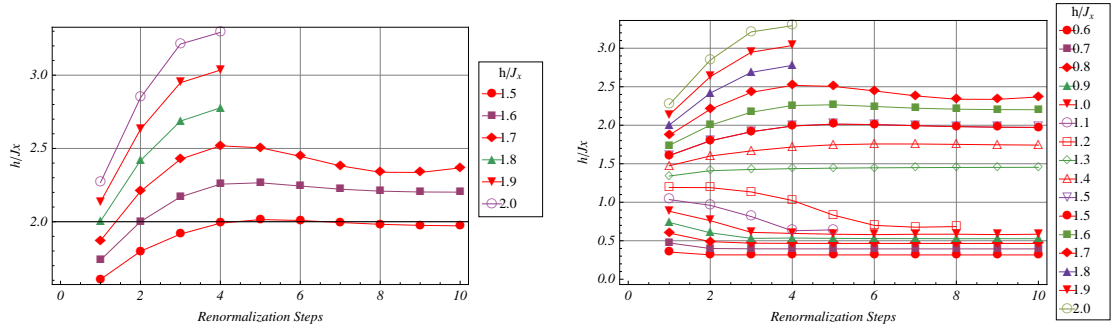
The plot (3.3a) shows that the renormalized ratios h/J_x is going towards the other fix point $h/J_x \rightarrow \infty$ for all the starting ratios greater than 1.3.



(a) The evolution of the renormalized parameter ratio $\frac{h}{J_x}$ for the starting parameter of $\frac{h}{J_x} = \{0.6, 0.7, 0.8, 0.9, 1.0\}$ with each of the CORE renormalization step. (b) The evolution of the renormalized parameter ratio $\frac{h}{J_x}$ for the starting fraction of $\frac{h}{J_x} = \{1.1, 1.2, 1.3, 1.4, 1.5\}$ with each of the CORE renormalization step.

Figure 3.2: Evolution of the renormalized parameter ratio $\frac{h}{J_x}$ with CORE simulations at range-2.

In the plot (3.2b), the critical point appears to be between the starting value of $h/J_x = \{1.2\}$ and $h/J_x = \{1.3\}$, which is away from the actual value of critical point $h/J_x = \{1.0\}$. Considering



(a) The evolution of the renormalized parameter ratio $\frac{h}{J_x}$ for the starting fraction of $\frac{h}{J_x} = \frac{h}{J_x}$ for all the starting simulated starting ratio. $\{1.5, 1.6, 1.7, 1.8, 1.9, 2.0\}$ with each of the CORE renormalization step.

(b) The evolution of the renormalized parameter ratio $\frac{h}{J_x}$ for all the starting simulated starting ratio. $\{0.6, 0.7, 0.8, 0.9, 1.0, 1.1, 1.2, 1.3, 1.4, 1.5, 1.6, 1.7, 1.8, 1.9, 2.0\}$ with each of the CORE renormalization step.

Figure 3.3: Evolution of the renormalized parameter ratio $\frac{h}{J_x}$ with CORE simulations at range-2.

the range-2 simulations with the smallest single block configuration of two sites, this is not a bad estimate for the critical point. For a good estimate of critical point, the simulations can be improved by selecting feasible options (big single blocks, more retained states and improving range of simulations) for the CORE algorithm.

3.3.2 Extraction of Parameters from range-3 calculations

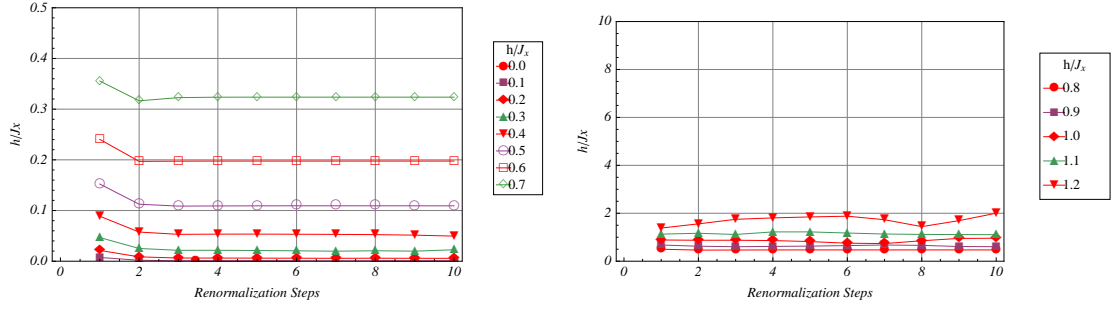
The CORE range-2 simulations did not give a good results for the critical point. To improve the results, one can switch to range-3 simulations. In these simulations a single block of three single sites is chosen with two retained states. For range-3 simulations, it is not recommended to make single block of less than three sites. The renormalized hamiltonians at range-3 are made from three renormalized sites after each of the CORE renormalized iteration. The first ten iterations with this geometry corresponds to the microscopic sites $\{9, 27, 81, 243, 729, 2187, 6561, 19683, 59049, 177147\}$ approaching the thermodynamics limit behaviour much earlier than CORE range-2 simulations.

From the plot (3.4b), one can see that extracted parameter h/J_x remains constant for the starting ratio of $h/J_x = 1.1$, close to the exact value $(h/J_x)_c = 1.0$. More exactly speaking, the critical point from range-3 simulations will be somewhere between $h/J_x = 1$ and $h/J_x = 1.1$. The exact value of the starting parameter can be found with bi-section method. The range-3 simulations show a big improvement of the results over the range-2 simulations. But since, the result is already close to the exact value so one can move on to other methods for finding the critical point.

Here the evolution of the renormalization flow spectrum with h/J_x will be discussed against the renormalization steps. In the region $\frac{h}{J_x} < \left(\frac{h}{J_x}\right)_c$, the renormalized controlling parameter $\frac{h}{J_x}$ decays from the starting value and remains constant to a converged value close to zero which is specific to each of the starting ratio.

The behaviour of the renormalization flow of the controlling parameter $\frac{h}{J_x}$ remains constant to the starting value within the range, which is close to the critical point. The critical point also lies within this range. This behaviour is shown in the (3.4b).

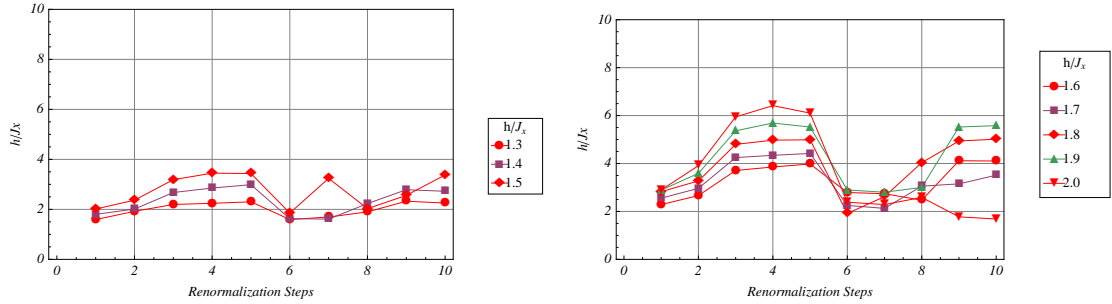
As the starting regime goes towards the regime $\frac{h}{J_x} > \left(\frac{h}{J_x}\right)_c$, the renormalization flow of the



(a) The evolution of $\frac{h}{J_x}$ for the starting parameter of $\frac{h}{J_x} < \left(\frac{h}{J_x}\right)_c$ with each of the CORE iterations. (b) The evolution of $\frac{h}{J_x}$ for the starting parameter of $\frac{h}{J_x} \approx \left(\frac{h}{J_x}\right)_c$ with each of the CORE iterations.

Figure 3.4: Evolution of $\frac{h}{J_x}$ with CORE renormalization transformation iterations at range-3.

parameter $\frac{h}{J_x}$ start to change its constant behaviour going towards the other direction as shown in the figure (3.5). This is very novel behaviour as the renormalization behaviour is going in both the directions increasing, then decreasing. The exact values are controlled by the value of the starting parameters.



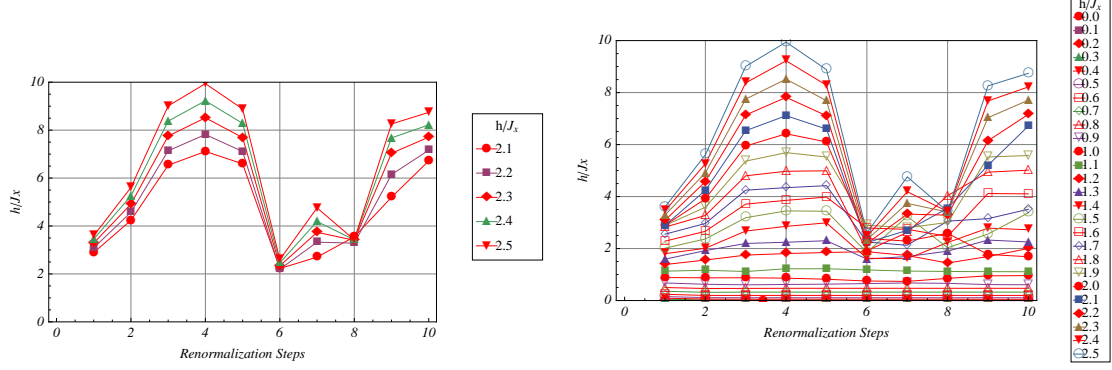
(a) The evolution of $\frac{h}{J_x}$ for the starting parameter of $\frac{h}{J_x} > \left(\frac{h}{J_x}\right)_c$ with each of the CORE iterations. (b) The evolution of $\frac{h}{J_x}$ for the starting parameter of $\frac{h}{J_x} \gg \left(\frac{h}{J_x}\right)_c$ with each of the CORE iterations.

Figure 3.5: Evolution of $\frac{h}{J_x}$ with CORE renormalization transformation iterations at range-3.

As one goes far away from the critical point, this zigzag behaviour is far more elaborated. Each curve have its own course for this zigzag behaviour, but the point of maximum depression is generally common. This behaviour is shown in the plot (3.6a). The CORE results with increasing iterations did not remain as accurate, therefore the data from first ten iterations is shown, otherwise this elaborated zigzag behaviour upto fifteen CORE iterations is seen.

In the last plot (3.6b), the renormalization flow curves for all the starting parameters are shown. This is a complex behaviour in contrast to other techniques, where a single line curve is showing the renormalization flow diagram as shown in figure (3.1). So for the starting regime $\frac{h}{J_x} < \left(\frac{h}{J_x}\right)_c$, the renormalization flow of $\frac{h}{J_x}$ goes to fix point, the value of which depend on the starting ratio. The critical point is found at $\left(\frac{h}{J_x}\right)_c = 1.1$. For the starting regime $\frac{h}{J_x} >$

$\left(\frac{h}{J_x}\right)_c$, a zigzag behaviour is shown with the point of constant depression. Therefore CORE does not predict a fix point in this regime, or at least with the parameters taken for these CORE simulations.

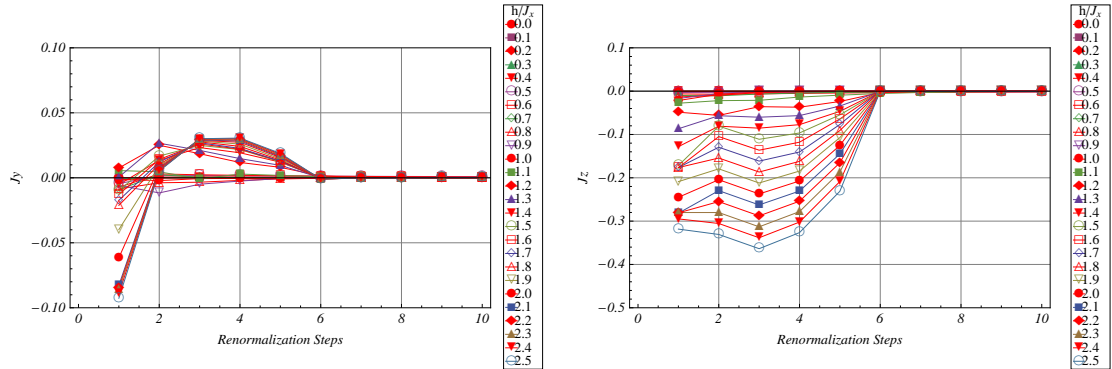


(a) The evolution of $\frac{h}{J_x}$ for the starting parameter of $\frac{h}{J_x} \gg \left(\frac{h}{J_x}\right)_c$ with each of the CORE iterations. (b) The evolution of $\frac{h}{J_x}$ for all the starting parameter with each of the CORE iterations.

Figure 3.6: Evolution of $\frac{h}{J_x}$ with CORE renormalization transformation iterations at range-3.

Comparing Results of RSRG and CORE

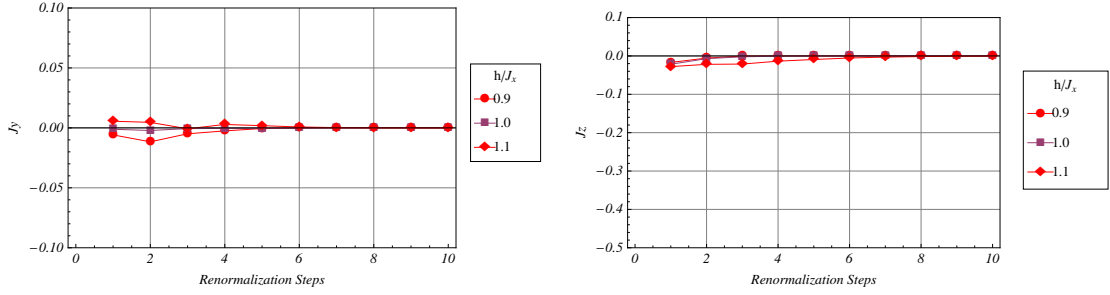
In the naive RSRG, $\frac{h}{J_x}$ is the only controlling parameter for the renormalization flow of the Ising model to one of its fix points. Therefore the evolution of the ratio $\frac{h}{J_x}$ is mainly responsible for the renormalization flow in the naive RSRG. But the situation is much more complex in the case of the CORE algorithm, since there is also evolution of parameters J_y and J_z , which are part of the renormalized hamiltonians but were not part of the starting hamiltonians after each of the CORE iteration as shown by the equation (3.2). So the phase diagram by CORE method is different from the phase diagram by the real space renormalization group.



(a) The evolution of J_y for the spectrum of starting parameters with CORE iterations. (b) The evolution of J_z for all the starting parameters $\frac{h}{J_x}$ as given in the legend.

Figure 3.7: Evolution of J_y and J_z with CORE renormalization transformation iterations.

3.4. EVALUATION OF THE RENORMALIZED MAGNETIZATION OPERATOR IN $(1 + 1)$ ISING MODEL



(a) The evolution of J_y for the starting parameters close to the critical point (b) The evolution of J_z for the starting parameters close to the critical point

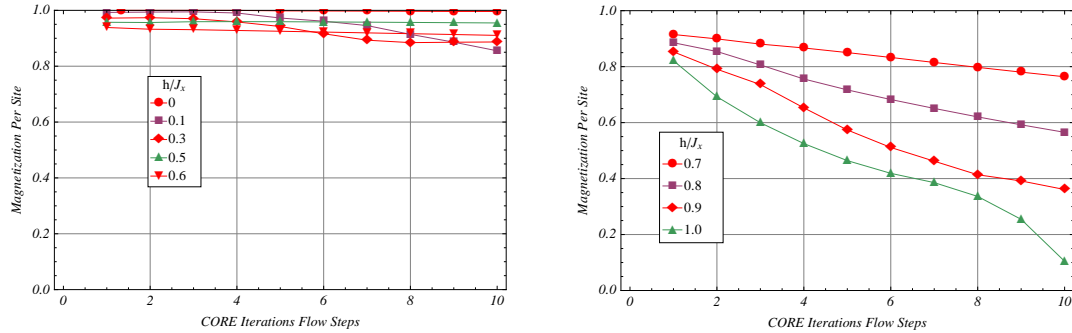
Figure 3.8: Evolution of J_y and J_z with CORE renormalization transformation iterations close to the critical point

The plots (3.8), show the evolution of the renormalized parameters J_y and J_z close to the critical point. It shows close to the critical point the renormalization parameters J_y and J_z remains zero corresponding to their values in the starting hamiltonians. So the critical point of the phase transition can be studied with the evolution of the renormalized parameter $\frac{h}{J_x}$.

3.4 Evaluation of the Renormalized Magnetization Operator in $(1 + 1)$ Ising Model

The evolution of magnetization operator with the increasing CORE iterations will serve as the pre-requisite in the latter sections. The renormalized magnetization operator after each of the CORE iteration along with the renormalized hamiltonian is found by applying the CORE algorithm. After each of the CORE transformation iterations, there will be range-1, range-2 and range-3 operators m_1 , m_2 and m_3 analogously to the h_1 , h_2 and h_3 hamiltonians respectively.

In the plot (3.9a), away from the critical point, the magnetization remains the same with the increasing CORE iterations for the starting parameter $\frac{h}{J_x}$.

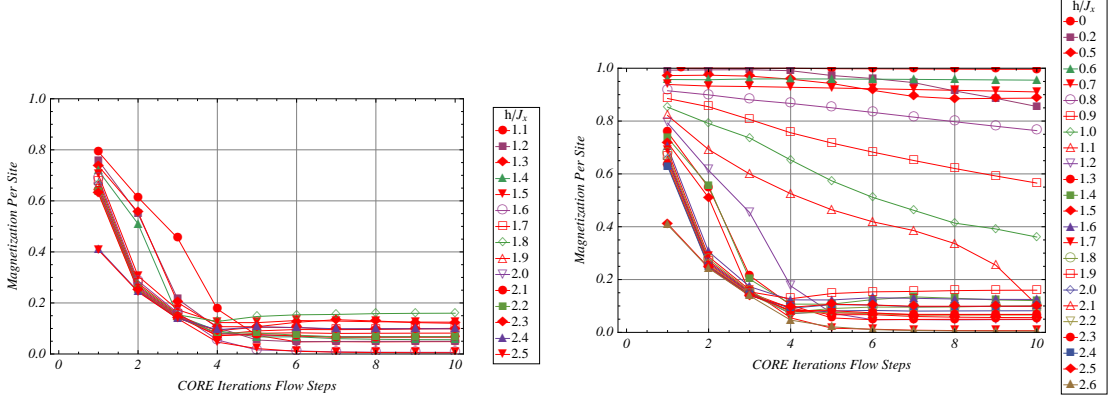


(a) The evolution of magnetization in Ising(1+1) model with CORE transformation iterations. The starting ratio or near the critical point. is in ferromagnetic regime. (b) The evolution of the magnetization in Ising(1+1) at

Figure 3.9: Plots of magnetization of $(1+1)$ -Ising model for various starting parameters

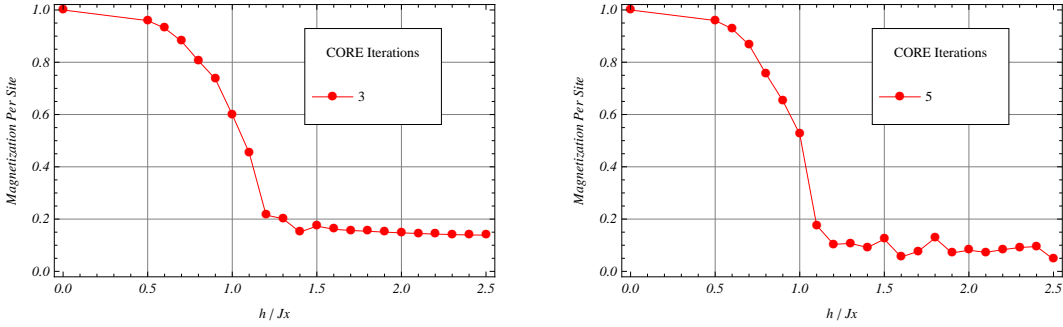
3.4. EVALUATION OF THE RENORMALIZED MAGNETIZATION OPERATOR IN $(1+1)$ ISING MODEL

In the plot 3.10a, after the critical point, $\frac{h}{J_x} > \left(\frac{h}{J_x}\right)_c$. The ordered state has been changed into disordered state with the vanishing of the magnetization.



(a) The evolution of the magnetization in Ising(1+1) in the paramagnetic regime. (b) The evolution of the magnetization for all the starting parameters.

Figure 3.10: Plots of magnetization of $(1+1)$ -Ising model for various starting parameters



(a) The magnetization after convergence for the various starting parameters. The magnetization is calculated for three renormalized sites after the three CORE transformation for a total microscopic sites of 81. (b) The magnetization after convergence for the various starting parameters. The magnetization is calculated for three renormalized sites after the four CORE transformation for a total microscopic sites of 243

Figure 3.11: Evolution of $\frac{h}{J_x}$ with CORE renormalization transformation iterations at range-3.

For all these plots, the expectation value of magnetization operator is calculated. The ground state of the Ising model in the regime $\left(\frac{h}{J_x}\right)_c < \frac{h}{J_x}$ is two fold degenerate, so the magnetization operator matrix is made using these two degenerate states. The eigen values of this magnetization matrix will be the expectation value of the magnetization of the Ising model. The magnetization operator eigenvalues in the regime $\left(\frac{h}{J_x}\right)_c < \frac{h}{J_x}$ can be specified by $\pm m$ and one can take m as the expectation value. It is the method used to calculate the expectation values for the magnetization in all the regimes.

For finding the critical exponents of the magnetization, the converged magnetization per site is plotted with that of the starting parameters $\frac{h}{J_x}$. Since magnetization is also the order parameter

ter of the spin- $\frac{1}{2}$ $(1 + 1)$ Ising model, this plot also gives the critical point of phase transition. At increasing CORE iterations, there will be more sharp curve of the magnetization i.e., the order parameter. This behaviour is plotted in (3.11), for CORE renormalized transformation iteration three and four. These plot give of evidence of critical point being 1, since after $\frac{h}{J_x} = 1$, there is a vanishing magnetization. To find the critical exponents, one has to go for more CORE renormalized iterations to get magnetization converged. Since this approach has already been used in [17], a different approach for finding these two quantities will be undertaken. The objective was to demonstrate the evolution of the renormalized operator along with the renormalized hamiltonian with the increasing CORE iterations, and finding the expectation value. This renormalized magnetization operator will serve as the basics for finding the critical point and critical exponents using a different approach, namely, finite size scalings.

Prior to going forward, the results in the reference [17], for the $(1 + 1)$ -Ising model can be discussed in detail. The CORE simulations are done by taking three sites per single block with two retained states. The approach was to apply multiple iterations of CORE algorithm finding the renormalized hamiltonian at each of the iteration. From these renormalized hamiltonians, the bulk limit energy density, mass gap and converged value of magnetization per site were calculated. The plots were made corresponding to the starting ratio $\frac{h}{J_x}$ from zero to ∞ . For the bulk energy density, the CORE estimates follow the exact results, except for the starting parameters ratio near the critical point. From $\frac{h}{J_x} = 0.3$ to $\frac{h}{J_x} = 3.0$, there is a fractional error between the CORE estimates and that of the exact results of the order of 10^{-4} at its maximum. The behaviour is something like bell curve with fractional error dropping to 10^{-3} at the critical point. For mass gap, the CORE estimates exactly overlap the exact results in the paramagnetic regime from $\frac{h}{J_x} = 1.0$ to $\frac{h}{J_x} = \infty$. In the ferromagnetic regime, there is some very little deviation close to the critical point. Two methods were used to extract the critical coupling and the critical exponent of the magnetization. In the first method, where the prior knowledge of the critical coupling is not used, the critical coupling is found at the point $\frac{h}{J_x} = 0.9885$ and the critical exponent of magnetization β between 0.01 and 0.11, where the exact value of critical coupling is $\frac{h}{J_x} = 1.0$ and that of the critical exponent of magnetization $\beta = 0.125$. This discrepancy can be seen on log of the magnetization fitting curve. This discrepancy can be removed by trying different values of the critical couplings for obtaining the best fit resulting in the critical coupling at $\frac{h}{J_x} = 1.0063$ and the critical exponent of the magnetization between 0.1236 and 0.126. This led the authors to conclude that for a system with unknown solution, to be treated with CORE method, 1% of the error can be supposed due to the accumulation of the numerical errors during the CORE iterations and the limited range of calculations upto the range-3.

3.5 Critical Exponents using the CORE Algorithm

The CORE algorithm gives the liberty of choosing different approaches for finding the critical exponents. Although the CORE algorithm is designed to study the critical behaviour of a system, where the correlation length is infinite, it also gives equally good results for the mediocre size lattice systems. For small lattice sizes there are other techniques available, like exact diagonalization, lanczos method of finding the lowest eigen values and eigen vectors. Sometimes going for big lattice sizes, where the infinite behaviour sets in, give some additional difficulties for CORE simulations. For example, the low energy eigen values and eigenvectors should be accurate enough, so that the CORE algorithm can be iterated many times. Then there is a issue with accumulated numerical and approximation errors. Although these issues can be addressed, but with mediocre computational resources. To gain an insight in the working of the CORE algorithm, two approaches based on mediocre lattice sizes and big lattice sizes will be used to

find the critical exponents.

In the first approach, incorporating mediocre lattice sizes, will be based on the finite size scaling, implemented and evaluated by CORE algorithm. The advantage of using finite size scaling is that one can get accurate results, even by using only a few CORE transformation iterations. One can use finite size scaling to find the critical exponents with nominal computational resources.

The second approach is based on the conventional use of iterations of CORE renormalization transformations to find the critical exponent.

3.6 Critical Exponents Using Finite Size Scaling

Finite size scaling is the standard technique used to study the critical phenomena. At the critical point, the correlation length of the system diverges so the lattice length “L” becomes a relevant quantity. The scaling functions describing the relevant thermodynamic quantities incorporate lattice length of the quantum system. The magnetization from finite size scaling can be written as [24]

$$\mathcal{M}_L(t) = L^{-\frac{\beta}{\nu}} \tilde{\mathcal{M}} \left[\left\{ \frac{h}{J_x} - \left(\frac{h}{J_x} \right)_c \right\} L^{\frac{1}{\nu}} \right] \quad (3.5)$$

where β and ν are the critical exponents of magnetization and the correlation length. The singular behaviour of the magnetization can be described by $\mathcal{M}_L \sim \left[\frac{h}{J_x} - \left(\frac{h}{J_x} \right)_c \right]^\beta$ for the ferromagnetic regime $\frac{h}{J_x} \leq \left(\frac{h}{J_x} \right)_c$. The singular behaviour of the correlation length is given by $\xi \sim \left| \frac{h}{J_x} - \left(\frac{h}{J_x} \right)_c \right|^\nu$. The quantity \mathcal{M}_L is the average magnetization also called the expectation value of the magnetization operator and $\tilde{\mathcal{M}}$ is called the scaling function.

These critical exponents of correlation length ν and magnetization β will be found using finite size scaling technique. The simulations will be done at CORE algorithm at range-3.

3.6.1 CORE Algorithm and Finite Size Scaling

One can use the hamiltonian equation (3.1) and the magnetization operator as the starting point of the CORE algorithm. The single block is taken of three sites and the CORE algorithm will be applied at range-3. There will be two lowest energy retained states. For finite size scaling, three CORE iterations will be enough.

First of all, the reason for using CORE algorithm with finite size scalings will be described. The available computational resources allow to diagonalize a hamiltonian matrix of 18 sites with 2 states per site, i.e., the dimensions of $2^{18} = 262144$ for low energy eigen values and eigen vectors. For hamiltonians, not so much sparse, even this dimension is not feasible as it will need a good amount of time to diagonalize. By using only the three iterations of the CORE simulations, one is able to find the low energy hamiltonians from 21 microscopic sites to 270 microscopic sites, well above the computational limits of the available resources.

The average magnetization is plotted against the controlling parameter $\frac{h}{J_x}$ for various system sizes as shown in the figure (3.12) using the 1st CORE iteration. From this figure, it can be seen that as the phase transition controlling parameter $\frac{h}{J_x}$ is increased, there will be a phase transition from the ordered phase of the ferromagnetic regime to the disordered phase of the paramagnetic regime. The second-order phase transition shows a singular behaviour in the thermodynamic limit, so with the increasing system size, the phase transition curve will be more sharp at the

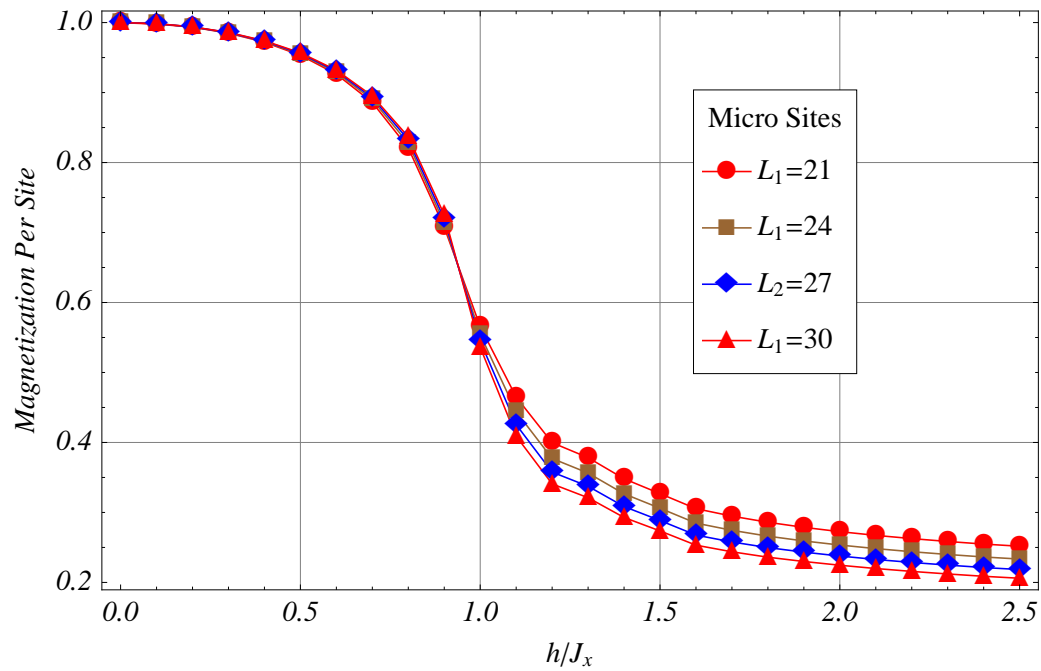
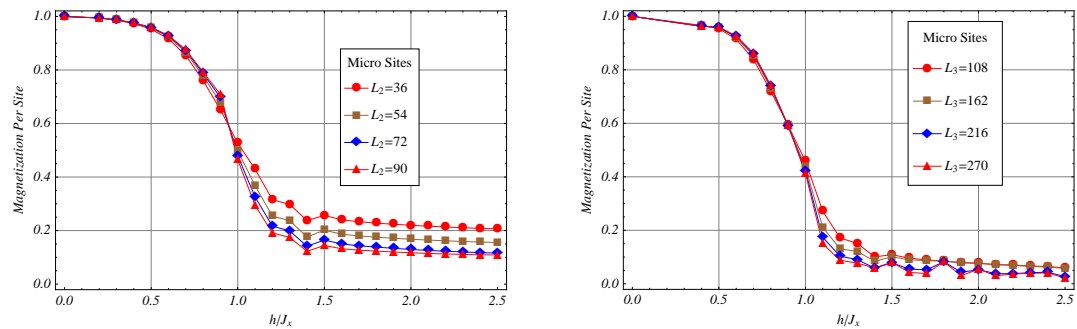


Figure 3.12: Average Magnetization for different site lattices in relation to the starting parameter $\frac{h}{J_x}$ using only the first CORE iteration.



(a) The average magnetization in Ising-(1+1) for different lattice sizes using the CORE 2^{nd} iteration.

(b) The average magnetization in Ising-(1+1) for different lattice sizes using the CORE 3^{rd} iteration.

Figure 3.13: Plots of magnetization of (1+1)-Ising model for various starting parameters using CORE 2^{nd} and 3^{rd} iteration.

phase transition point. It can also be seen from the figure that this phase transition occurs precisely at the point $\frac{h}{J_x} = 0.95$. There can be some finite size effects while using only the 1st iteration. These finite size effects can be nullified by going to higher iterations. Upto 3rd CORE iteration, one can see the evidence of critical point being equal to $\frac{h}{J_x} = 0.95$.

In the next step, the critical exponents of the magnetization β and that of the correlation length ν is to be determined. For this purpose one can use the equation (3.5). One can re-write the equation (3.5) as

$$\mathcal{M}_L(t) L^{\frac{\beta}{\nu}} = \tilde{\mathcal{M}} \left[\left\{ \frac{h}{J_x} - \left(\frac{h}{J_x} \right)_c \right\} L^{\frac{1}{\nu}} \right] \quad (3.6)$$

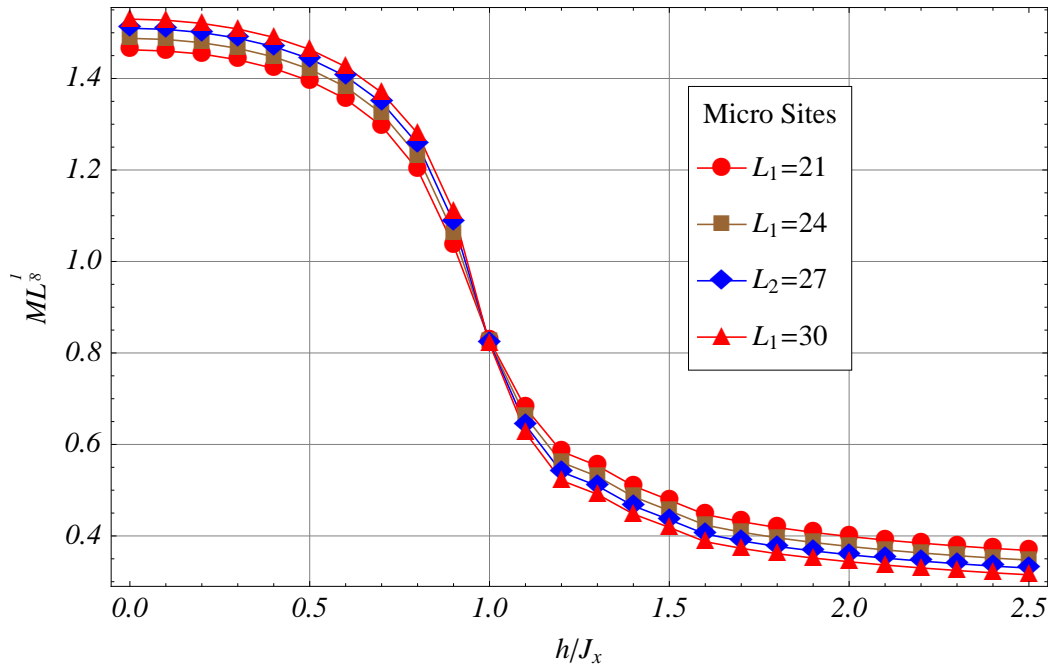
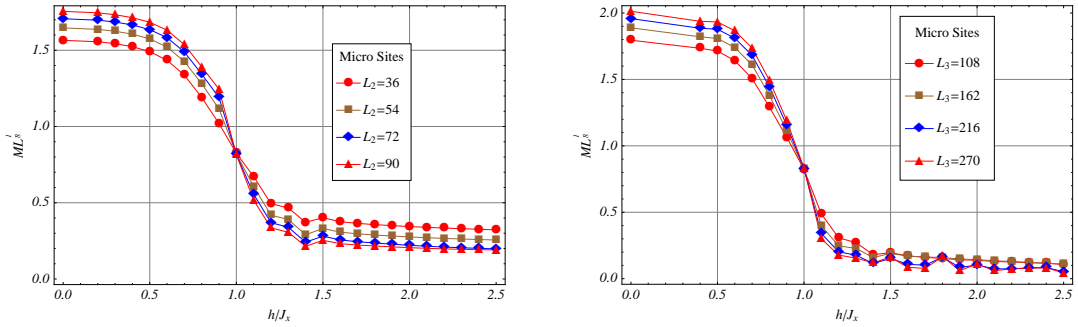


Figure 3.14: The crossing of the scaling parameter $mL^{\frac{1}{8}}$, in relation to the starting parameter $\frac{h}{J_x}$ for the 1st CORE iteration.

Now one will be plotting $\mathcal{M}_L(t) L^{\frac{\beta}{\nu}}$ with respect to the controlling parameter $\frac{h}{J_x}$. To plot these quantities, one need to know the values for the critical exponent of magnetization β and that of the correlation length ν . One can try a range of these values. The problem here is that there is a ratio between the two exponents β and ν in the equation 3.6. So at the best, one can only find the ratios between the two exponents from this plot. For a perfect match, the quantity $\mathcal{M}_L(t) L^{\frac{\beta}{\nu}}$ will have a perfect cross at the critical point $\frac{h}{J_x} = 1$ at different length scales. The perfect cross will be at the exact critical point $\left(\frac{h}{J_x} \right)_c = 1$. By experimenting with different values, a perfect match is found with the values $\frac{\beta}{\nu} = \frac{1}{8}$. So by using CORE simulations, one finds the ratio between the critical exponent for the magnetization and that of the critical



(a) The crossing of the scaling parameter $mL^{\frac{1}{8}}$, in relation to the starting parameter $\frac{h}{J_x}$ using the 2^{nd} CORE iteration. (b) The crossing of the scaling parameter $mL^{\frac{1}{8}}$, in relation to the starting parameter $\frac{h}{J_x}$ using the 3^{rd} CORE iteration.

Figure 3.15: Plots of the scaling parameter $mL^{\frac{1}{8}}$, in relation to the starting parameter $\frac{h}{J_x}$ using the 2^{nd} and 3^{rd} CORE iteration.

exponent for the correlation length

$$\frac{\beta}{\nu} = \frac{1}{8} \quad (3.7)$$

In the next step, the critical exponent for the correlation length will be determined using the CORE simulations.

3.6.2 Critical Exponent of the Correlation Length ν

To this point, there are many known results. The exact value of the critical point of the phase transition is $\left(\frac{h}{J_x}\right)_c = 1$. The ratio between the critical exponents magnetization to that of the correlation length is $\frac{\beta}{\nu} = \frac{1}{8}$. One re-consider the equation (3.6) and plot the quantity $\mathcal{M}_L(t) L^{\frac{\beta}{\nu}}$ with that of the $\left\{\frac{h}{J_x} - \left(\frac{h}{J_x}\right)_c\right\} \times L^{\frac{1}{\nu}}$. Now, there is only one unknown quantity, the critical exponent for the correlation length ν . So one can experiment with different values for the critical exponent of the correlation length. The plot will collapse to the universal scaling curve for the correct value of the critical exponent of the correlation length. The best collapse is seen for the value of correlation length to be $\nu = 1$.

So the critical exponent of the correlation length of the spin- $\frac{1}{2}$, $(1 + 1)$ -dimensional Ising model will be

$$\nu = 1 \quad (3.8)$$

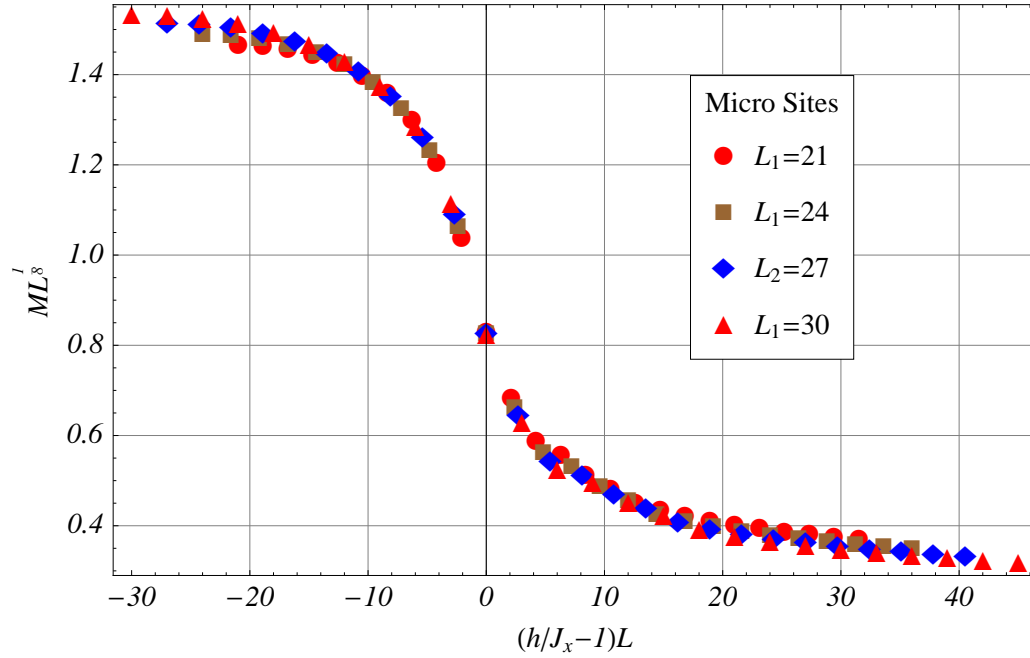
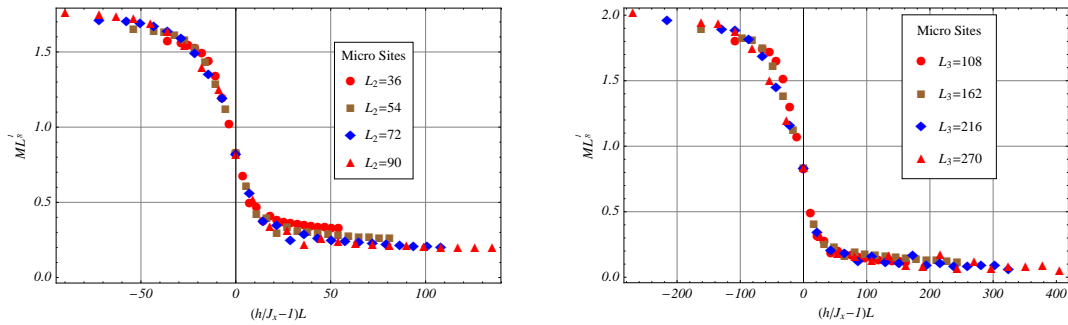


Figure 3.16: the best collapse on the universal curve gives the critical exponents of $\nu = 1$ for the CORE 1st-iteration



(a) the best collapse on the universal curve gives the critical exponents of $\nu = 1$ for the CORE 2nd-iteration (b) the best collapse on the universal curve gives the critical exponents of $\nu = 1$ for the CORE 3rd-iteration

Figure 3.17: The collapse on the universal curve for the critical exponents of correlation length $\nu = 1$ for the CORE 2nd- and 3rd-iteration

3.6.3 Critical Exponent of Magnetization β

From the equation 3.7, the critical exponent of the magnetization of the spin- $\frac{1}{2}$, $(1+1)$ -dimensional Ising model will be

$$\beta = \frac{1}{8} \quad (3.9)$$

For finding the accuracy of the critical exponents of magnetization β and correlation length ν , the plot (3.16) is plotted by varying the values of critical exponents. It is seen that as soon as correlation length is changed by a value of 0.02, the collapse curve is no longer there. Therefore the critical exponent of correlation length can be seen as 1 ± 0.01 . Similarly, the critical exponent of magnetization can be seen as 0.12 ± 0.01

3.7 Dynamical Critical Exponent z

Till now, the critical exponents are found by using mediocre size lattices by using only a few CORE iterations. In case of finding the dynamical critical exponent for the gap, one has to go for large number of CORE iterations at the critical point, thus testing CORE algorithm for large lattices.

The dynamical critical exponent describes the behaviour of the energy scales with that of the length scales close to the critical point. It can be described as

$$\Delta_s \propto y^{-z} \quad (3.10)$$

where Δ_s is the characteristic energy of the system. y denotes the characteristic length of the system, which is smaller between the correlation length and the system size. z is the dynamical critical exponent of the energy scales. For the Ising model in 1-dimension, the system is gapless in the ferromagnetic regime, while there is a gap in the paramagnetic regime, so the gap can be taken as characteristic energy scale. When CORE algorithm is used for the simulations, the system size is the total microscopic sites for which the hamiltonian is calculated. For 1-dimension it can be generally given as b^{I+1} , where I is the number of CORE renormalization iterations and b is the lattice sites per single block.

The transition in the energy scales (gap) happens close to the critical point. The correlation length at the critical point diverges. So one can say that close to the critical point, the system size is $b^{I+1} \leq \xi$, where ξ is the correlation length. Therefore $y = b^{I+1}$

$$b^{-z(I+1)} \propto \Delta_s \quad (3.11)$$

While using the CORE algorithm, there are some implementation points for finding the energy gap. There will be large number of CORE iterations needed to find the dynamical energy critical exponent, so one has to use shifting and scaling as given in the appendix (A) to carry out large number of CORE iterations. During the CORE iterations, all the hamiltonians h_1 , h_2 and h_3 are rescaled by dividing the energy by some specified value, so that the energy spectrum of the h_3 hamiltonian remains 1. After the desired number of CORE renormalized iterations, there will be no need to switch back the energy density as subtracted at each step, but there will be a need to undo the rescaling. For this purpose, one has to multiply the gap in the last step with all the scaling factors as documented for all the previous iterations. Mathematically it will be equivalent to

$$\Delta_s = \prod_{j=1}^{ren+1} \Delta_j^{sf} \quad (3.12)$$

where Δ_j^{sf} is the scaling factor of the CORE j th CORE iteration. Away from the critical point, these scaling factors keep on changing until the system reaches to one of the fix points. But close enough to the critical point, these scaling factors do not change significantly and so one can write

$$\Delta_s = \Delta^{I+1} \quad (3.13)$$

After some mathematical manipulation, one gets [32]

$$z = -\frac{\ln \Delta}{\ln b} \quad (3.14)$$

The z -exponent as given in eq. (3.14) is plotted against the renormalization steps. The eq. (3.14) is only valid at or near the critical point, which in the previous section is found to be $\frac{h}{J_x} = 1$. From the plot (3.18), it is seen that at the critical point, the dynamical gap exponent can be seen fluctuating around the value 1. This can be interpreted as the approximation $z = 1 \pm 0.1$, which matches the exact value of 1 found by theoretical methods. In the plot (3.18), *R.S.* stands for the renormalized sites. The simulations are carried out by taking three sites single block at range-3 with two retained states, but plots are made by making the renormalized hamiltonians for the renormalized sites $\{1, 2, 3, 4, 5, 6\}$, after each of the CORE renormalization iterations.

The result is quite good, keeping in view that it needed a large number of CORE iterations to be accomplished.

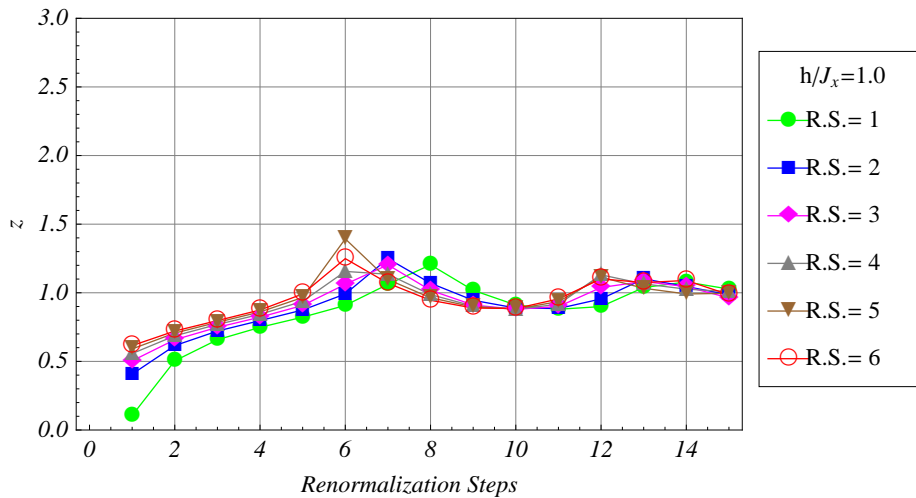


Figure 3.18: Dynamical gap critical exponent z at starting parameter $\frac{h}{J_x} = 1$ against the renormalization steps

3.8 Conclusion

The $(1 + 1)$ -Ising model with externally applied transverse field in one-dimension is investigated with CORE simulations. CORE simulations are done to study the quantum phase transitions at zero temperature. The controlling parameter of this quantum phase transition is $\frac{h}{J_x}$, where h is the externally applied magnetic field and J_x is the interaction between the spins in x -direction. There are two trivial fix points of the system, i.e., $\frac{h}{J_x} \rightarrow 0$ and $\frac{h}{J_x} \rightarrow \infty$. As the externally applied transverse field is varied in its strength, the system undergoes a quantum phase transition to one of these fix points. The phase transition is also seen in terms of the ratio of the extracted controlling parameters $\frac{h}{J_x}$ after each of the CORE iteration. These parameters are extracted at range-2 and range-3 CORE simulations. It is seen that the system is iterated to one the fix points depending on the starting ratio $\frac{h}{J_x}$. At the critical point, the correlation length is infinite and the system remain invariant with increasing CORE iterations. This critical behaviour is shown for the starting ratio of $\frac{h}{J_x} = 1.3$ for range-2 simulations and at $\frac{h}{J_x} = 1.1$ for the range-3 simulations, which is very close to the exact value of $\frac{h}{J_x} = 1.0$. The renormalization flow spectrum of parameter $\frac{h}{J_x}$ is also plotted, which is very different from those found at other techniques. No fix point is found for the range $\frac{h}{J_x} > \left(\frac{h}{J_x}\right)_c$, where the evolution of renormalized parameter $\frac{h}{J_x}$ shows zigzag behaviour along with the renormalization steps. The other parts of the renormalized spectrum generally agree with other techniques, except the fix point depends on the starting parameters. The reason for this mismatching is that there is contribution of more parameters during the iteration process obeying the symmetry of hamiltonian than that of the starting parameters.

To categorize the nature of quantum phase transition, the critical exponents of the transverse Ising model will be found. As the strength of the externally applied magnetic field is varied starting from zero to 2.5 for the simulations, there is a quantum phase transition from ordered ferromagnetic phase to disordered paramagnetic phase. The order parameter of this quantum phase transition is the magnetization in the direction of spin interaction. The renormalized magnetization operator is found along with the renormalized hamiltonians during the simulations after each of the CORE renormalized iterations. For $\frac{h}{J_x} < \left(\frac{h}{J_x}\right)_c$, there will be spontaneous magnetization. At $\frac{h}{J_x} > \left(\frac{h}{J_x}\right)_c$, this long range order (magnetization) vanishes.

The CORE algorithm gives us the liberty of choosing different approaches for finding the critical exponent. In the first approach CORE algorithm is iterated so that the lattice approaches to the thermodynamic limit. Some of the critical exponents, like critical exponent of magnetization β , based on this approach have already been calculated [17]. The dynamical critical exponent z is calculated by using this approach. The dynamical critical exponent is found to be $z = 1$ matching the exact result.

The other critical exponents for the transverse Ising model are found by using the finite size scaling technique. First of all, the critical point of the quantum phase transition of the transverse Ising model was found. The second-order phase transition shows a singular behaviour in the thermodynamic limit, so with the increasing system size, the magnetization (order parameter) curve will be more sharp at the phase transition point. This property is used by varying lengths with 1^{st} , 2^{nd} and 3^{rd} CORE iterations, which give 0.95 as the critical point of the phase transition. This is good result considering only three site single block with two retained states at range-3 simulations. At 5^{th} CORE iteration, the plots for different lattice lengths seem to converge as the results start to approach to the thermodynamics limits.

The finite size scaling does allow to find the critical exponents revealing phase transitions. These phase transition in principle can only be known in thermodynamics limits. From CORE

algorithm point of view, it also have advantages. There are accumulated approximation and numerical errors with the increasing iterations of the CORE algorithm. In spite of the fact, that the CORE algorithm is designed to work at or close to the critical point, it also gives good results for smaller lattice sizes for lower CORE iterations. For higher CORE iterations, one has to switch mediocre computational resources. For normal computational resources, finite size scaling with the CORE algorithm give very good results. Other techniques, suitable for working with finite size scaling (like exact diagonalization, lanczos methods) hardly fulfill the requirements even for small lattice sizes. By using CORE algorithm, one can find the low energy renormalized hamiltonian starting from small lattice sizes going upto the thermodynamics limits. The results for small lattice sizes on normal computational resources are more accurate. So one has the option of choosing the method based on the computational resources available. For finding the critical exponents in this work by the finite size scaling, lattice sizes from 21 sites to 270 were used. If the finite size scaling is used, one gets results comparable to the exact results by using the CORE algorithm with far less computational resources than needed by other techniques solving low energy hamiltonians of the same system sizes . The approximation for the critical exponent of the magnetization is found as $\beta = 0.12 \pm 0.01$ and that of the correlation length as $\nu = 1 \pm 0.01$.

Then CORE algorithm is also tested for finding the dynamical critical exponent for the energy gap in which going for a large number CORE iterations are necessary. The dynamical critical exponent approximation for the energy gap as found by CORE simulations is $z \approx 1 \pm 0.1$, compared to the the exact value of 1.

So the approximate critical exponents are found by CORE simulations by using both types of techniques, one needing large number of iterations and the other needing finite size scalings in which CORE simulations are done with only three iterations.

So the critical exponents for the correlation length, magnetization and dynamical energy scales (gap) of the 1D Ising model as found by using CORE simulations are in good approximation to the exact results.

Chapter 4

Critical Exponent (Energy Gap) of XXZ Model in Transverse Field

In low dimensional systems, the effect of the external magnetic fields is a subject of great interest in recent years. One can study the effects of the external magnetic field on the one dimensional spin- $\frac{1}{2}$ XXZ model [38]. CORE simulations will be used to study the effects of the external field on the low energy behaviour of the XXZ model. The hamiltonian of the 1-dimensional chain of XXZ-model can be written as

$$H = J \sum_{i=1}^L (S_i^x S_{i+1}^x + S_i^y S_{i+1}^y + \Delta S_i^z S_{i+1}^z - h S_i^x) \quad (4.1)$$

where L is the number of sites in the 1-dimensional chain. $J > 0$ is the antiferromagnetic exchange coupling in the xy-plane, $J\Delta$ is the anisotropy along the z -direction. h is the magnitude of the external magnetic field as applied in the transverse direction (to the z -axis). The properties of the XXZ-model with externally applied field depends on the direction of the field. If the field is applied in the longitudinal direction (z -axis), then the applied field commutes with the hamiltonian and the system remains integrable [39]. But if the field is applied in the transverse direction (x - or y -axis), it does not commute with the hamiltonian, the system loses its integrability and the numerical methods become one of the options to deal with these systems.

4.1 Phase Diagram of the XXZ-model

First, one can discuss the phase diagram with no applied externally field i.e., $h = 0$. In this case the XXZ model remains integrable and the Bethe ansatz [47, 48] gives the exact solution.

On the basis of anisotropy in the z -direction Δ , there are three regimes in the phase diagram

For $\Delta \leq -1$, the system has a ferromagnetic ground state (two fold degeneracy) and there is a gap after the ferromagnetic state.

For $-1 < \Delta \leq 1$, the system has a gapless spin-fluid ground state. With the inclusion of externally applied transverse magnetic field ($h \neq 0$), the gap in the excitation spectrum begins to open up [45, 46].

For $\Delta > 1$, the system may be seen as in Ising-like regime (as Δ works as h in the Ising model), there is a Neel long range order (LRO) along z -axis in the ground state. This regime is also characterized by a gap in the excitation spectrum.

For a detailed discussion on phase diagram, please refer to [45]. The CORE simulations done in this chapter will be focused on the anisotropy regime ($-1 < \Delta \leq 1$).

4.2 Critical Exponent of the Energy Gap With Applied Transverse Field

According to the 2^{nd} -order phase transition, for an infinite system, the gap in XXZ-chain with the introduction of the external field can be written as [46]

$$G(h) \sim h^\lambda \quad (4.2)$$

where $G(h)$ is the gap induced by external field h near the critical point and λ is the critical exponent of the gap.

According to the field theoretical studies, the total regime ($-1 < \Delta \leq 1$) can be divided into two different regimes, each having the Gap exponent as given by following equations [45, 46]

$$\lambda_\tau \sim \frac{1}{1 - \frac{\theta}{2}} \quad -1 < \Delta \leq 0 \quad (4.3)$$

$$\lambda_\tau \sim \frac{2}{4 - \theta - \frac{1}{\theta}} \quad 0 < \Delta \leq 1 \quad (4.4)$$

The τ indicates that critical exponent is given by field-theoretical studies and θ is given by

$$\theta = 1 - \frac{\text{Cos}^{-1}(\Delta)}{\pi} \quad (4.5)$$

The eq. (4.5) shows that the critical exponents of the energy gap depends on the anisotropy parameter Δ .

The gap exponent of the XXZ model for different anisotropy parameters Δ as calculated by field theoretical approach from the equations (4.3,4.4) are given in the following table (4.1).

| anisotropy Δ | Critical Exponent λ_τ |
|------------------------|-------------------------------------|
| 0.25 | 1.17875 |
| 0.5 | 1.09091 |
| 0.7 | 1.04484 |
| -0.25 | 1.26548 |
| -0.5 | 1.2 |
| -0.7 | 1.14494 |

Table 4.1: critical exponents of the gap for anisotropy parameters ($-1 < \Delta \leq 1$).

In this chapter, the critical exponents of the energy gap for the given anisotropy parameter will be calculated by using the CORE simulations. The anisotropy parameters given in the table (4.1), $\Delta = \{-0.7, -0.5, -0.25, 0.25, 0.5, 0.7\}$ are selected for these simulations. The results can be compared with that of the field theoretical studies.

4.3 Evaluation of the Energy Gap Critical Exponent

In the anisotropy regime ($-1 < \Delta < 1$), with no externally applied field ($h = 0$), the system is gapless. The application of small amount of external field opens the gap, so the energy gap in XXZ model depends on the externally applied field. The gap for the XXZ model having L number of sites in one dimension as dependent on the externally applied field h can be written as

$$G(L, h) = E_m(L, h) - E_0(L, h) \quad (4.6)$$

where E_0 will be the ground state energy and E_m will be first excited state. Here m refers to the excited state that is not degenerate with the ground state. For example, if the ground state is two fold degenerate, i.e., E_0 and E_1 , then m takes a value of 2 and the spin gap becomes $E_2(L, h) - E_0(L, h)$.

Re-writing equation (4.2) for the second order phase transition, for an infinite system

$$G(h) \sim h^\lambda \quad (4.7)$$

The gap depends on the externally applied field h . At the critical point ($h_c = 0$), the gap $G(h_c)$ vanishes. This behaviour of the gap can be expressed by the equation.

$$G(h \rightarrow h_c) \rightarrow 0 \quad (4.8)$$

Another equation can be formed showing the gapless behaviour of the XXZ-model in the anisotropy range of ($-1 < \Delta < 1$) with no external field. For this purpose, inverse chain length $\frac{1}{L}$ is taken as the relevant quantity. Since as $L \rightarrow \infty$ then $\frac{1}{L} \rightarrow 0$. So the gapless behaviour with the relevant parameter (inverse chain length) can be described as

$$\lim_{L \rightarrow \infty} G(L, h = 0) \rightarrow \frac{A}{L} \rightarrow 0 \quad (4.9)$$

where A will be some constant.

These two conditions (4.8,4.9) can be used to describe the gapless behaviour of the XXZ-chain in the thermodynamic limit $L \rightarrow \infty$.

The gapless behaviour of the XXZ-model in 1-dimensional chain can be described as [38]

$$\frac{G(L, h)}{G(L, 0)} = 1 + x^\phi \quad (4.10)$$

where x^ϕ is a scaling function showing the asymptotic behaviour. The scaling parameter is $x = Lh^\lambda$ [50].

The combined limit of the gapless behaviour in the XXZ-model can be written as

$$L \rightarrow \infty \quad h \rightarrow 0 \quad (x \gg 1) \quad (4.11)$$

The equation (4.10) can be structured for the combined limit ($x \gg 1$).

So the ϕ -exponent will be found in this combined limit as given in equation (4.11).

Using equations (4.7),(4.8) and (4.9) in (4.10), one gets

$$\lim_{L \rightarrow \infty} LG(L, h) \sim (Lh^\lambda)^\phi \quad (4.12)$$

To make equation (4.12) to be true in the combined limit (4.11), the ϕ -exponent will have to be 1.

There is a constraint specific to this model. There will be level crossing with the application of the external field. When CORE simulations were first tested for more than five iterations, it was seen that depending on the external field, there was a level-crossing at some higher iterations. With the increasing external field, the level-crossing happens much earlier. To avoid the level crossing, and to remain close to the critical point, the external field is kept ($h < 0.01$). Even keeping the external magnetic fields extremely low does not solve this problem. The simulations will run upto 4th-iteration maximum without the level crossings. At 5th-iteration, the level crossing is generally observed for the low energy renormalized hamiltonians for more than four renormalized sites. Due to these reasons, one cannot go for ($L \rightarrow \infty$) in the XXZ model with externally applied magnetic field. For this reason, the combined limit behaviour ($\phi = 1$), for the equation (4.10), cannot be taken for granted. So the ϕ -exponent will also have to be found using CORE simulations, while working with finite lattice length L .

So the equation (4.10) can be written as

$$K(L, h) = \frac{G(L, h)}{G(L, 0)} = 1 + L^\phi h^{\lambda\phi} \quad (4.13)$$

one can put $\alpha = \lambda\phi$, and the equation 4.13 becomes

$$K(L, h) = \frac{G(L, h)}{G(L, 0)} = 1 + L^\phi h^\alpha \quad (4.14)$$

The exponents ϕ and α are to be computed using CORE simulations. Then the critical exponent for the energy gap λ can be computed as

$$\lambda = \frac{\alpha}{\phi} \quad (4.15)$$

The critical exponent λ will be specific to anisotropy parameter Δ in the anisotropy regime of ($-1 < \Delta < 1$).

4.4 Evaluation of the Critical Exponent of the Gap λ

The critical exponent of the energy gap λ can be determined by using the equation (4.15). For this purpose, one has to find the ϕ -exponent and the α -exponent using the equation (4.14).

4.4.1 Evaluation of the ϕ -Exponent

The *LHS* of the eq. (4.14), called gap ratio $K(L, h)$, is plotted using the CORE simulations for the increasing lattice sizes, while fixing the value of the external field. The *RHS* of eq. (4.14) is also plotted by fixing the external field to the same value and incrementing lattice sizes in correspondence to the microscopic sites of the CORE simulations. These two plots are to be superimposed. All the variables of equation (4.14) are known, same as given by CORE simulations, except for the ϕ -exponent. Different values of the ϕ -exponent are tried until the plot from *RHS* of the equation (4.14) overlaps the plot from CORE simulations. This will be the ϕ -Exponent corresponding to the particular anisotropy.

4.4.2 Evaluation of the α -Exponent

The same procedure is adopted for finding the α -Exponent except that the CORE simulations for the gap are done with fixing the lattice length and incrementing the external field. This curve

is then superimposed by the curve given by equation (4.14). The equation (4.14) have all the known quantities except the α -exponent for which, experimentation with different values will be done. For some specific value of the α -exponent, the gap ratio from CORE simulations and the *RHS* of equation (4.14) overlap. This overlapping value is the α -exponent.

4.5 Numerical Perspective : CORE simulations

CORE algorithm produces the renormalized hamiltonians for the renormalized sites equivalent to the corresponding microscopic sites. Whenever the dimensions of the renormalized hamiltonian reaches to the limits of the computational resources, one can switch to the next CORE iteration which gives low dimensional renormalized hamiltonian for even more microscopic sites.

Going for the next iteration also involves accumulation of CORE approximation and numerical errors. In this work, one goes to next CORE iteration only when it is needed. At higher range of simulations, like range-3, the approximation error will be minimized in going for the next renormalization transformation iteration, so the simulations are done at range-3 to achieve better accuracy. Two schemes with different parameters will be used for these simulations.

In the first scheme, there will be two sites single block, so the range-2 super block will comprise of four sites and the range-3 super block will comprise six sites. The degeneracy of the hamiltonian is such that one can retain three lowest states for a single block hamiltonian. These options will be called CORE simulation scheme-1. In the second scheme, a single block made of three sites with two retained states will be used. It will be called CORE simulation scheme-2. First, the CORE simulations are done using both the schemes. Based on the percentage error of the results with that of the field-theoretical results, the scheme with better accuracy will be adopted. There may be many other possible options for the simulations with CORE algorithm, but these schemes are chosen for the comparative studies of accuracy between bigger blocks and more retained states.

It should be noted that increasing the block size in different simulations schemes, while retaining same number of states results in having the same number of states for each of the renormalized sites after each of the CORE iteration. This results in the same dimension of the renormalized hamiltonians after each iteration. In this case, the microscopic sites corresponding to the renormalized sites increases more rapidly for the bigger blocks.

In case of the increasing retained states in different simulations schemes, but with the same size of single block, the number of states for each of the renormalized site increases corresponding to the increase in the retained states. This results in the increase in the dimension of the renormalized hamiltonians with the increasing retained states for the same number of renormalized sites.

Having defined the tools (schemes) needed to find the critical exponents of the energy gap in the XXZ model, with the introduction of the external field in the anisotropy regime of ($-1 < \Delta < 1$), one can start simulations.

4.6 scheme 1: Gap Exponent at ($\Delta = 0.5$)

This scheme focuses on the more retained states, while considering small single blocks. The dimensions of the starting single block hamiltonian, range-2 super block hamiltonian and range-3 super block hamiltonian are $2^2 = 4$, $2^4 = 16$ and $2^6 = 64$. After the first CORE iteration and for all the subsequent CORE iterations, the dimensions of the renormalized single block hamiltonian, renormalized range-2 super block hamiltonian and renormalized range-3 super block hamiltonian

have increased to $3^2 = 9$, $3^4 = 243$ and $3^6 = 729$. So the exponents are evaluated from this scheme as follows.

4.6.1 Scheme 1: Evaluation of the ϕ -Exponent at ($\Delta = 0.5$)

First, the scheme-1 parameters will be used for CORE simulations. One can use the value of anisotropy as ($\Delta = 0.5$) as a test case and fix the externally applied field to $h = 0.001$. In these plots gap ratio is found by CORE simulations for increasing CORE iterations. Increasing CORE iterations corresponds to the increasing lattice sizes.

In the plot (4.1a), the total number of sites $\{6, 8, 10, 12, 14\}$ and $\{16, 20, 24, 28\}$ is taken from the CORE 1st and 2nd renormalization transformation iterations respectively. In the plot (4.1b), the overlap between the CORE simulations and equation (4.14) is found for $\phi = 1.6$.

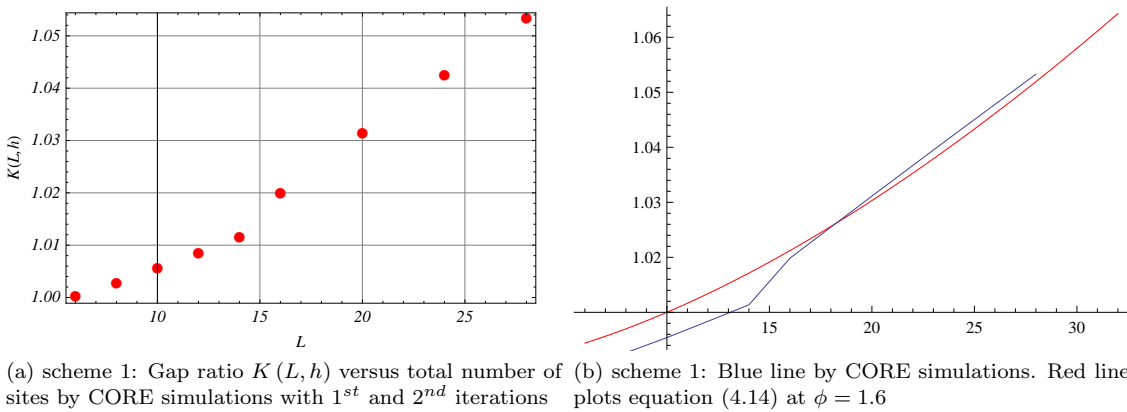


Figure 4.1: Scheme 1: CORE simulations and finite size scaling at $\Delta = 0.5$ and $h = 0.001$

In the plot (4.2a), the total number of sites $\{6, 8, 10, 12, 14\}$, $\{16, 20, 24, 28\}$, $\{32, 40, 48, 56\}$ is taken from the CORE 1st, 2nd and 3rd renormalization transformation iterations respectively. The overlap exists for $\phi = 1.6$.

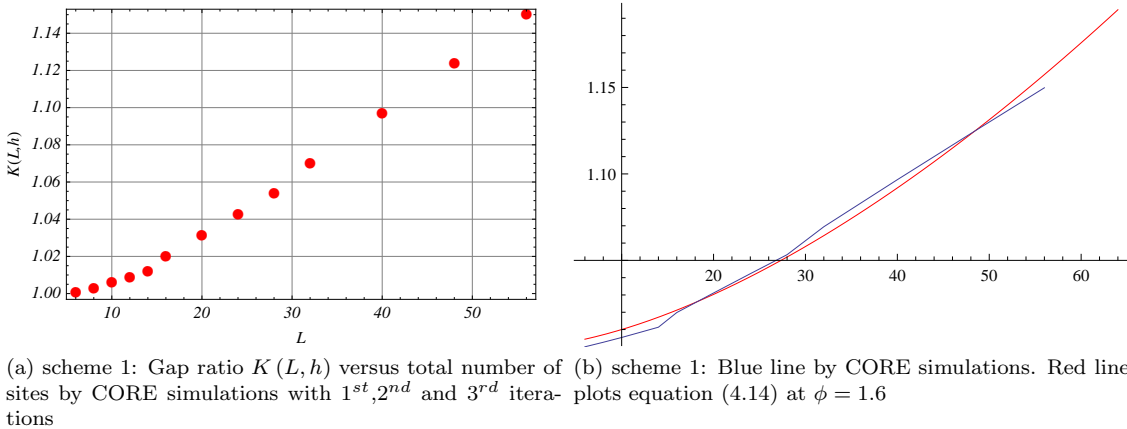
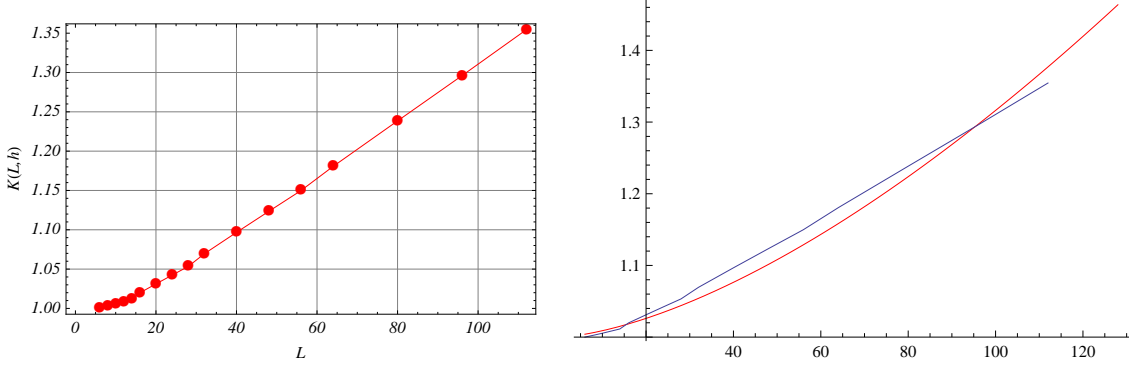


Figure 4.2: Scheme 1: CORE simulations and finite size scaling at $\Delta = 0.5$ and $h = 0.001$

4.6. SCHEME 1: GAP EXPONENT AT ($\Delta = 0.5$)

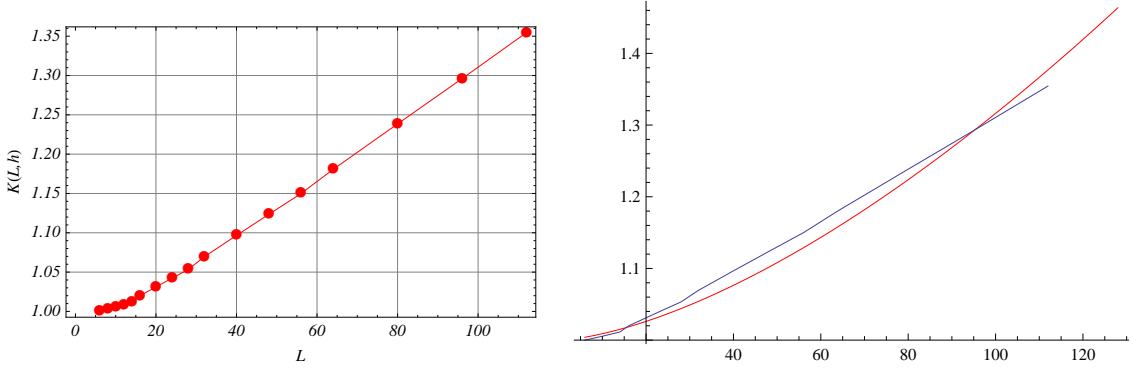
In the plot (4.3a), the total number of sites $\{6, 8, 10, 12, 14\}$, $\{16, 20, 24, 28\}$, $\{32, 40, 48, 56\}$ and $\{64, 80, 96, 112\}$ is taken from the CORE 1st, 2nd, 3rd and 4th renormalization transformation iterations respectively.



(a) scheme 1: Gap ratio $K(L, h)$ versus total number of sites by CORE simulations with 1st, 2nd, 3rd and 4th iterations. (b) scheme 1: Blue line by CORE simulations. Red line plots equation (4.14) at $\phi = 1.55$

Figure 4.3: Scheme 1: CORE simulations and finite size scaling at $\Delta = 0.5$ and $h = 0.001$

In the plot (4.4a), gap ratio $K(L, h)$ versus total number of sites $\{6, 8, 10, 12, 14\}$, $\{16, 20, 24, 28\}$, $\{32, 40, 48, 56\}$, $\{64, 80, 96, 112\}$ and $\{128, 160, 192, 224\}$ is taken from the CORE 1st, 2nd, 3rd, 4th and 5th renormalization transformation iterations respectively. In the plot (4.14), the best value for the overlap is $\phi = 1.5$



(a) scheme 1: Gap ratio $K(L, h)$ versus total number of sites by CORE simulations with 1st, 2nd, 3rd, 4th and 5th iterations. (b) scheme 1: Blue line by CORE simulations. Red line plots equation (4.14) at $\phi = 1.5$

Figure 4.4: Scheme 1: CORE simulations and finite size scaling at $\Delta = 0.5$ and $h = 0.001$

The ϕ -exponent does not depend on the system size. But for small lattice sizes, there is a possibility of finite size effects. So it is best to go for more CORE iterations, so that the microscopic lattice size increases with each iteration. The value of ϕ -exponent should be the same for all the CORE iterations. This is the case for first three CORE iterations. There is a slight change in the value of ϕ -exponent in the 4th and 5th iterations. One possible cause of

this behaviour is the accumulation of CORE approximation and numerical errors with higher CORE iterations. One has found out the values of the ϕ -exponent as $\{1.6, 1.6, 1.6, 1.55, 1.5\}$ using CORE low energy renormalized hamiltonians for upto 5th iterations.

Since with more CORE renormalization transformation iterations, there will be more accumulated errors, one can average the ϕ -exponent value from the first three CORE renormalization transformation iterations only. So the ϕ -exponent using CORE scheme-1 is 1.6.

4.6.2 Scheme 1: Evaluation of the α -Exponent at ($\Delta = 0.5$)

While keeping the lattice size constant, the external field is varied to values $h = \{0, 0.001, 0.002, 0.003, 0.004, 0.005, 0.006, 0.007, 0.008, 0.009, 0.01\}$.

In the plot (4.5a), the renormalized hamiltonian is made by taking three renormalized sites after the first CORE iteration. The best overlap for the α -exponent is found to be at $\alpha = 2.0$.

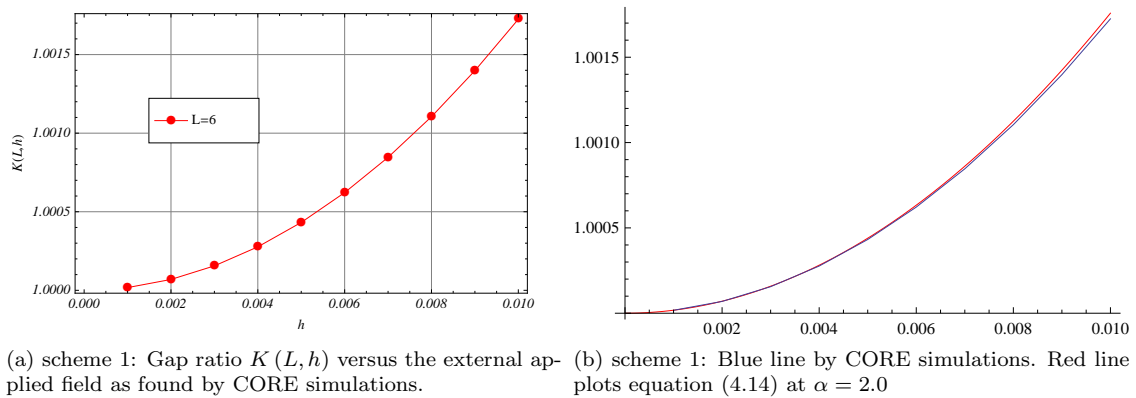


Figure 4.5: Scheme 1: CORE simulations and finite size scaling at $\Delta = 0.5$ and $L = 6$

4.6.3 Scheme 1: Evaluation of the Gap-Exponent λ at ($\Delta = 0.5$)

After finding the ϕ - and α -exponents, the gap-exponent λ can be found by CORE simulations scheme-1 by using equation (4.15). The gap-exponent by CORE scheme-1 is found to be $\lambda = 1.25$. It can be compared with field theoretical value of 1.09091 of the table (4.1). It shows an error of 14%. This error may be large but considering only 2-site single block geometry, the CORE simulations needed much less computational resources. The accuracy of the ϕ -exponents and α -exponents and therefore the resulting gap exponent λ can be checked by plotting the equation (4.14). In the figure (4.6), the gap ratio by CORE simulations and the scaling function $L^\phi h^\alpha$ are plotted for the finite 1-dimensional lattice consisting of sites $L = \{6, 10, 14\}$ with the varying external field

$h = \{0.001, 0.002, 0.003, 0.004, 0.005, 0.006, 0.007, 0.008, 0.009, 0.01\}$. The α -exponent is taken as $\alpha = 2.0$, while the ϕ -exponent is taken as $\phi = 1.6$. As the equation (4.14) shows all the gap ratios $K(L, h)$ should be on the same universal scaling curve for different lattice sizes L and magnetic fields h . The scattered data instead of being on the same universal curve show that the ϕ - and α -exponent do not have the good accuracy. So one can now move onto the CORE simulations scheme-2 to find still better results.

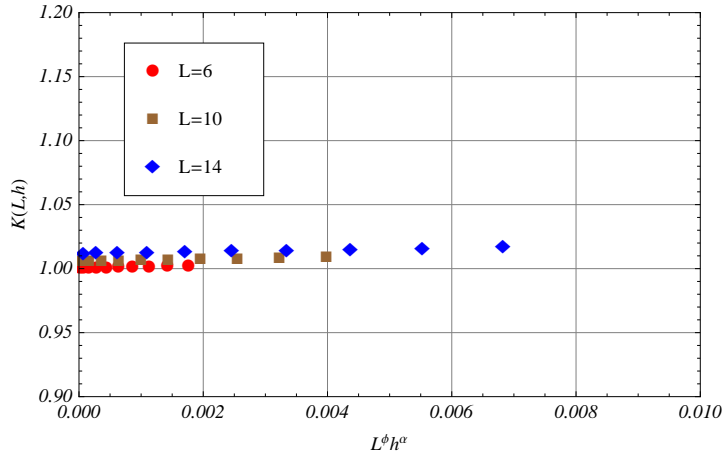


Figure 4.6: scheme 1: Plot for gap ratio $K(L, h)$ versus the scaling function $L^\phi h^\alpha$ using CORE simulations.

4.7 scheme 2: Gap Exponent at ($\Delta = 0.5$)

This is also a range-3 scheme based on bigger blocks and less retained states than that of scheme-1. These parameters have more advantages from the previous scheme from the computational point of view. Due to only two retained states in the scheme-2 with three site single block, the renormalized hamiltonians remain of the same form as the original hamiltonian. The dimensions of the hamiltonians remain the same during all the simulations. Then the range-3 super block hamiltonian has the dimensions $2^9 = 512$. In the previous scheme-1, for the three retained states and two site single block the range-3 super block renormalized hamiltonian after the 1st CORE iteration has dimensions was $3^6 = 729$. So the CORE simulations using these options becomes very fast and straight forward.

4.7.1 scheme 2: Evaluation of the ϕ -Exponent at ($\Delta = 0.5$)

Again, the external field is fixed at $h = 0.001$. In the plot (4.7a), $K(L, h)$ for the number of sites $\{6, 12, 18, 24, 36, 54, 72\}$ is taken from the CORE renormalization transformations upto 2nd-iteration. In the plot (4.7b), the best overlap between the equation (4.14) and CORE simulation is found to be at value of $\phi = 2.13$

Table (4.2) shows the ϕ -exponents for all the iterations done with CORE simulations.

| Renormalized Hamiltonians using CORE iterations | ϕ -exponent |
|---|------------------|
| 1 st | 2.17 |
| 1 st and 2 nd | 2.13 |
| 1 st , 2 nd and 3 rd | 2.17 |
| 1 st , 2 nd , 3 rd and 4 th | 2.20 |

Table 4.2: ϕ -exponents for the best overlap between the CORE simulations and equation (4.14) for anisotropy ($\Delta = 0.5$)

4.7. SCHEME 2: GAP EXPONENT AT ($\Delta = 0.5$)

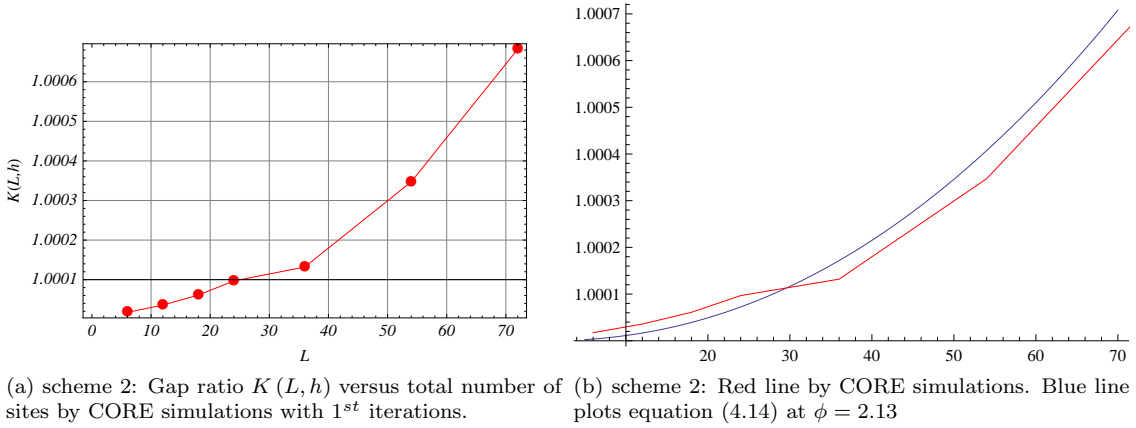


Figure 4.7: Scheme 2: CORE simulations and finite size scaling at $\Delta = 0.5$ and $h = 0.001$

In the 5th CORE iteration, one can calculate the gap for the microscopic lattice size of 972. But due to level crossing and the gap data does not remain consistent. As from the previous simulations, the ϕ -exponent for the first four CORE renormalized iterations is averaged. In this case, the averaged value of the ϕ -exponent from the first four CORE renormalization transformation iterations turns out to be $\phi = 2.17$.

4.7.2 scheme 2: Evaluation of the α -Exponent at ($\Delta = 0.5$)

While keeping the finite lattice size constant to $L = 36$, and varying the external field $h = \{0, 0.001, 0.002, 0.003, 0.004, 0.005, 0.006, 0.007, 0.008, 0.009, 0.1\}$, one can get the best overlap value of the α -exponent.

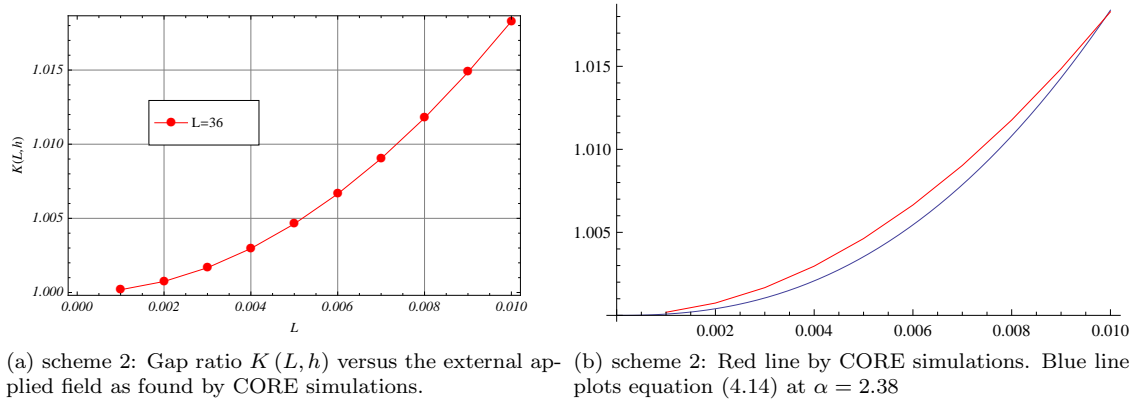


Figure 4.8: Scheme 2: CORE simulations and finite size scaling at $\Delta = 0.5$ and $L = 36$

One can find the α -exponent by super-imposing the CORE simulations results with that of finite size scaling ansatz (4.14) for the parameter α , as done in the plots (4.8b).

After the 1st CORE iteration, the plot (4.8a) is made from the twelve renormalized sites. In these simulations, for each plot, the total number of microscopic sites corresponding to the renormalized sites are fixed to 24, 30 and 36 respectively, while the external field varies with the

values

$h = \{0, 0.001, 0.002, 0.003, 0.004, 0.005, 0.006, 0.007, 0.008, 0.009, 0.01\}$. The α -exponent is found to be $\alpha = \{2.34, 2.36, 2.38\}$ from these three plots respectively. The α -exponent is taken as the average of these three values and is found to be $\alpha = 2.36$. If there is a very good overlap for the 1st-CORE iteration and that of the finite size scaling ansatz (4.14), then the higher CORE iterations becomes unnecessary as the 1st-CORE iteration is giving the best results. The overlap between the CORE simulations 1st-CORE iteration and the equation (4.14) is so good that more CORE iterations for the exploration of α -exponent are not undertaken.

4.7.3 Scheme 2: Evaluation of the Gap-Exponent λ at ($\Delta = 0.5$)

The ϕ -exponent is equal to 2.17 and the α -exponent is 2.36 for anisotropy ($\Delta = 0.5$) as found in the previous sections. The gap exponent is calculated to be $\lambda = 1.09$ by the equation (4.15).

This gap-exponent is exactly the same as the gap exponent given by the field theoretical studies $\lambda_\tau = 1.09$ in table (4.1).

The accuracy of ϕ - and the α -exponents and therefore the gap exponent can be seen by plotting the scaling function for different values of L and h . The data points are taken for different lattice sizes $L = \{24, 30, 36\}$ and for the external field $h = \{0, 0.001, 0.002, 0.003, 0.004, 0.005, 0.006, 0.007, 0.008, 0.009, 0.01\}$. The gap ratio $K(L, h)$ with different lattice sizes L and different externally applied transverse fields h appears to be on the same universal scaling curve. This shows the validity of the gap exponent as found by the CORE simulations scheme-2.

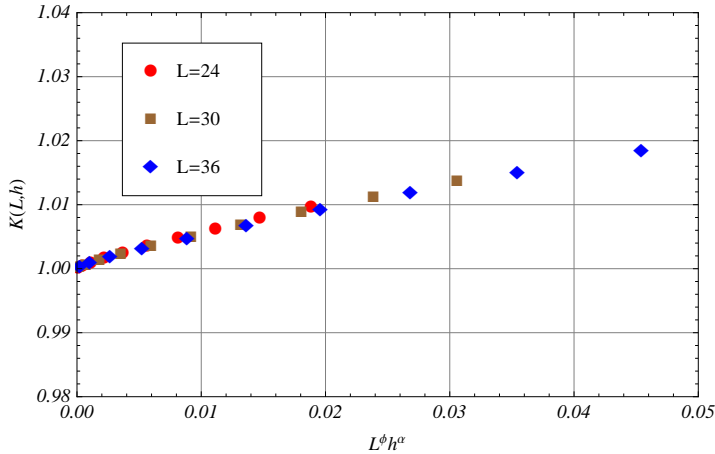


Figure 4.9: scheme 2: Plot for gap ratio $K(L, h)$ versus the scaling function $L^\phi h^\alpha$ using CORE simulations at $\Delta = 0.5$.

One can conclude from the scaling plots (4.6,4.9) that the CORE simulations parameter options of the scheme-2 are better than that of scheme-1 for the 1-dimensional XXZ model. The scheme-1 is also more resource intensive than that of the scheme-2 due to the more retained states resulting in the increasing dimensions of the resulting hamiltonians.

For the subsequent simulations in this chapter, only scheme-2 parameters of the CORE simulations will be adopted.

4.8 Gap Exponents using CORE simulations For Different Anisotropy Parameters

One can find the Gap exponents for different anisotropy parameters in the span of $(-1 < \Delta \leq 1)$ using the CORE simulations. These simulations will be done for six different anisotropy parameters namely $\Delta = \{-0.25, -0.5, -0.7, 0.25, 0.5, 0.7\}$. The purpose of these simulations is to compare the gap exponents by CORE with that of field theoretical studies to study their behaviour. The gap exponents will also be compared with other numerical techniques.

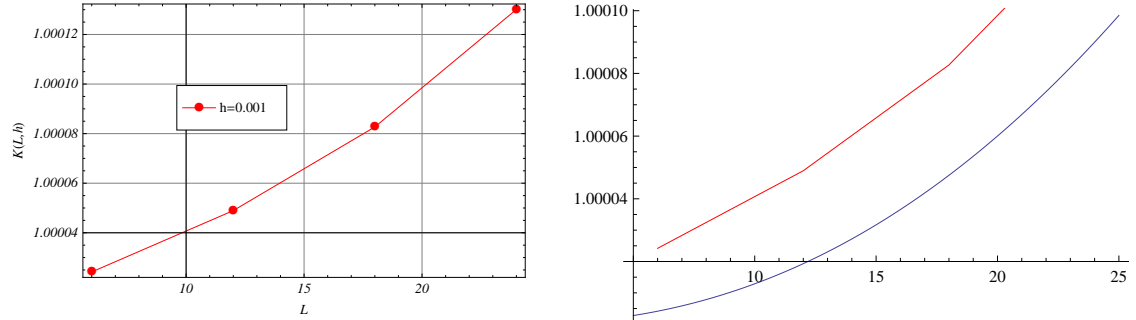
4.8.1 Evaluation of ϕ -exponent For Different Anisotropy Parameters

For finding the ϕ -exponent for the XXZ-Model with all the given anisotropy parameters $\Delta = \{-0.25, -0.5, -0.7, 0.25, 0.5, 0.7\}$, one can plot the scaling gap with changing (increasing) finite lattice length and fixing the external field to $h = 0.001$.

After 1st, 2nd, 3rd, 4th and 5th CORE iterations, the hamiltonians are made for the $\{4, 6, 8\}$ renormalized sites, equivalent to $\{12, 18, 24\}$, $\{36, 54, 72\}$, $\{108, 162, 216\}$, $\{324, 486, 648\}$ and $\{972, 1458, 1944\}$ microscopic sites respectively. At the 5th CORE iterations, the level crossing happens generally for all the simulations. The simulations for upto four CORE iterations are possible for studying the scaling behaviour of the gap. So the results from only the first four CORE iterations will be used for the calculation of ϕ -exponent.

All the plots for different anisotropies are of the same nature, giving different ϕ -exponents for different anisotropies. For illustrating the method used for finding the ϕ -exponents, the plots for anisotropy 0.7 will be shown. It shows the method, used for obtaining these highly accurate results.

In the figure (4.10a), energy gap ratio $K(L, h)$ is plotted for CORE 1st iteration corresponding to the $\{6, 12, 18, 24\}$ microscopic sites. The anisotropy parameter is $\Delta = 0.7$. The figure (4.10b) shows an overlap for the ϕ -exponent $\phi = 2.22$. There is some distance between the curves as the scale on the vertical axis is expanded to see the two separate curves. If the scale is condensed with a factor of ten, there will be a complete overlap.



(a) Gap ratio $K(L, h)$ versus total number of sites by CORE simulations with 1st-iteration. (b) Red line by CORE simulations. Blue line plots equation (4.14) at $\phi = 2.22$

Figure 4.10: CORE simulations and finite size scaling at $\Delta = 0.7$ and $h = 0.001$

The ϕ -exponents as found by CORE simulations for different anisotropies are shown in table (4.3). The CORE simulations are done for first four CORE iterations. The final ϕ -exponent is taken by averaging the values from the four CORE iterations. The CORE approximation and

4.8. GAP EXPONENTS USING CORE SIMULATIONS FOR DIFFERENT ANISOTROPY PARAMETERS

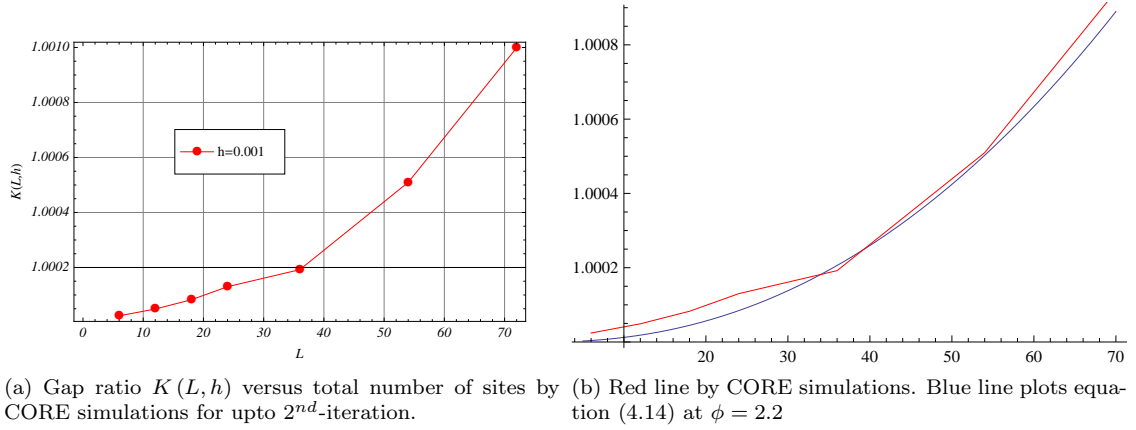


Figure 4.11: CORE simulations and finite size scaling at $\Delta = 0.7$ and $h = 0.001$

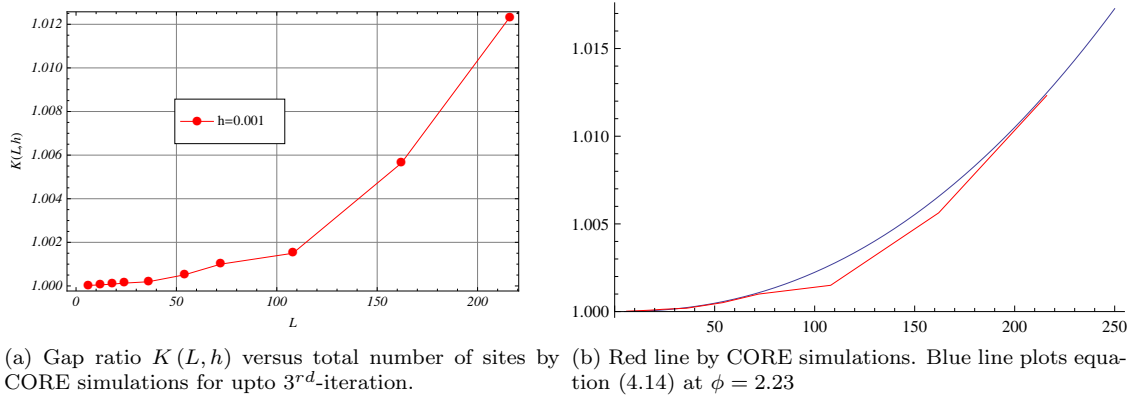


Figure 4.12: CORE simulations and finite size scaling at $\Delta = 0.7$ and $h = 0.001$

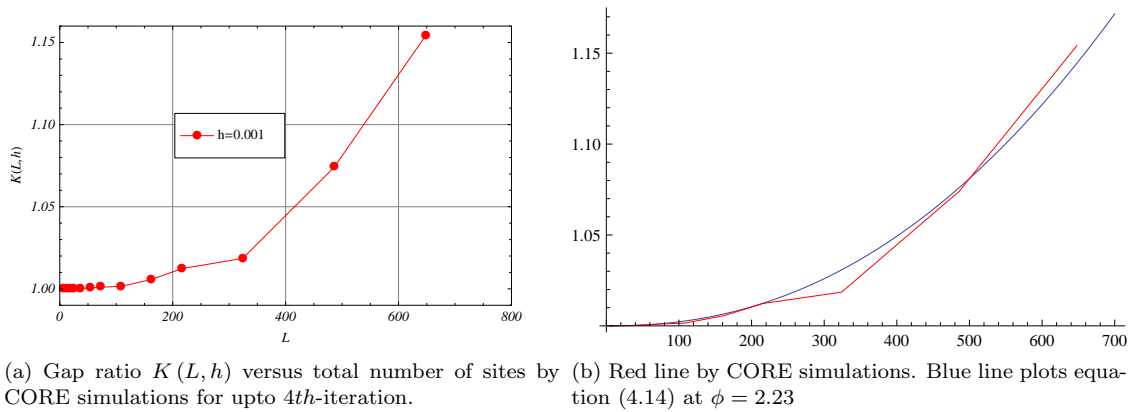


Figure 4.13: CORE simulations and finite size scaling at $\Delta = 0.7$ and $h = 0.001$

4.8. GAP EXPONENTS USING CORE SIMULATIONS FOR DIFFERENT ANISOTROPY PARAMETERS

| CORE simulation ϕ -exponent | | | | | |
|--|------------------------------|------------------------------|------------------------------|------------------------------|-------------------------|
| Best Overlap for CORE simulations upto | | | | | |
| Anisotropy Δ | 1 st Iteration | 2 nd Iteration | 3 rd Iteration | 4 th Iteration | Best Overlap Average |
| 0.7 | 2.22 | 2.2 | 2.23 | 2.23 | 2.22 |
| 0.5 | 2.17 | 2.13 | 2.17 | 2.20 | 2.17 |
| 0.25 | 2.09 | 2.05 | 2.09 | 2.1 | 2.08 |
| -0.25 | 1.85 | 1.85 | 1.85 | 1.85 | 1.85 |
| -0.5 | 1.95 | 1.91 | 1.96 | 1.96 | 1.95 |
| -0.7 | 2.1 | 2.04 | 2.04 | 1.99 | 2.04 |

Table 4.3: ϕ -exponent for different anisotropy parameters

numerical errors are also at their minimum, so one gets a very good estimate of ϕ -exponent by using this method.

4.8.2 Evaluation of α -Exponent For Different Anisotropy Parameters

The α -exponent are calculated by fixing the length of the lattice chain by making renormalized hamiltonians of $\{24, 30, 36\}$ microscopic sites after CORE 1^{st} -iterations. The external field increases from 0.001 to 0.1 for each of the plots.

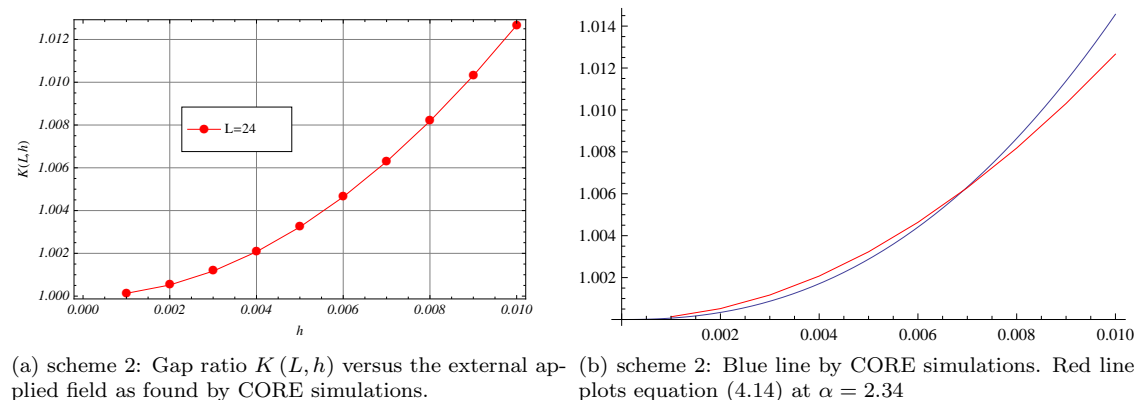


Figure 4.14: Scheme 2: CORE simulations and finite size scaling at $\Delta = 0.7$ and $L = 24$

In the figure (4.14b), the overlap between CORE simulations and finite size scaling ansatz is shown for the energy gap ratio at anisotropy ($\Delta = 0.7$).

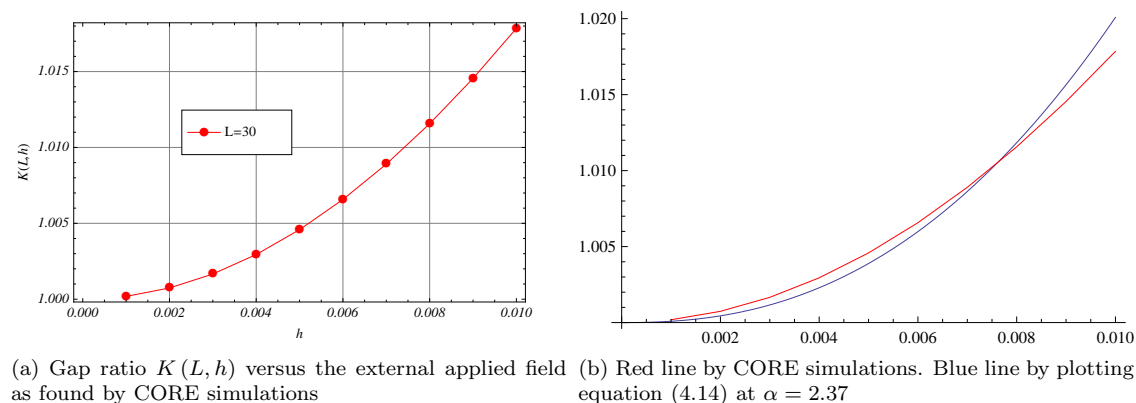


Figure 4.15: CORE simulations and finite size scaling at $\Delta = 0.7$

Table (4.4) shows the summary of the α -exponents for different anisotropy parameters. One gets a very good overlap using the CORE 1^{st} -iteration. There are sufficient points in each plot due to increasing external field, so there is no need for going to the higher iterations. The α -exponent do not depend on the lattice size of the system so the three values found at different lattice sizes are averaged to find the α -exponent for particular anisotropy.

4.8. GAP EXPONENTS USING CORE SIMULATIONS FOR DIFFERENT ANISOTROPY PARAMETERS

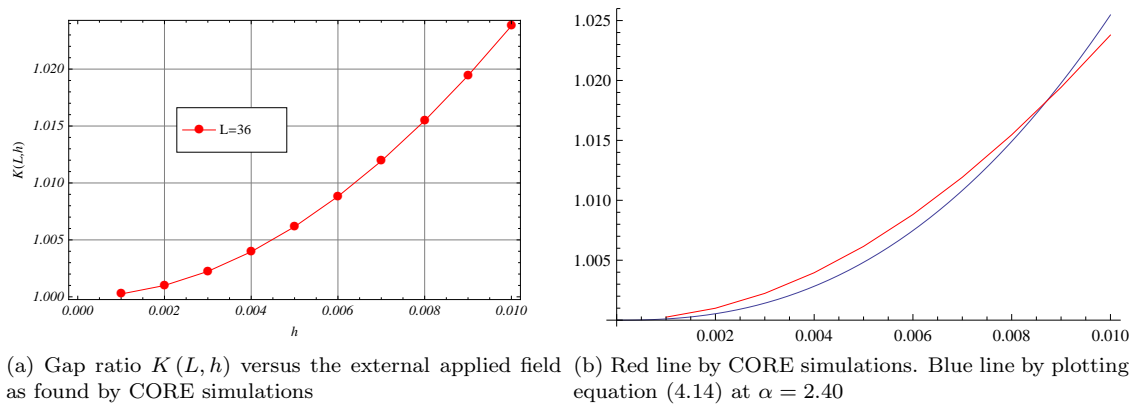


Figure 4.16: CORE simulations and finite size scaling at $\Delta = 0.7$

| CORE simulation α -exponent | | | | | |
|------------------------------------|---------------------|-----------------------|-----------------------|-----------------------|----------------------|
| Itr.No. | Anisotropy Δ | Best Overlap $L = 24$ | Best Overlap $L = 30$ | Best Overlap $L = 36$ | Best Overlap Average |
| 1 | 0.7 | 2.34 | 2.37 | 2.40 | 2.37 |
| 1 | 0.5 | 2.34 | 2.36 | 2.38 | 2.36 |
| 1 | 0.25 | 2.36 | 2.38 | 2.40 | 2.38 |
| 1 | -0.25 | 2.26 | 2.26 | 2.26 | 2.26 |
| 1 | -0.5 | 2.30 | 2.32 | 2.34 | 2.32 |
| 1 | -0.7 | 2.28 | 2.30 | 2.32 | 2.30 |

Table 4.4: α -exponent for different anisotropy parameters

4.8.3 Validity of ϕ -exponent and α -exponent For Different Anisotropy Parameters

To see the validity of the ϕ -exponent and α -exponent, finite size scaling ansatz (4.14) will be used. The gap ratio $K(L, h)$ for the microscopic sites L and the applied external field h will be calculated by using the CORE simulations. Then it is plotted against the scaling function $L^\phi h^\alpha$. If the points are on the universal scaling curve, then the ϕ -exponent and α -exponents are calculated with sufficient accuracy.

In the plot (4.17), gap ratio $K(L, h)$ versus the scaling function $L^\phi h^\alpha$ is plotted. The plot shows the points on the universal curve. In addition the CORE simulation, while finding the ϕ -exponent and α -exponents, the overlapping is done manually. The universal scaling curve shows the acceptable results for both of the exponents. But from some of the plots of this series, there is room for improvement.

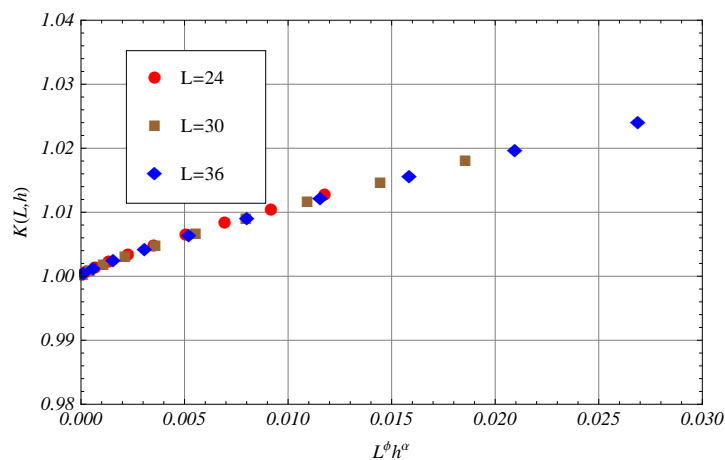
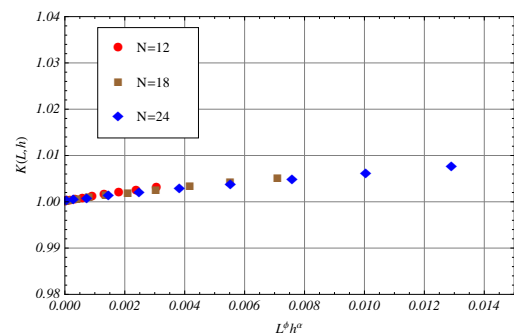


Figure 4.17: CORE simulations for the gap plotted against the scaling function $L^\phi h^\alpha$ at $\Delta = 0.7$

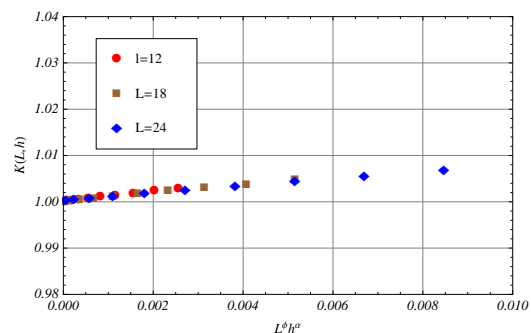
The lattice length is taken differently for all the plots, so it can be seen on respective plots.

The ϕ - and α -exponents are also found by modified lanczos method having the ground and excited states with same accuracy [38]. In that technique the curve fitting is used against the manual overlap as done in this chapter. Having found all the ϕ - and α -exponents, the equation (4.15) can be used to find the gap exponent (λ) as shown in the table (4.5).

4.8. GAP EXPONENTS USING CORE SIMULATIONS FOR DIFFERENT ANISOTROPY PARAMETERS

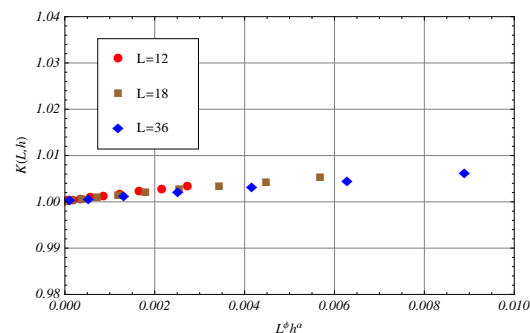


(a) CORE simulations for the gap plotted against the scaling function $L^\phi h^\alpha$ at $\Delta = 0.25$

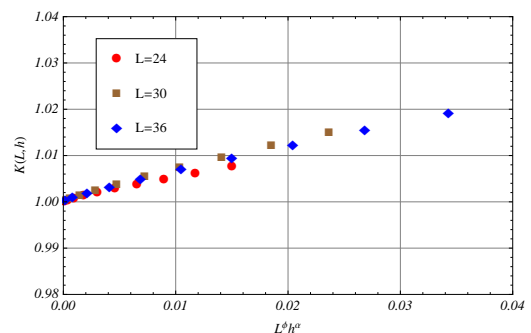


(b) CORE simulations for the gap plotted against the scaling function $L^\phi h^\alpha$ at $\Delta = -0.25$

Figure 4.18: Each anisotropy have its particular ϕ - and α -exponent given by tables (4.3) and (4.4) respectively.



(a) CORE simulations for the gap plotted against the scaling function $L^\phi h^\alpha$ at $\Delta = -0.5$



(b) CORE simulations for the gap plotted against the scaling function $L^\phi h^\alpha$ at $\Delta = -0.7$

Figure 4.19: Each anisotropy have its particular ϕ - and α -exponent given by tables (4.3) and (4.4) respectively.

| CORE simulation Gap exponent (λ) | | | | | |
|--|---------------|------------------|-----------------|--------------------|------------------|
| Anisotropy Δ | ϕ_{CORE} | $\phi_{M.Lancz}$ | α_{CORE} | $\alpha_{M.Lancz}$ | λ_{CORE} |
| 0.70 | 2.22 | 2.07 | 2.37 | 2.00 | 1.07 |
| 0.50 | 2.17 | 1.94 | 2.36 | 2.00 | 1.09 |
| 0.25 | 2.08 | 1.85 | 2.38 | 2.00 | 1.14 |
| -0.25 | 1.85 | 1.56 | 2.26 | 2.00 | 1.22 |
| -0.05 | 1.95 | 1.47 | 2.32 | 2.00 | 1.19 |
| -0.07 | 2.04 | 1.50 | 2.32 | 2.00 | 1.14 |

Table 4.5: ϕ - and α -exponent by CORE and Modified Lanczos

4.9 Conclusion

The XXZ-model shows a gapless behaviour in the anisotropy range of $(-1 < \Delta \leq 1)$ with no applied external field. If an external field is applied, transverse to the anisotropy in the z -direction, the gap starts to open up. The critical exponent of the gap with range-3 simulations is calculated. According to the field theoretical approach, there are different formulas for the critical exponent of the energy gap in the anisotropy range of $(-1 < \Delta \leq 0)$ and that of the $(0 < \Delta \leq 1)$. The value of the critical exponent also depends on the anisotropy parameter Δ . Using the CORE simulations, same procedure is adopted for finding the critical exponent for the specific values of the anisotropy. The backbone for finding the critical exponent is the scaling ansatz, in which gap ratio is calculated for any length L of the XXZ-model. There are two exponents which are to be calculated using this approach. The first is the ϕ -exponent, which is calculated by fixing the external field and then varying the length of the chain lattice. The second is the α -exponent, which is calculated by fixing the XXZ-chain length and then varying the external field. The ratio of these exponents give the critical exponent of the gap with that of the applied external field.

The approximation critical exponents found by CORE have a very good match to their field-theoretical counter-parts. The reason for the good results is in the multiple iterations of the CORE algorithm. The multiple CORE iterations made available many points, giving enough trajectory, resulting in finding the exponents approximations correctly. These simulations can be improved further as the computational resources allow to do that, but there is no reason to do it in this problem.

| anisotropy Δ | λ_τ | λ_{CORE} | $\lambda_{M.Lancz}$ |
|---------------------|----------------|------------------|---------------------|
| 0.7 | 1.04 | 1.07 | 0.96 |
| 0.5 | 1.09 | 1.09 | 1.03 |
| 0.25 | 1.18 | 1.14 | 1.08 |
| -0.25 | 1.26 | 1.22 | 1.28 |
| -0.5 | 1.20 | 1.19 | 1.36 |
| -0.7 | 1.14 | 1.14 | 1.33 |

Table 4.6: gap-exponents by different Methods

These results can be compared with other techniques, like modified lanczos, which gives all the lowest states of a hamiltonian with same accuracy, but it cannot go for the big lattice sizes as done by CORE simulations. From the table (4.6), the difference in the results is quite evident.

Chapter 5

Alternating spin- $\frac{1}{2}$ Heisenberg Chains (AHC)

The spin- $\frac{1}{2}$ uniform Heisenberg chain is a simple quantum spin system, which has a gapless excitation spectrum in reference with the ground state. The ground state of the spin- $\frac{1}{2}$ uniform Heisenberg chain is also characterized by strong quantum fluctuations making it unstable with small alternations and frustrations [55], which will be investigated by using the CORE algorithm in this chapter.

There is a vast space for the application of the CORE algorithm to the quantum spin systems near criticality. As near the criticality the correlation length diverges, so there is a need to find the low energy hamiltonians for sufficiently big lattice sizes. The exact diagonalization and other techniques, working on small lattice sizes, in general, cannot get rid of the finite lattice effects and are not able to get convergence for the critical exponents and therefore their results cannot be taken for granted to study the critical behaviour for quantum spin systems. So the critical behaviour of the quantum spin systems are good candidates for study with the techniques which are able to simulate systems upto thermodynamics limits, like DMRG etc. CORE algorithm is also one of the technique designed to study the critical phenomena, in which after only a few CORE renormalization iterations, one reaches to low energy renormalized hamiltonian of the sufficiently large microscopic lattice sizes. The CORE algorithm can be applied to alternating Heisenberg model to study its critical behaviour of the energy density and the spin gap. This chapter is divided into three sections. In the first section, the simulations are done with range-2, in the second section the simulations are done with range-3, while in the third section, the range-3 simulations are done by using bigger blocks for the study of spin- $\frac{1}{2}$ uniform Heisenberg chain with alternations.

5.1 Alternating Heisenberg Chain (AHC)

The alternating Heisenberg chain (AHC) can be used to describe the magnetic behaviour of large number of materials e.g., $Sr_{14}Cu_{24}O_{41}$, $(VO)_2P_2O_7$ and $CuGeO_3$ [53]. The spin- $\frac{1}{2}$ alternating Heisenberg chain (AHC) can be viewed as the generalization of the spin- $\frac{1}{2}$ uniform Heisenberg chain. The alternating Heisenberg chain is characterized by two alternating spin-couplings, say (j_1, j_2) , between the consecutive spins in the chain. The ground state of alternating Heisenberg chain is a spin singlet for even number of sites, while the translational symmetry in the uniform spin- $\frac{1}{2}$ Heisenberg chain is reduced by alternations, so there is gap between the ground state $S = 0$

and the first excited state, which is a spin-triplet $S = 1$. In this way the alternating Heisenberg chain can be viewed as an isotropic spin system in 1-dimension characterized by a gap [53]. So the alternating Heisenberg chain (AHC) can be compared with 1D isotropic quantum spin systems with a similar gap like integer spin chains (haldane conjecture) or spin- $\frac{1}{2}$ Heisenberg even leg ladders. This makes the alternating Heisenberg chain (AHC) of major theoretical interest.

The alternating Heisenberg antiferromagnetic model can be viewed as uniform Heisenberg chain, with the nearest neighbour couplings are added by two alternating couplings of the magnitude say $+J\delta$ and $-J\delta$ repeating one after another along the length of the 1-dimensional lattice, where J is the nearest neighbour couplings and δ is the alternation parameter. The hamiltonian for the spin- $\frac{1}{2}$ alternating Heisenberg model can be written as

$$H = \sum_{j=1}^L J [1 - \delta (-1)^j] \vec{S}_j \cdot \vec{S}_{j+1} \quad (5.1)$$

This model is also called dimerization model, if the couplings are seen as $J(1 + \delta)$ and $J(1 - \delta)$ repeating alternatively.

There are two quantities in relation to the hamiltonian (5.1), for which the critical behaviour of this model is to be studied by CORE simulations. The first of these quantities is the energy per spin or energy density

$$e_o(L, \delta) = \frac{E_o(L, \delta)}{L} \quad (5.2)$$

where $E_o(L, \delta)$ is the total energy of the alternating Heisenberg model (5.1) for the lattice of length L at alternation parameter δ , whereas $e_o(L, \delta)$ is the energy density (energy per spin).

The second quantity in relation to the hamiltonian (5.1) for which the critical behaviour is to be studied is the singlet-triplet gap $\Delta(L, \delta)$ (the simulations will be done for even number of sites) as defined by

$$\Delta(L, \delta) = E_1(L, \delta) - E_o(L, \delta) \quad (5.3)$$

Where $E_1(L, \delta)$ is the first excited state. For even number of sites, $E_1(L, \delta)$ is a spin-triplet and $E_o(L, \delta)$ is a spin singlet.

Now, if one can put $\delta = 0$ in the equation (5.1), then the alternating Heisenberg antiferromagnetic chain converts into the uniform spin- $\frac{1}{2}$ Heisenberg chain. So the model becomes gapless and the energy density of the uniform Heisenberg chain is understood to have the value $e_o = \frac{1}{4} - \ln 2$.

The CORE simulations will be done for the alternations approaching to the uniform chain limit $\delta \rightarrow 0$. So a span of alternations starting from $\delta = 0.001$ to $\delta = 0.1$ is chosen. The alternating Heisenberg model has a more complicated higher excited states [53] which will not be discussed using CORE simulations.

The early study of the alternations on the uniform Heisenberg model was done by Cross and Fisher [55]. Their approach yield the critical exponent of the spin gap as defined by the power law $\Delta(\delta) \propto \delta^{\frac{2}{3}}$. So the power law describing the critical exponent of the spin gap can be stated as [52]

$$\Delta(\delta) = A\delta^\alpha \quad (5.4)$$

where A is the co-efficient of the power law describing the gap scaling with alternations δ , while α is the critical exponent of the gap for alternating Heisenberg model.

The Cross-Fisher approach for the critical behaviour of the energy density yield the power law as $e_o - e_o(\delta) \propto \delta^{\frac{4}{3}}$ which can be generalized [52] as

$$e_o - e_o(\delta) = B\delta^\beta \quad (5.5)$$

where B is the co-efficient of the power law describing the energy density scaling with alternations δ , while β is the critical exponent of the quantity also called energy stabilization for alternating Heisenberg model.

There are logarithmic corrections found by Black and Emery [58] to these power laws. For the energy stabilization, the logarithmic correction to the power law is

$$e_o - e_o(\delta) \propto \frac{\delta^{\frac{4}{3}}}{|\ln \delta|} \quad (5.6)$$

and for the spin gap, the logarithmic correction to the power law is

$$\Delta(\delta) \propto \frac{\delta^{\frac{2}{3}}}{|\ln \delta|^{\frac{1}{2}}} \quad (5.7)$$

The numerical study by CORE will also study the span of the alternations for which the critical behaviour of the quantities overlap the power law and the span of alternations for which the logarithmic corrections are needed.

In a perturbation analysis [53, 51], the gap exponent is given by $\alpha \sim \frac{3}{4}$ and $A = 2$ for the alternations to be in the range of $0 \leq \delta \leq 1$. In some of the previous numerical studies, a combination of the exact diagonalization with that of the extrapolation [53, 54] is used to find the critical exponents for the energy density and that of the spin gap. The exact diagonalization is used for the system size of upto ~ 30 . DMRG studies were also used to find the critical exponent for the system sizes of upto $L = 192$ [51], giving the gap exponent as $\alpha = 0.73$ and energy density exponent $\beta = 1.45$.

In the next sections, the CORE algorithm will be applied to find these critical exponents and the span of the alternations for which the power laws are valid without logarithm corrections. The accuracy of these exponents as calculated by the CORE algorithm depends on the range of the calculation. So the exponents as found by the CORE algorithm can be stated along with the range of the calculations. The CORE simulations can be used to obtain these exponents by using CORE algorithm at range-2 and range-3. In these simulations, generally, a large single block with more retained states is used to increase the accuracy of the results.

5.2 Application of CORE to the Alternating Heisenberg Model

The application of the CORE algorithm can be started in a usual way. First the sub-lattice making a single block is chosen. The consideration of the number of sites in a single block depend on the model used for the simulations. Big sized blocks give more accuracy. In this case for even number of sites, there will be singlet-triplet as the lowest energy states for the alternating hamiltonian (5.1). So for the even number of sites single block, the most feasible option for the number of the retained states will be $M = 4$, i.e., a singlet and a triplet (the triplet can only be taken as a whole).

At first, CORE simulation with single block of odd number of sites taking five and seven sites per single block was tried. These simulations were done at range-2 with two retained states. The

maximum dimensions of the range-2 hamiltonian for these two simulations were 1024 and 16384 respectively. These hamiltonians can be solved for few lowest eigenvalues and eigenvectors with mediocre computer resources. The energy stabilization from these simulations appear to follow the Cross-Fisher power laws in the alternation span of 0.02 to 0.1 (the total alternation span for the simulation is 0.001 to 0.1), comparable to results by other techniques, but the critical exponents calculated were not as accurate. For example, for a seven site single block, the critical exponent for the energy stabilization was approximated to be 1.1 which has quite a notable difference with the Cross-Fisher exponent for the energy stabilization, i.e., 1.33. So in order to increase the accuracy of finding the critical exponent, a scheme with more retained states was adopted which greatly enhanced the accuracy of the critical exponents as will be discussed later.

To achieve better results, the simulations were done with even number of sites. There will be four retained states consisting of a singlet and a triplet. These options in the CORE algorithm present some additional difficulties, which can be discussed. The starting hamiltonian has a two states per site. But after retaining four states in the first iteration of the CORE algorithm, the new renormalized site after the first CORE iteration has four states. Now, if more than one iteration is needed, all the new renormalized sites from the 2^{nd} iteration onwards have four states. The dimensions of the corresponding hamiltonian from 2^{nd} iteration onwards for the single block, super block range-2 and super block range-3 are enhanced compared to the dimensions of the hamiltonians in the first CORE iteration. (Dimension of the hamiltonian = M^L , where M is the number of retained states and L is the number of sites.)

The computational resources available for these simulations can diagonalize a matrix for few lowest eigen values and eigen states of the dimension $2^{16} = 65536$ by Arnoldi's method taking some feasible time for the simulations. The needed time depend on zeros in the matrix with more zeros needing less time. The computational system is also able to diagonalize a matrix of the dimension $2^{18} = 262144$ for few lowest eigen values and eigen states, but it takes a lot of time. More than one hamiltonian of this dimension per simulation is not recommended. It is also seen that the hamiltonian matrices after first iteration do not remain very much sparse. In case of four retained states, after the first CORE iteration, each of the renormalized sites has four states. If the computational resources are already used to their full capacity in the first iteration, one will not be able to go for more CORE iterations using the same computational resources. There are two possible solutions for this problem. The first solution is that the single block for the first iteration is chosen in such a way, that the hamiltonian dimensions for the given range of the calculation remains well within the limits, even if the states of the renormalized site are increased in 2^{nd} or any other CORE iteration. This solution will make the single block of the first CORE iteration small enough so that when the states of the renormalized site increases, the dimensions of the resulting super block hamiltonians remains within the capability of the computational system. This solution may be successful in some kind of problems but is generally not successful for getting good critical exponents in the alternating Heisenberg hamiltonian system. The reason is that the alternating term in the alternation Heisenberg model demands that big sub-lattice blocks should be used for CORE simulations. During the tests with simulations, it was seen that at least four site single block at range-3 is necessary to calculate the appropriate critical exponents. So for obtaining good results, one have to take the single blocks of at least four microscopic sites in the 1^{st} CORE iteration. For the 2^{nd} CORE iteration, the states of each renormalized site will be increased to four resulting in the increase in the dimensions of the renormalized hamiltonian. So with four site single block at range-3, the first super block range-3 hamiltonian will be $2^{12} = 4096$, well within the computational limits of available resources. From CORE 2^{nd} iterations onwards, the dimensions of super block range-3 hamiltonian will be $4^{12} = 16777216$, well out of limits of our computational resources. So this technique will not be applicable for the alternating Heisenberg Model.

The second option is devised in such a way that all the objectives are met. The first objective was to make big sub-lattice single block in the first CORE iteration. This is very important step as it enhances the accuracy of the simulations. For the alternating Heisenberg model, there are two states per site. The single block are chosen in such a way that super block range-2 and super block range-3 remain within the available computational limits. Then the problem comes for the second CORE iteration, as the renormalized sites have four states, the range-2 and range-3 hamiltonians do not remain diagonalizable due to their increased size in the available computational resources. To make the size of renormalized hamiltonian in the 2^{nd} CORE iteration equivalent to the CORE first iteration hamiltonians, one can reduce the size of sub-lattice constituting the single block so that overall dimension of the range-2 or range-3 hamiltonian remains within computational limits of the computational resources.

In pursuing this approach, the question arises that the smaller blocks of the renormalized sites from 2^{nd} iteration onwards will not give good results as achieved in the first CORE iteration. But on doing simulations, it was seen that the accuracy achieved in the first CORE iteration step is somewhat maintained in the sub-sequent CORE iterations apart from the approximation and numerical errors of the technique, which are incorporated at each CORE iteration. The reason is that the reduced size renormalized blocks from 2^{nd} CORE iteration onwards have effectively more microscopic sites than the microscopic sites of the blocks in the first CORE iteration. So this scheme will be adopted for studying the critical behaviour of alternating Heisenberg model.

The plots are made using two different CORE renormalized iteration schemes, i.e., range-2 and range-3. Then the range-3 simulations will be done with two different types of parameters. In the range-2 simulations, the CORE algorithm is implemented on eight site single block with four retained states, while in the range-3 simulations, the single block of six sites will be taken with four retained states. The reason for the second scheme will be discussed in the next section. There will be some difference in results using the two schemes, which will also be discussed. The energy stabilization as calculated for different number renormalized sites at different CORE iterations corresponds to the different number of the microscopic sites. These equivalent microscopic sites are indicated in the plots.

5.3 CORE Simulations for AHC at Range-2

In this section, the range-2 simulations of the critical behaviour of energy stabilization and gap for the alternating Heisenberg chain (AHC) (5.1) will be studied. To achieve the best accuracy in the available computational resources, the eight sites single block is chosen. This makes the range-2 super block of 16 sites. For the first CORE iteration the dimensions of the single block will be $2^8 = 256$, while that of the super block range-2 is $2^{16} = 65536$, is within the computational limits of the available resources. As only a few lowest energy eigen states of the super-block hamiltonian are needed, in this particular configuration, $M^R = 4^2 = 16$, i.e., sixteen states if there is no zero scalar product between the tensor product states of two single blocks and the lowest exact eigen states of the super-block range-2 hamiltonian. Supposing there are some zero scalar products, one can diagonalize the super block range-2 hamiltonian for the forty lowest energy eigen states. These lowest eigen states can be calculated by using Arnoldi method. From 2^{nd} CORE iteration onwards, the single block will be made of four renormalized sites that makes the range-2 super-block of eight renormalized sites. Each of these renormalized sites has four states. This makes the dimension of the single block renormalized hamiltonian as $4^4 = 256$ and that of range-2 super block hamiltonian $4^8 = 65536$. These renormalized hamiltonians from 2^{nd} CORE iteration onwards have the same dimensions as that of the hamiltonians in the first CORE iteration.

After each iteration of the CORE algorithm, one get the hamiltonian h_1 and h_2 from which one can calculate renormalized hamiltonians for the desired number of the renormalized sites. A simulation of total of five Core iterations will be done and renormalized hamiltonians of upto six renormalized sites are computed after each CORE iteration. The microscopic sites corresponding to each of the renormalized hamiltonian is also computed. The number of microscopic sites are indicated in the plots. These renormalized hamiltonians will be used to compute the desired quantities as given in equations (6.2,6.3) showing their critical behaviour.

5.3.1 Critical Exponent for the Energy Stabilization at Range-2

For the CORE 1st iteration, eight sites single block is taken, while that for the 2nd CORE iteration and onwards, the single block is made of four renormalized sites. There will always be the four retained states and the simulations will be at range-2. The renormalized hamiltonians for a single plot are made from the results of the specific CORE iterations as indicated by the subscript to L in the plot. If the microscopic sites are repeated for different CORE iterations in the plots, then the renormalized hamiltonian is made using the results from the lowest CORE renormalized iterations. in fig.(5.1), energy difference of the uniform Heisenberg chain with that of alternating Heisenberg chain is plotted with alternations δ . The renormalized hamiltonian are made using the results from CORE 1st and 2nd renormalization transformation Iterations. Each curve represents different microscopic sites of the lattice as indicated in the plot. This microscopic sites in this plot approximately correspond to the lattice sizes in other studies [51]. This is the first reason for the plot (5.1) to be used as reference plot. The second reason is the simulations from CORE 2nd iteration means that it contains minimum of the approximations and numerical errors. The critical exponent of the power law is calculated, which is valid without logarithmic corrections in the alternation span of 0.02 to 0.1. The coefficient and the critical exponent of the energy stabilization power Law (5.5) gives $A = 0.39$ and $\beta = 1.45$ respectively. These values are approximated by using the outputs of CORE 2nd iteration, forming hamiltonian of upto six renormalized sites corresponding to 192 microscopic sites.

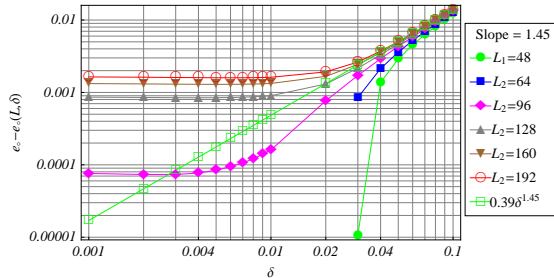


Figure 5.1: log-log plot of Energy Stabilization with alternation parameters. Hamiltonians are made from CORE 1st and 2nd iterations. Single block of 1st iteration consist of 8 sites, while subsequent iterations single blocks consist of 4 renormalized sites.

The plot (5.2a) is made by using the CORE 1st-iteration. As the total number of microscopic sites is ≤ 50 , there is no convergence in the results. The critical exponent of 48 lattice sites is also calculated, as shown in the figure, but these values are only of symbolic value, as the microscopic lattice sizes are so small that the energy density has not converged. It can also be seen from the plot that only exact diagonalization is not enough for the study of the critical behaviour of these

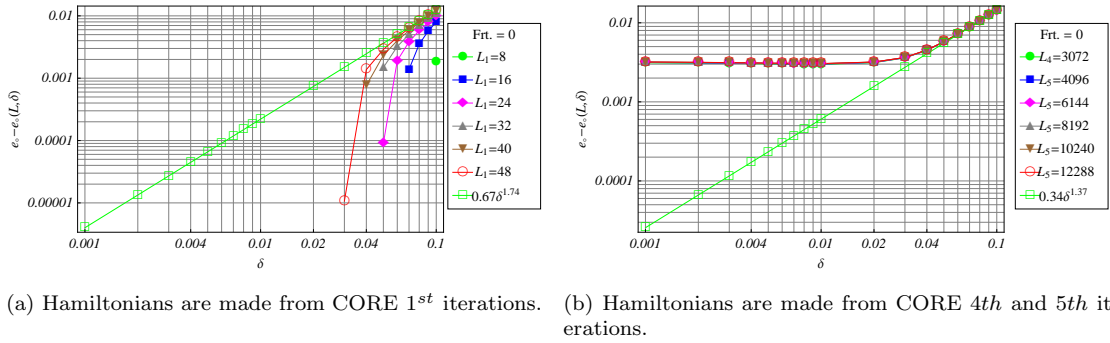


Figure 5.2: log-log plot of Energy Stabilization with alternation parameter. CORE simulations are done at range-2.

types of systems as indicated by [51].

From the CORE 3rd iteration, equivalent to upto 768 microscopic sites, the energy stabilization start going for convergence. It means that from CORE 2nd iteration equivalent to 192 sites to CORE 3rd iteration equivalent to 768 sites, there exists a thermodynamics limit behaviour, showing the behaviour for the infinite lattice. For the CORE 4th iteration, equivalent to upto 3072 microscopic sites, there is almost a complete convergence, and there is a very small change in the critical exponent. The appearance of small change in the critical exponents is due to the accumulated approximation and numerical errors. The plot (5.2b) using the 5th iteration shows a complete convergence of curves with different equivalent microscopic sites. The critical exponent is already converged to a value of 1.37, which is very near to $L \rightarrow \infty$ behaviour of the conformal theory with critical exponent 1.33 [55]. So the result achieved by CORE algorithm at range-2 is very close to the result from the conformal theory.

5.3.2 Critical Exponent for the Gap for (AHC) at Range-2

The critical exponent for the energy stabilization is found with good accuracy using the CORE algorithm at range-2, but the same is not true for the gap. In the CORE simulations at range-2, it has been seen that convergence is not achieved for the singlet-triplet gap. The gap follows the required pattern but the value of critical exponent cannot be relied beyond the 2nd CORE iteration. The is because, for the gap calculation in alternation Heisenberg model, one is dealing with a singlet and a triplet, i.e., more than the lowest state as have been the requirement of the energy stabilization in the previous section. The results for the gap exponent will be mentioned with using only the first CORE iteration. The solution to this problem will be addressed in the next section.

In the plot (5.3), the evolution of the singlet-triplet gap is plotted with the alternation parameter δ simulated by CORE 1st and 2nd-iterations. CORE simulation are done at range-2. The value for the critical exponent for the gap is 0.734252 and the co-efficient is found to be 1.84599 with using four renormalized sites after the first iteration. The microscopic lattice size is not approaching the thermodynamics limits and there is no convergence of the gap exponent with the increasing CORE iterations, therefore it is only a symbolic value.

These simulations for the energy stabilization are done with five CORE renormalization transformation iterations, with renormalized hamiltonians made of upto six renormalized sites. One can go for further CORE renormalization transformation iterations, but that will be un-

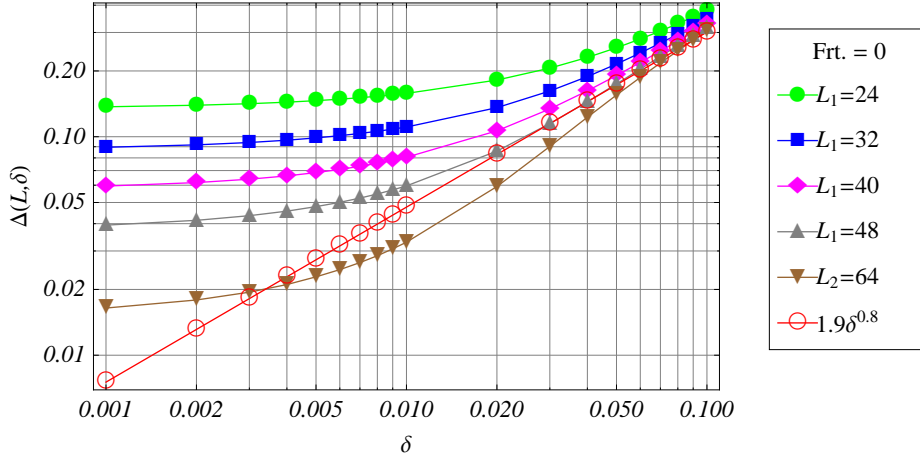


Figure 5.3: log-log plot for singlet-triplet gap with alternation parameters using CORE 1st and 2nd iteration at range-2.

necessary for this problem, as the required quantities like energy densities and gap are already converged resulting in the convergence of the critical exponents.

| CORE Algorithm range-2 | | | | | | | |
|------------------------|--------------|------------------|-----------------------------|---------------------|--------------|------------------|----------------------|
| Energy Stabilization | | | | Singlet-Triplet Gap | | | |
| Itr.No. | Micro. Sites | Critical Co-eff. | Critical Expt. Energy Stab. | Itr.No. | Micro. Sites | Critical Co-eff. | Critical Expt. (Gap) |
| 1 | 48 | 0.670457 | 1.74154 | 1 | 24 | 1.5921 | 0.6552266 |
| 2 | 192 | 0.390588 | 1.45349 | 1 | 32 | 1.84599 | 0.734252 |
| 3 | 768 | 0.348796 | 1.39186 | 1 | 40 | 2.07358 | 0.801299 |
| 4 | 3072 | 0.339407 | 1.37692 | 1 | 48 | 2.26394 | 0.854373 |
| 5 | 12288 | 0.33713 | 1.37321 | 2 | 64 | 2.54031 | 0.921435 |

Table 5.1: critical exponents by CORE simulations at range-2

The range-2 results are shown in the table (5.1), indicating the convergence of critical exponent of the energy stabilization with the increasing CORE iterations but it is not the case with gap exponent.

5.4 CORE Simulations For (AHC) at Range-3

In the previous section, the CORE simulations were done at range-2 with four retained states. There were very good results for the critical exponent of energy stabilization, but convergence for the gap exponent was not achieved. There is also more than ground state (a singlet and a triplet) involved in case of the gap calculation. So to achieve a better accuracy, one can go for the CORE simulations at range-3 with four retained states.

For the first CORE iteration, each site has two states, so for the 1st CORE iteration at range-3, one can take the single block of six microscopic sites. This makes the dimensions of single block hamiltonian as $2^6 = 64$, the dimensions of the super block range-2 hamiltonian becomes $2^{12} = 4096$ and that of the super block range-3 hamiltonian becomes $2^{18} = 262144$. The dimension of range-3 super block is touching the limits of the available computational resources as indicated in the section (5.2). With the four retained states, the lowest eigen values and eigen vectors needed from the super block range-2 hamiltonian is $M^R = 4^2 = 16$ and for the super block range-3 is $M^R = 4^3 = 64$. These are the minimum number of eigenvectors required, if there is no zero scalar product between the tensor product states of the retained states of the two single block hamiltonian and that of the super block exact lowest eigen states. Suppose there may be some exact eigen states whose scalar product with the tensor product states of the single block may be zero, one should find some extra lowest states of the super block range-2 and range-3 hamiltonian so that during the simulations, there will be no interruption. So one can find 40 lowest states for the super block range-2 instead of $M^R = 4^2 = 16$ and 200 lowest states instead of $M^R = 4^3 = 64$ for the super block range-3 hamiltonian. For the single block only four lowest eigen values and eigen states are needed. Now these are the inputs for the range-3 simulation. It is to be noted that to find the lowest eigen values and the eigen vectors of the hamiltonian matrices of the dimensions $2^{18} = 262144$ is the time consuming job. The hamiltonian matrices are not so much sparse, so it increases the time consumption of the computations at range-3 as compared to the time consumption of range-2 computation as done in the previous section.

Another issue while addressing the CORE iteration at range-3 is the dimension of the input hamiltonians in the CORE algorithm after the 1st CORE iteration. After the first iteration each renormalized site has four states. For example the dimension of the renormalized super block range-3 hamiltonian will be $4^{18} = 68719476736$. The hamiltonian with this dimension cannot be written in the available computational resources as discussed in section (5.2). So the blocking scheme used for the CORE 1st iteration cannot be used for the CORE 2nd iteration. From CORE 2nd iteration onwards, even four renormalized sites per single block is impractical, as in this case the dimensions of the super block renormalized range-3 hamiltonian will be $4^{12} = 16777216$. Even the hamiltonian of this dimensions is impractical to the available computational resources. The practical number of renormalized sites with four retained states come at three renormalized sites per single block, where the dimension of the super block range-3 hamiltonian becomes $4^9 = 262144$. But this option also becomes impractical due to time factor involved to diagonalize the hamiltonian at each iteration step. So the most practical blocking scheme after 1st CORE iteration at range-3 is two renormalized sites per single block. The dimension of super block range-3 hamiltonian in this case will be $4^6 = 4096$. So the main time consumption in this case will be in the 1st CORE iteration (as it involves diagonalizing a super block range-3 hamiltonian of the dimension of $2^{18} = 262144$). It is also seen that making a small block in the 2nd CORE iteration step will have no major effects on the accuracy of the results, as for the 2nd CORE iteration single renormalized block still represents the 12 microscopic sites, making 24 microscopic sites for range-2 super block and 36 microscopic sites for the range-3 super block. These renormalized hamiltonians even have more effective microscopic sites than that of the microscopic sites of the first CORE iteration. In this range-3 simulation, due to the two renormalized sites single block from 2nd CORE iteration onwards, the microscopic sites do not increase rapidly with the increasing CORE iterations. There will be 576 microscopic sites compared to 12228 sites reached in the previous range-2 scheme for going to six renormalized sites at 5th CORE iteration. So one has to look at 4th and 5th CORE iteration for the results. The range-3 simulations are more accurate than the range-2 simulations, therefore the results from even higher CORE renormalization iterations are acceptable. It is also noted that the matrix of the dimension $2^{18} = 262144$ is to be diagonalized by the Arnoldi method only once in the

CORE iterations for each alternation, so timing requirements do not considerably increase with the increasing CORE iterations. One can now start simulations for finding critical exponents using this scheme.

5.4.1 Critical Exponent for the Energy Stabilization at Range-3

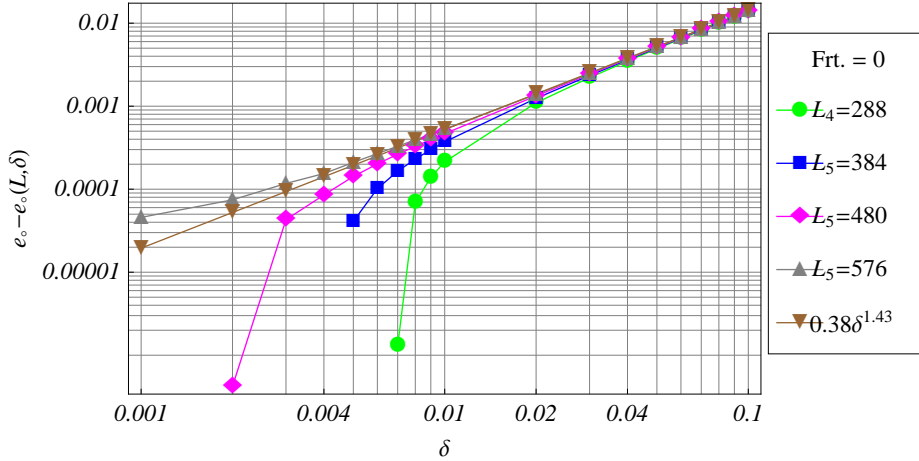
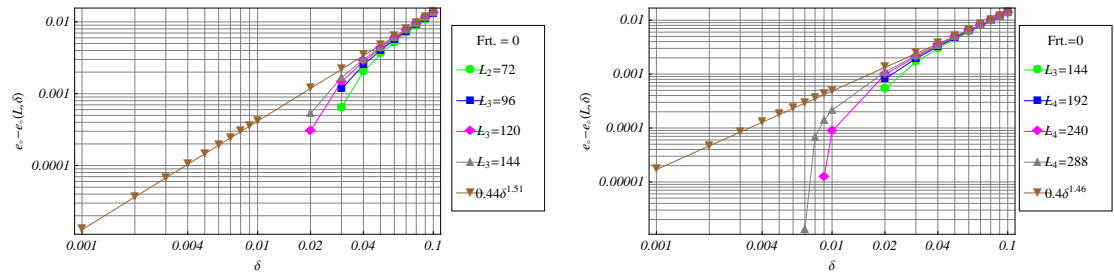


Figure 5.4: log-log plot of Energy Stabilization with alternation parameters. Hamiltonians are made from CORE 4th and 5th iterations at range-3.

In plot (5.4), energy difference of the uniform Heisenberg chain with that of alternating Heisenberg chain with alternation parameter δ is plotted with alternation parameter δ . The renormalized hamiltonian are made using the results from CORE 4th and 5th renormalization transformation Iterations. The results of the range-3 calculation endorse the results of the range-2 calculation, with the exception that range-3 results follow the Cross-Fisher Power Law upto the alternation parameter of 0.008 as opposed to 0.02 for the range-2. This also matches calculation from Papenbrock [51], but that simulation is done with lattice size of $L = 576$, which is a bigger lattice from the lattice size of $L = 192$ used in the study [51]. This shows that at lattice chain length at $L = 576$, the system is already at the thermodynamics limit.

The plot (5.5a) shows that thermodynamics limit is not reached for CORE 2nd and 3rd iteration equivalent to 144 microscopic sites. So one has to go for CORE 3rd and 4th iteration equivalent to 288 microscopic sites. Here the convergence for the energy stabilization can be seen. So for observing critical properties, one has go at least 288 sites for alternating Heisenberg chain.



(a) log-log plot for energy stabilization using CORE 2^{nd} and 3^{rd} iteration. (b) log-log plot for energy stabilization using CORE 3^{rd} and 4^{th} iteration.

Figure 5.5: Energy stabilization for (AHC) with CORE simulations at range-3.

5.4.2 Critical Exponent for the Gap for (AHC) at Range-3

The reason for doing the CORE simulations at range-3 for the alternating Heisenberg chain (AHC) is to find the improved convergence of the critical exponent of the singlet-triplet gap with the increasing CORE renormalization iterations.

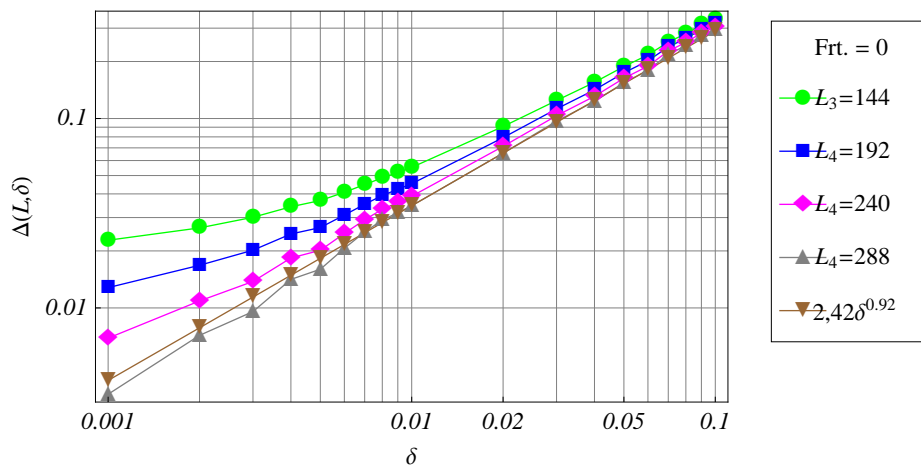
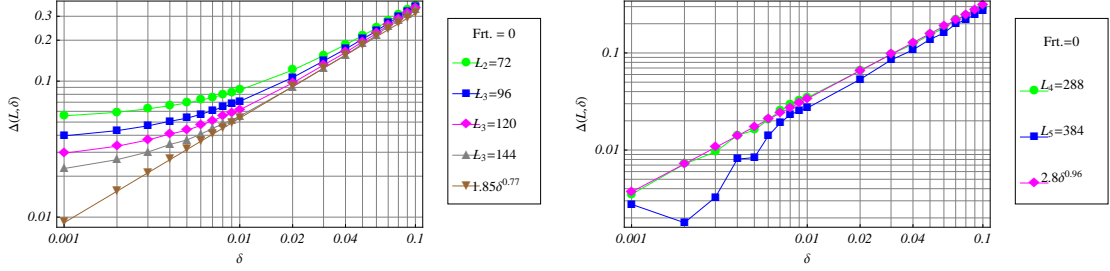


Figure 5.6: log-log plot of singlet-triplet gap with alternation parameters using CORE 3^{rd} and 4^{th} -iterations at range-3.

In the figure (5.6), the evolution of the singlet-triplet gap is plotted with the alternation parameter δ using CORE 3^{rd} and 4^{th} -iterations.

In the plot (5.7), a relatively good convergence for the spin gap critical exponent with the increasing number of CORE iterations.

5.5. CORE SIMULATIONS FOR (AHC) AT RANGE-3, BIGGER ITERATED SINGLE BLOCKS



(a) log-log plot for the singlet-triplet gap using CORE 2^{nd} and 3^{rd} iteration. (b) log-log plot for the singlet-triplet gap using CORE 4^{th} and 5^{th} iteration.

Figure 5.7: singlet-triplet gap with CORE simulations at range-3.

The CORE-simulation at range-3 give good convergence for both the energy stabilization and singlet-triplet gap critical exponents. However for exploring the CORE algorithm further, the available computational resources allow to go a step further, i.e., to make single block of three renormalized sites from 2^{nd} CORE iteration onwards at range-3. This will be topic of study in the next section.

| CORE Algorithm at range-3 | | | | | | | |
|---------------------------|--------------|------------------|-----------------------------|---------------------|--------------|------------------|----------------------|
| Energy Stabilization | | | | Singlet-Triplet Gap | | | |
| Itr.No. | Micro. Sites | Critical Co-eff. | Critical Expt. Energy Stab. | Itr.No. | Micro. Sites | Critical Co-eff. | Critical Expt. (Gap) |
| 1 | 36 | 0.954598 | 1.92326 | 1 | 36 | 1.79155 | 0.6552266 |
| 2 | 72 | 0.548715 | 1.63272 | 2 | 72 | 2.04561 | 0.734252 |
| 3 | 144 | 0.438115 | 1.51173 | 3 | 144 | 2.31861 | 0.814229 |
| 4 | 288 | 0.39545 | 1.45591 | 4 | 288 | 2.41438 | 0.885019 |
| 5 | 576 | 0.376381 | 1.42873 | 5 | 384 | 2.80356 | 0.959777 |

Table 5.2: critical exponents with increasing lattice sizes with CORE simulations at range-3.

5.5 CORE Simulations For (AHC) at Range-3, Bigger iterated single Blocks

The CORE algorithm at range-3 gives better results both for the critical exponents of the energy stabilization and the gap as seen in the section (5.4). Bigger blocks in CORE simulations give better results. The available computational resources allow to make single block of three renormalized sites from 2^{nd} CORE iteration onwards. This makes dimensions of the super-block range-3 from 2^{nd} CORE iteration onwards $4^9 = 262144$. The trade-off will be the increase in the computational time. Due to time constraints, the simulations will be done for only three CORE iterations. The drawback of computing only three CORE iterations is that the renormalized hamiltonian of only 324 microscopic sites are reached. At this lattice length, the infinite length behaviour should set in [64], but from the CORE simulation study, this much lattice length is not enough for the finding the critical exponents showing the true infinite lattice behaviour. Therefore a proper convergence will not been seen but the results can be compared for the same

number of sites of other numerical studies. The aim of this study is to see how bigger blocks for the subsequent CORE iteration after the first CORE iteration improve the results.

5.5.1 Critical Exponent for the Energy Stabilization for (AHC) at Range-3 (Bigger Blocks)

In the plot (5.8), the renormalized hamiltonian are made using the results from CORE 2^{nd} and 3^{rd} renormalization transformation Iterations. The plots endorse the results for the critical exponents of the energy stabilization from the previous sections. The overlap of the energy stabilization with that of the power law exists for the alternation span between 0.02 to 0.1. As from previous range-3 study, the overlap was for the alternation span of 0.008 to 0.1, but for equivalent 576 microscopic sites. This result shows that at 324 microscopic sites, the thermodynamics limit is not reached.

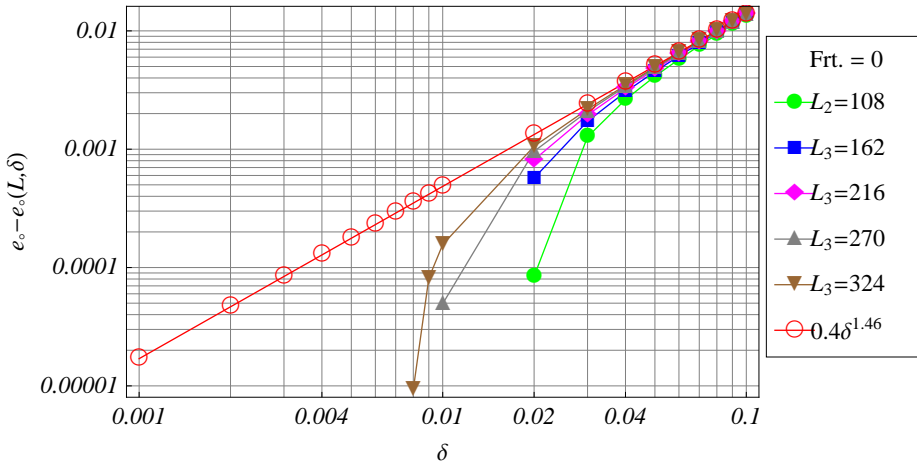


Figure 5.8: log-log plot of Energy Stabilization with alternation parameters. Hamiltonians are made from CORE 2^{nd} and 3^{rd} iterations at range-3 with bigger blocks.

5.5.2 Critical Exponent for the Singlet-Triplet Gap for (AHC) at Range-3 (Bigger Blocks)

In the figure (5.9), evolution of the singlet-triplet gap is plotted with the alternation parameter δ by the CORE algorithm using 2^{nd} and 3^{rd} iterations. The critical exponent of the spin gap is the main reason that CORE simulations to the full capacity of the available computational resources is done. This scheme has also paid-off, as for the lattice size of $L = 324$, the critical exponent of the gap is approximated to be $\alpha = 0.82$. This is a big improvement on the previous range-3 simulation results. In the plot 5.9, the curves are also seen going for convergence with the increasing size of the lattice.

5.5. CORE SIMULATIONS FOR (AHC) AT RANGE-3, BIGGER ITERATED SINGLE BLOCKS

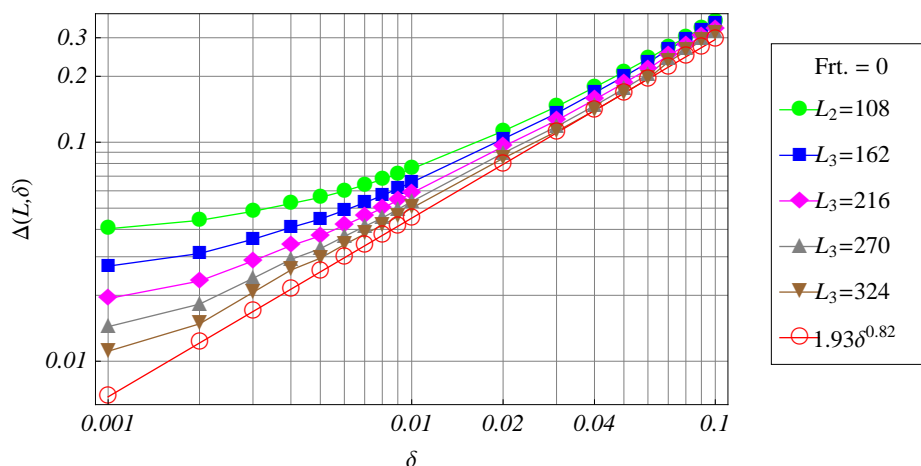


Figure 5.9: log-log plot of singlet-triplet gap with alternation parameters. Hamiltonians are made from CORE 2nd and 3rd iterations at range-3 with bigger blocks.

| CORE Algorithm range-3 Bigger Blocks | | | | | | | |
|--------------------------------------|--------------|------------------|-----------------------------|---------------------|--------------|------------------|----------------------|
| Energy Stabilization | | | | Singlet-Triplet Gap | | | |
| Itr.No. | Micro. Sites | Critical Co-eff. | Critical Expt. Energy Stab. | Itr.No. | Micro. Sites | Critical Co-eff. | Critical Expt. (Gap) |
| 1 | 36 | 0.954833 | 1.92336 | 1 | 36 | 1.71533 | 0.653433 |
| 2 | 108 | 0.474981 | 1.55506 | 2 | 108 | 1.76164 | 0.694697 |
| 3 | 324 | 0.395563 | 1.45575 | 3 | 324 | 1.92729 | 0.815797 |

Table 5.3: critical exponents of energy stabilization and gap by CORE simulations at range-3 with bigger blocks

5.6 Renormalization Flow of the alternation Parameter δ , couplings J

CORE allows to find the renormalization flow of the alternation parameter and the couplings against the starting alternation parameters. The method undertaken to find the renormalization flow from the CORE algorithm has a constraint requiring the renormalized hamiltonian to be of the same form as that of the starting hamiltonian. It restricts only two retained states in a single block for CORE simulations. It excludes many configurations of the CORE simulations, which are giving good results as discussed in this chapter.

There were extensive simulations with different input parameters for the CORE simulations to find the best results. It was found that a single block of considerable number of even sites with four retained states (a singlet and triplet) gives the most accurate results. So the optimum configurations for the alternation Heisenberg model have more than two retained state along with other requirements. In case of the four retained states, the renormalized hamiltonian does not keep the form of the original hamiltonian. This results in new form of the renormalized hamiltonian having new types of the renormalized parameters. These new parameters can be found by introducing a orthonormal basis of the renormalized hamiltonian. Then new relevant parameters corresponding to the starting parameters in the new form of renormalized hamiltonian can be found.

For studying the renormalization flow of the original parameters, the scheme followed in this work is with two retained states resulting in the renormalized hamiltonian of the same form as that of the original hamiltonian. The other parameters are five site single block at range-3. This scheme did not give the desired results as in the previous simulations of this chapter due to which it was discarded. Therefore using this scheme, one does not expect to find the results, but only a generalized behaviour. Another consideration is to not going beyond the 1st CORE iteration. This will led to the renormalized hamiltonian equivalent to 25 microscopic sites, not enough for study an infinite converged behaviour.

To draw such a diagram, the starting hamiltonian can be viewed as consisting of two alternating coupling terms as called strong couplings $J(1 + \delta)$ and weak couplings $J(1 - \delta)$ [67]. Once the renormalized couplings corresponding to these are found, the renormalized J^1 and δ^1 renormalized alternations after the 1st CORE iteration can be known.

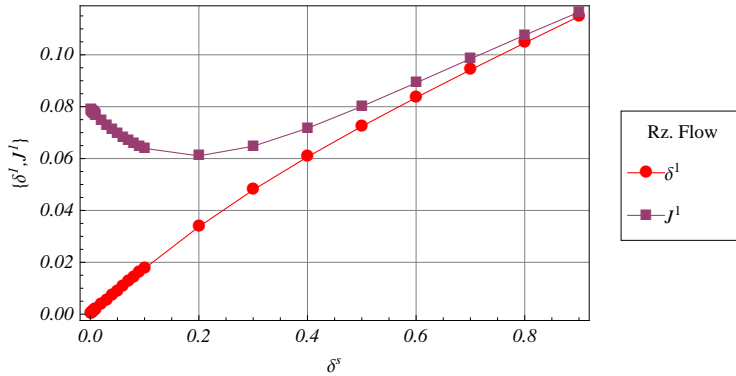


Figure 5.10: Renormalization flow of coupling J and alternation parameter δ

The renormalization flow diagram (5.10) shows the renormalized parameters $\{J^1, \delta^1\}$ going to the same accumulation point. This is consistent with reference [67]. Beyond this no further information can be extracted as the plot (5.10) is not showing the bulk behaviour.

5.7 Conclusion

In this chapter, CORE algorithm is used to investigate the critical behaviour of spin- $\frac{1}{2}$ alternating Heisenberg chain (AHC). The CORE simulations are done for finding the critical behaviour of singlet-triplet gap and energy stabilization. These two quantities are approximated from the renormalized hamiltonians as simulated from the CORE algorithm, for the alternation span of values from 0.001 to 0.1. Three different schemes with individual parameters were used to carry out the CORE simulations. One of the schemes is range-2, while the other two schemes are range-3. In these simulations, the approach of the energy density of uniform Heisenberg model to the energy density of the alternating Heisenberg model (AHC) is plotted against the alternations. This evolution of the energy density difference also called energy stabilization is described by the Cross-Fisher power law $B\delta^\beta$, where β is the critical exponent of the energy stabilization and B is a constant. Similarly the evolution of gap with alternation parameter δ in the alternating Heisenberg model is described by the Cross-Fisher power law $A\delta^\alpha$, where α is the critical exponent of the gap and A is a constant.

By using the range-2 simulations, the value of critical exponent of energy stabilization β is approximated to be $\beta = 1.45$, while that of the co-efficient of the power law is $B = 0.39$ for the lattice size of $L = 192$ sites. This result is approximately the same as that by Papenbrock [51]. The power law is approximately obeyed for the alternation span starting from 0.02 to 0.1 for the CORE range-2 simulations. Further, the CORE simulations with increasing iterations were also done. At 5th CORE iteration, there is a total convergence of the energy stabilization. It is also interesting that at the 5th-CORE iteration corresponding to the microscopic lattice size of 12288, the critical exponent of the energy stabilization is approximated to be 1.37, which is very close to the critical exponent 1.33 as found by Cross-Fisher [55]. The critical exponent of the singlet-triplet gap by using the range-2 simulations does not show convergence with the increasing CORE iterations. The critical exponent of the singlet-triplet gap at range-2 simulations has good estimates by using only CORE first or second iterations. At the first CORE iteration, one gets the gap exponent $\alpha = 0.80$ and coefficient $A = 2.07$, for four renormalized sites, corresponding to the microscopic lattice size of $L = 32$. These values are only of symbolic nature showing that the critical behaviour of the gap follows the Cross-Fisher power law, but the convergence is not achieved with the increasing CORE iterations.

The non-convergence of the gap plots in the range-2 CORE simulations is the reason that CORE range-3 simulations are also done for the evaluation of the critical exponents. Two schemes for range-3 CORE simulations were followed. In the first scheme, a single-block of six sites was used for the first CORE iteration, while from 2nd CORE iteration onwards, a single block is made of two renormalized sites. In the second scheme, a single block of six renormalized sites was used like the first scheme, while from 2nd iteration onwards, a single block is made of three renormalized sites.

In the first scheme, the approximated critical exponent of the energy stabilization is again 1.42 for the 5th CORE iteration for lattice size of $L = 576$. This critical exponent is again consistent with the critical exponent of other studies [51]. But due to the smaller size of the single block used in the CORE range-3 simulations from 2nd iteration onwards, one does not go to the lattice sizes large enough to see total convergence by CORE algorithm, as seen by range-2 simulations. There is an improvement achieved in the gap exponent of the alternating Heisenberg

model. For the 2nd CORE iteration, the critical exponent of the gap is 0.73 for the lattice size of $L = 72$. Even for the 3rd and 4th iteration the approximation for the critical exponent for the gap remains 0.80 and 0.85 for the microscopic lattice sizes of $L = 144$, $L = 288$, which is quite significant improvement over the range-2 simulations considering the errors involved in going to the higher CORE iterations.

In the previous range-3 scheme, the critical exponents for the energy stabilization and the gap were calculated. While the critical exponent for the energy stabilization converged to a value consistent with other numerical studies, the critical exponent of the gap gives good results for upto 4th CORE iteration. Considering using the available computational resources to their maximum, the simulations are also done with the second scheme of the range-3 core algorithms as stated earlier. Due to the large time involved in these simulations and the number of alternations for which the simulations are to be carried out, the total number of CORE iterations is restricted to three. In this scheme, the results for the critical exponent of the energy density as calculated earlier are verified. In the 3rd CORE iteration the critical exponent of the energy density is approximated to be 1.46, which is consistent with other CORE simulations and other numerical studies. The critical exponent of the gap definitely improved from the first scheme of the range-3 simulations, as it approximates $\alpha = 0.82$ for the 3rd CORE iteration corresponding to the microscopic lattice size of $L = 324$. Approximately for the same microscopic lattice size, in the first scheme of range-3, the critical exponent for the gap is found to be 0.88. It is seen that both schemes are giving respective good results, and having a bigger blocks at any CORE iteration improves results even better. However, to have an insight in the critical behaviour of the system, using large single blocks at the first CORE iteration is enough and one can carry on simulations with smaller blocks from 2nd iteration onwards.

So by using the CORE algorithm, critical exponent of the gap and the energy stabilization is approximated to be $\alpha = 0.82$ and $\beta = 1.46$ respectively. These exponents are generally following the power law in the span of alternations from 0.008 to 0.1 for range-3 simulations. The results are compatible with Papenbrock [51], which are done for even smaller lattice sizes than the lattice sizes CORE algorithm allowed to undertake. These results can also be compared for percentage error with the DMRG-extrapolated results as in [52]. The approximations for the critical exponents of the energy density and the gap at CORE range-3 simulations have a difference of 1% and 9% respectively, from that of the DMRG-extrapolated results for infinite limit.

Chapter 6

Heisenberg spin- $\frac{1}{2}$ Chain with Alternations and Frustrations

In the previous chapter, CORE algorithm was used to find the co-efficients and the critical exponents of the power laws for the energy stabilization as well as for the singlet-triplet gap for the spin- $\frac{1}{2}$ alternating Heisenberg chain (AHC). The span of alternations for which these power laws are valid were also be found by CORE simulations. In the antiferromagnetic system, the inclusion of the frustration is another topic of interest [63]. So one can add the frustration in spin- $\frac{1}{2}$ alternation Heisenberg chain with nearest neighbour interactions. Frustration can be introduced in the antiferromagnetic hamiltonian, by the introduction of J_2 , the next-nearest (second-nearest) coupling as

$$H = \sum_{j=1}^L J [1 - \delta (-1)^n] \vec{S}_j \cdot \vec{S}_{j+1} + J_2 \vec{S}_j \cdot \vec{S}_{j+2} \quad (6.1)$$

where δ is the alternation parameter, J is the nearest neighbour coupling that will be taken as 1, i.e., $J = 1$, and $J_2 > 0$ is the next-nearest neighbour coupling. It is a typical model for competing interactions (frustration). To recover the spin- $\frac{1}{2}$ uniform Heisenberg chain hamiltonian, one has to put alternations and frustrations equal to zero. i.e., ($\delta = 0, J_2 = 0$) in the equation (6.1).

At ($\delta = 0, J_2 = 0$), the ground state of the hamiltonian (6.1) has gapless excitation and is called the spin-fluid state. While in case of ($\delta = 0, J_2 = \frac{1}{2}$), the ground state of the system is the dimer state [60, 61] and there will be an excitation gap between the ground state and the first excited state. This shows the scaling of the gap depends on J_2 . From these facts, one can say that there will be fluid-dimer transition in the ground state at ($\delta = 0, J_2 = J_{2c}$) between ($\delta = 0, J_2 = 0$) and ($\delta = 0, J_2 = \frac{1}{2}$). With the help of conformal field theory, the value of the transition point is found to be $J_{2c} = 0.2411 \pm 0.0001$ [59].

At ($\delta = 0, J_2 = 0$), in the equation (6.1), the spin- $\frac{1}{2}$ Heisenberg antiferromagnetic chain with frustration converts into the uniform spin- $\frac{1}{2}$ Heisenberg chain. The energy density of the uniform Heisenberg chain in the thermodynamic limit can be written as $e_o (J_2 = 0) = \frac{1}{4} - \ln 2$ and the vanishing singlet-triplet gap can be written as $\Delta (J_2 = 0) = 0$.

At ($\delta = 0, J_2 \leq J_{2c}$), in the equation (6.1), the energy density of the alternating Heisenberg chain in the thermodynamic will be found by using the CORE algorithm, and there will be vanishing singlet-triplet gap can be written as $\Delta (\delta = 0, J_2 \leq J_{2c}) = 0$.

The gap in the Heisenberg hamiltonian with finite frustrations ($\delta = 0, J_2 > 0$) opens at $J_{2c} = \frac{J_2}{J_1} = 0.2411$ and it is also the transition point of this system from magnetic to non-magnetic

ground state [59]. The simulations with CORE will in the region of magnetic state.

The first quantity, for which the critical behaviour of this model is to be studied is energy per spin or energy density defined as

$$e_o(\delta, J_2) = \frac{E_o(\delta, J_2)}{L} \quad (6.2)$$

where $E_o(\delta, J_2)$ is the total energy of the hamiltonian (6.1) with alternations δ and frustration J_2 , computed at the microscopic lattice length L . $e_o(\delta, J_2)$ is the energy per spin of the same system.

The second quantity for which the critical behaviour is to be studied is the singlet-triplet gap defined as

$$\Delta(\delta, J_2) = E_1(\delta, J_2) - E_o(\delta, J_2) \quad (6.3)$$

Where $E_1(\delta, J_2)$ is the first excited state, which is a spin-triplet for the hamiltonian (6.1) with even number of sites.

The power law for the spin gap with the introduction of frustration can be stated as [52]

$$\Delta(\delta, J_2) = A\delta^\alpha \quad (6.4)$$

where α is the critical exponent of the gap and A is the coefficient of the power law.

and that of the energy stabilization as

$$e_o(0, J_2) - e(\delta, J_2) = B\delta^\beta \quad (6.5)$$

where β is the critical exponent of the energy stabilization and B is the coefficient of the power law.

The computation of the term $e_o(0, J_2)$ can also be discussed. In case of the power laws with both alternation and frustration to be zero, the energy density is understood to be $e_o(0, 0) = \frac{1}{4} - \ln 2$. So there was no need to find the value of $e_o(0, 0)$ with CORE algorithm or any other numerical technique. But in the case of finite frustration ($J_2 \neq 0$), the term $e_o(0, J_2)$ is to be calculated using the CORE algorithm. These bulk limit energy density for particular frustrations are calculated in some papers like [64, 65], but are not given for the entire range of the frustrations $\{0.05, 0.1, 0.15, 0.2, 0.2411\}$ planned for this chapter. These values by other techniques also have their own percentage errors, but these values from CORE simulations are accurate enough to give us reasonable critical exponents of the power laws.

| Bulk Energy Density of (AHC) with Frustration | | | |
|---|-------------------|--|--|
| Sr.No. | Frustration J_2 | CORE Algo. range-2 $e_o(\delta = 0, J_2)$ | CORE Algo. range-3 $e_o(\delta = 0, J_2)$ |
| 1 | 0.05 | -0.4345 | -0.4338 |
| 2 | 0.1 | -0.425925 | -0.425005 |
| 3 | 0.15 | -0.417631 | -0.416464 |
| 4 | 0.2 | -0.409637 | -0.408211 |
| 5 | 0.2411 | -0.403336 | -0.401692 |

Table 6.1: The bulk energy density of (AHC) with Frustration with CORE algorithm at range-2 and range-3

The bulk limit value of the energy density for CORE range-2 simulations is calculated by using CORE algorithm 2^{nd} iteration, three renormalized sites, equivalent to 96 micro-sites. For the range-3 simulations, the bulk energy density is taken from CORE 4th iteration at range-3 with six renormalized sites, equivalent to 288 micro-sites.

6.1 Renormalization Flow of parameters J_2 and J_1

By setting alternation parameter ($\delta = 0$) in (6.1), the Heisenberg model of competing interactions is obtained as given by

$$H = \sum_{j=1}^L J_1 \vec{S}_j \cdot \vec{S}_{j+1} + J_2 \vec{S}_j \cdot \vec{S}_{j+2} \quad (6.6)$$

The ground state of the hamiltonian (6.6) is already discussed. There will be a phase transition from the spin fluid state to dimer state with increasing next nearest neighbour from $J_2 = 0$ to $J_2 = \frac{1}{2}$. The critical point of this phase transition can also be calculated by using the CORE algorithm. In order to plot the renormalization flow diagram of the competing interactions against the starting ratio, the simulations were done with single block consisting of odd number of sites and retaining two states. Due to two retained states, the renormalized hamiltonian keeps its original form, helping in finding the renormalization flow of the renormalized parameters ratio $\frac{J_2}{J_1}$. In case of the four retained states, the renormalized hamiltonian does not keep the original form of hamiltonian. This new form of the renormalized hamiltonian has new renormalized parameters instead of the renormalized parameters J_1 and J_2 corresponding to the original hamiltonian.

For studying the renormalization flow of the original parameters, the scheme followed in this work is with two retained states giving the renormalized hamiltonian the same form as that of the original hamiltonian.

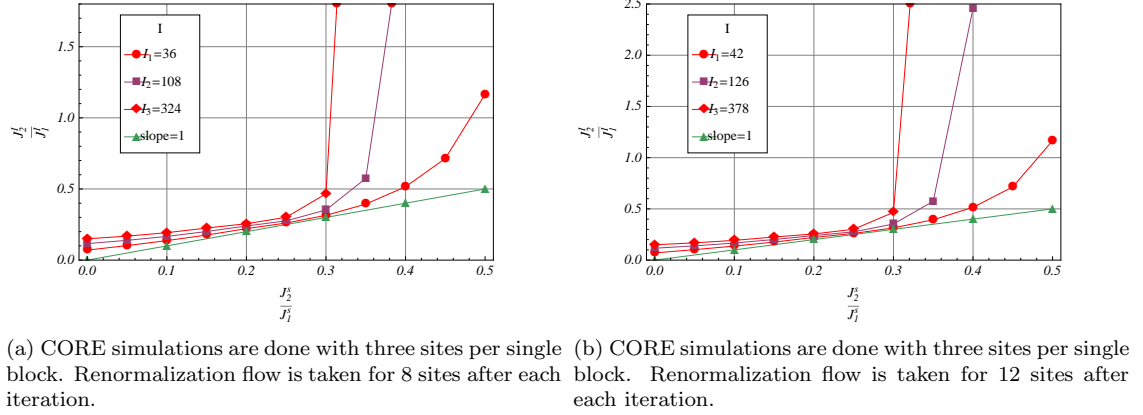
6.1.1 Renormalization Flow of competing interactions $\frac{J_2}{J_1}$ using CORE Simulations

Having decided that there should be only two retained states in a single block hamiltonian, the option remains for deciding the number of odd sites in a single block. To remain within the limits of the available computational resources (2^{18} dimensional matrices), two range-3 schemes can be followed. In the first scheme, the single block with three single sites is chosen while in the second scheme a single block with five sites is chosen. Doing large number of CORE iterations involve accumulation of approximation and numerical errors, only three CORE iterations are done. These number of CORE iterations are also enough for finding the phase transition point.

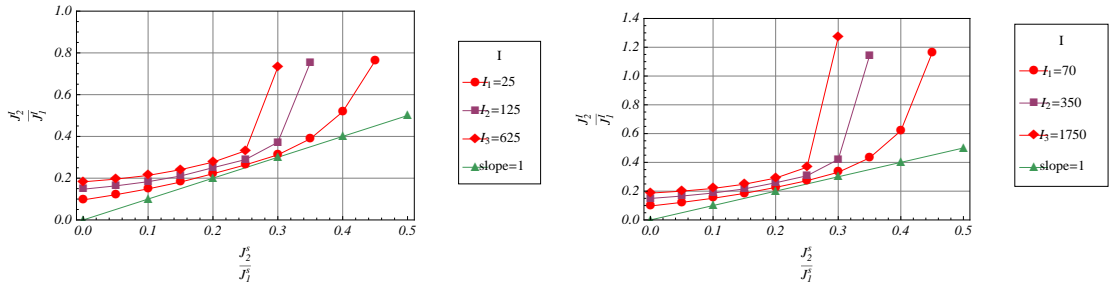
The second aim is to draw renormalization flow diagrams for sufficiently big lattices of varying sizes, so that the finite size effects are removed. Therefore the renormalized hamiltonians are made from the first three consecutive iterations for more renormalized sites than that of the number of sites in a single block taken during the CORE simulations.

The plots (6.1) are made from the CORE simulations, scheme-1. The CORE simulations are done with three sites single block with two retained states. Similarly the plots (6.2) for CORE scheme-2 are made by making single block of five sites with two retained states. In both the cases CORE simulations are done for three iterations.

The phase transition point can be found by following the procedure as given in reference [67]. The renormalization flow curves show an interesting behaviour. These multiple curves of varying lattice sizes have a minimum distance point from the straight line of slope 1. This point

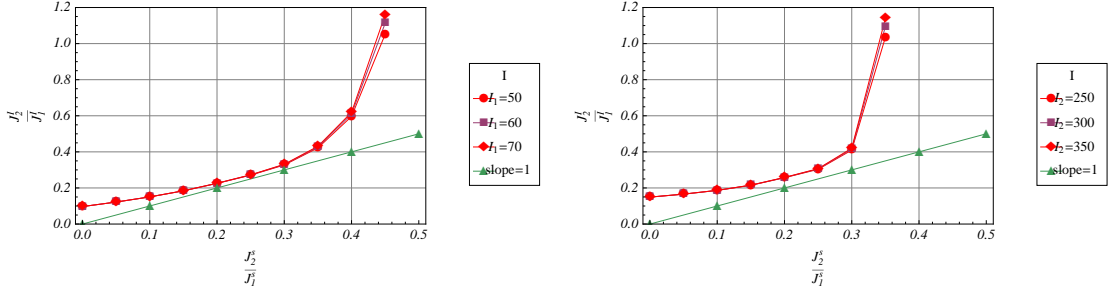

 Figure 6.1: Renormalization Flow of parameter $\frac{J_2^I}{J_1^I}$ with respect to starting ratio $\frac{J_2^S}{J_1^S}$

corresponds to the phase transition point [67]. The plots (6.1,6.2) have a resolution of 0.05. So the most relevant point in the vicinity of exact phase transition point is 0.25. The curves corresponding to different CORE iterations converge for the same minimum distance at 0.25. There is one more notable difference with the plots given in reference [67], where curves come close to the straight line of slope 1 on increasing the lattice length. In the CORE simulations, on increasing lattice length the minimum distance between the curve and the straight line increases until the lattice length is reached where all these curve converge. The CORE simulations for small size finite lattices are good enough to give the approximate phase transition point. There are several factors that can be responsible for this anomaly. The CORE simulations are done with the constraint of keeping the renormalized hamiltonian of the same form as the original hamiltonian. So the best configuration for CORE simulations for these types of model are excluded. It can also be due to the accumulated error for bigger lattice sizes. To find the phase transition point accurately one can switch to bisection method, but considering the constraints and the resolution of competing interactions taken for the simulations, 0.25 is a good enough estimate.


 Figure 6.2: Renormalization Flow of parameter $\frac{J_2^I}{J_1^I}$ with respect to starting ratio $\frac{J_2^S}{J_1^S}$

6.1.2 Critical Coupling (at bulk limit)

CORE also allowed to study the renormalization flow of the competing couplings $\frac{J_2}{J_1}$ at the bulk limit. The critical coupling was found by using the renormalization flow and then by switching to extrapolation in reference [67], given by $\frac{J_2}{J_1} = 0.241915$, while the exact value of the critical coupling is $\frac{J_2}{J_1} = 0.241167$. Using CORE, a different approach is undertaken based on finding the infinite limit behaviour. The CORE simulations will be done with parameters giving the best results, while remaining within the constraint. These parameters are five site single block with two retained states (constraint) at range-3.



(a) CORE simulations with five sites per single block. Renormalized hamiltonians are made taking $\{10, 12, 14\}$ renormalized sites after 1st CORE iteration. (b) CORE simulations with five sites per single block. Renormalized hamiltonians are made taking $\{10, 12, 14\}$ renormalized sites after 2nd CORE iteration.

Figure 6.3: Renormalization Flow of parameter $\frac{J_2^I}{J_1^I}$ with respect to starting ratio $\frac{J_2^s}{J_1^s}$

It is seen from the plots (6.3,6.4), showing the infinite limit behaviour that the renormalization flow of competing interactions takes a very sharp turn with respect to line of slope 1. This sharp turn is recognizable on the plots with small span of very precise scale. Therefore the point of minimum distance from the line of slope 1 is recognizable with the starting ratio of the competing couplings. It is also seen that with the increasing lattice sizes, the curves on the side of $\frac{J_2}{J_1} < \left(\frac{J_2}{J_1}\right)$ show a very good convergence.

For finding the bulk limit behaviour, one goes for finding the renormalized hamiltonian for large number of renormalized sites after each iteration. One can also go for 4th CORE iteration. The method used in the reference ([67]) can be applied for lattices of different finite sizes. This technique is already used in the previous section to find the approximate results. However, this technique seems not working, when the scale of input competing interactions is made more precise. The reason is that the overall span of the competing interactions has to be reduced due to the large number of the simulations involved. This results in the straight lines showing the renormalization flow of the competing interactions. It is very difficult to judge the point of minimum distance from the line of slope 1. This behaviour is shown in the figure (6.5a). Although the critical coupling point can be estimated, but going for infinite behaviour, the critical coupling point becomes more evident.

Therefore a plot of renormalization flow of the competing couplings is made in the vicinity of critical couplings point 0.25 as found by the CORE simulations. This plot will be on a much refined scale for the starting ratio from $\frac{J_2^s}{J_1^s} = 0.230$ to $\frac{J_2^s}{J_1^s} = 0.260$ with a increment of 0.01. In this way the estimate of critical coupling can be found on a three digit scale. With going to 4th iteration, it becomes quite clear that the point of minimum distance to the line of slope 1 is $\frac{J_2^s}{J_1^s} = 0.240$. So it is the point of critical coupling on a much refined scale. There is a possibility

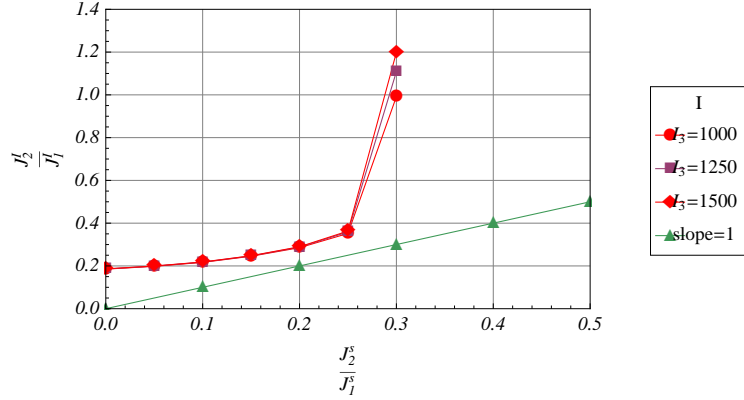
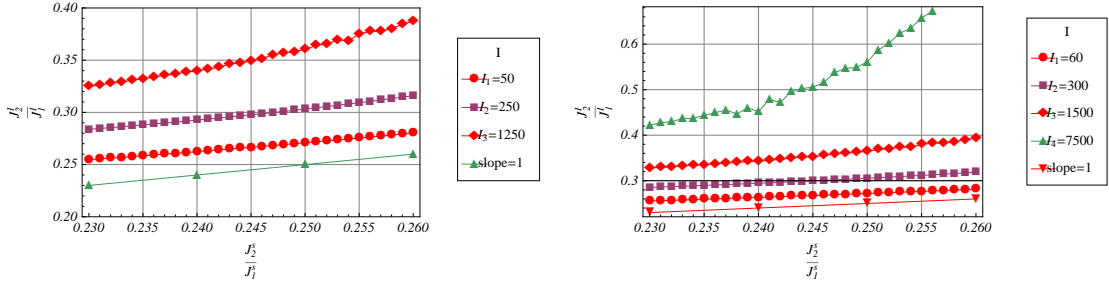


Figure 6.4: CORE simulations with five sites per single block. Renormalized hamiltonians are made taking $\{8, 10, 12\}$ renormalized sites after 3^{rd} CORE iteration.

of finding a more precise estimate using the CORE algorithm, but the available computational resources are not supporting a very large array of big matrices. The curves for the first three CORE iterations in the plot (6.5b) stack at minimum distance from the straight line of slope 1 for the critical coupling point at $\frac{J_2^s}{J_1^s} = 0.240 \pm 0.001$ showing 0.5% of error from the exact value.



(a) CORE simulations with five sites per single block. Renormalized hamiltonians also consists of 10 renormalized sites. (b) CORE simulations with five sites per single block. Renormalized hamiltonians also consists of 12 renormalized sites.

Figure 6.5: Renormalization Flow of parameter $\frac{J_2^s}{J_1^s}$ with respect to starting ratio $\frac{J_2^s}{J_1^s}$

6.2 Critical Exponents for Spin- $\frac{1}{2}$ Heisenberg model (Alternations and Frustrations)

In the previous chapter, CORE simulations were used on the alternating spin- $\frac{1}{2}$ Heisenberg chain (AHC) for finding the critical exponents of the Cross-Fisher power laws as well as the span of alternations for which the power laws were applicable. In the limit of $(\delta \rightarrow 0)$, there exists logarithmic corrections. The reason for the logarithmic corrections is the presence of marginal

operator. $H(\delta, J_2)$ as given by the equation (6.1), at $(\delta = 0, J_2 = 0)$, is not scale invariant. There exists a marginal operator which destroys the scale-invariance. The coefficient of the marginal operator decreases with increasing next nearest neighbour interactions J_2 and goes to zero at J_{2c} [52]. It means that at J_{2c} , there will be no logarithm corrections and the Cross-Fisher power laws should be obeyed for the whole (simulations) range of alternations. So by using CORE simulations, one will be able to find the coefficients and the critical-exponents and span of the alternations, for which the power laws are valid for a particular frustration. The power laws (6.4,6.5) are valid for the range of simulations ($J_2 \leq J_{2c}$) [66]. CORE simulations are done for the values of frustration $J_2 = \{0.05, 0.1, 0.15, 0.2, J_{2c} = 0.2411\}$. For all these values of frustrations, the power laws remain valid.

There will be two schemes to carry out CORE simulations for the Heisenberg alternating chain (AHC) with frustration. The first scheme is the range-2 scheme, while the second scheme is the range-3 scheme. In the first range-2 scheme, the CORE simulations are done with single block of eight sites for the first CORE iteration and four renormalized sites single block from 2^{nd} CORE iteration onwards. In the second range-3 scheme, the CORE simulations are done with single block of the six sites for the first CORE iteration and two renormalized sites single block from 2^{nd} CORE iteration onwards. In the previous chapter, there was an even one more scheme for the range-3 simulations with big blocks. In that scheme, CORE simulations were also done with single block of the six sites for the first CORE iteration and three renormalized sites single block from the 2^{nd} CORE iteration onwards. In that scheme bigger block from 2^{nd} CORE iteration onwards do give good results but it needs much more time to diagonalize the bigger hamiltonian matrices. So one can compromise on acceptable results by not going for the this scheme for simulations. All these simulations are done with four retained states single block.

6.3 CORE Simulations at range-2 for (AHC) with Frustration

The range-2 simulations are done for studying the bulk limit behaviour. Due to bigger blocks in the first and subsequent CORE iterations, the low energy renormalized hamiltonian reach upto 12228 microscopic sites corresponding to six renormalized sites in just five CORE renormalized iterations. This bulk limit behaviour has been shown by the convergence of the critical exponents of the energy stabilization.

The critical exponents of the singlet-triplet gap are not converging with the increasing CORE iterations, therefore range-2 simulations are not good for the evaluation of the gap. However, for the CORE 1^{st} and 2^{nd} iteration, there is some convergence of the singlet-triplet gap. But these renormalized hamiltonians are not describing the thermodynamics limit. The critical exponents of the gap are calculated from the 1^{st} CORE iteration, which have a symbolic value only due to small microscopic lattice sizes.

From the tables (6.2 \dots 6.6), it is seen that critical exponent of the energy stabilization show a good convergence with the increasing CORE iterations. This convergence starts to happen after 3^{rd} CORE iteration corresponding to the 768 microscopic sites. It means to study the critical behaviour at thermodynamics limits with range-2 CORE simulations, one has to go much beyond the 200 micro-sites as discussed in [64]. These approximate exponents taken from the 5^{th} CORE iteration decreases from 1.39 to 1.25 with the increasing frustrations from 0.05 to 0.2411 respectively. The alternations for which the power laws are obeyed remains within the span of 0.01 to 0.1. These converged values of the critical exponents also in agreement with other studies [52].

6.3. CORE SIMULATIONS AT RANGE-2 FOR (AHC) WITH FRUSTRATION

| CORE Algorithm at range-2, Frustration=0.05 | | | | | | | |
|---|--------------|------------------|-----------------------------|---------------------|--------------|------------------|----------------------|
| Energy Stabilization | | | | Singlet-Triplet Gap | | | |
| Itr.No. | Micro. Sites | Critical Co-eff. | Critical Expt. Energy Stab. | Itr.No. | Micro. Sites | Critical Co-eff. | Critical Expt. (Gap) |
| 1 | 48 | 0.642586 | 1.67873 | 1 | 24 | 1.69477 | 0.638219 |
| 2 | 192 | 0.423286 | 1.45661 | 1 | 32 | 1.95853 | 0.736254 |
| 3 | 768 | 0.386342 | 1.40724 | 1 | 40 | 2.18323 | 0.804413 |
| 4 | 3072 | 0.377844 | 1.39517 | 1 | 48 | 2.363 | 0.852004 |
| 5 | 12288 | 0.375759 | 1.39216 | | | | |

Table 6.2: critical exponents by CORE simulations at Range-2 with Frustrations=0.05

| CORE Algorithm at range-2, Frustration=0.1 | | | | | | | |
|--|--------------|------------------|-----------------------------|---------------------|--------------|------------------|----------------------|
| Energy Stabilization | | | | Singlet-Triplet Gap | | | |
| Itr.No. | Micro. Sites | Critical Co-eff. | Critical Expt. Energy Stab. | Itr.No. | Micro. Sites | Critical Co-eff. | Critical Expt. (Gap) |
| 1 | 48 | 0.609173 | 1.60777 | 1 | 24 | 1.80276 | 0.649379 |
| 2 | 192 | 0.4472 | 1.44347 | 1 | 32 | 2.07537 | 0.742674 |
| 3 | 768 | 0.416894 | 1.40576 | 1 | 40 | 2.29552 | 0.805142 |
| 4 | 3072 | 0.40977 | 1.396484 | 1 | 48 | 2.46389 | 0.847434 |
| 5 | 12288 | 0.408002 | 1.39414 | 2 | 64 | 2.68555 | 0.897548 |

Table 6.3: critical exponents by CORE simulations at Range-2 with Frustrations=0.1

| CORE Algorithm at range-2, Frustration=0.15 | | | | | | | |
|---|--------------|------------------|-----------------------------|---------------------|--------------|------------------|----------------------|
| Energy Stabilization | | | | Singlet-Triplet Gap | | | |
| Itr.No. | Micro. Sites | Critical Co-eff. | Critical Expt. Energy Stab. | Itr.No. | Micro. Sites | Critical Co-eff. | Critical Expt. (Gap) |
| 1 | 48 | 0.581014 | 1.53814 | 1 | 24 | 1.91207 | 0.657317 |
| 2 | 192 | 0.466309 | 1.42157 | 1 | 32 | 2.18831 | 0.744817 |
| 3 | 768 | 0.442923 | 1.39409 | 1 | 40 | 2.39858 | 0.801007 |
| 4 | 3072 | 0.437327 | 1.38728 | 1 | 48 | 2.55176 | 0.837798 |
| 5 | 12288 | 0.435929 | 1.38557 | 1 | 64 | 2.74341 | 0.879942 |

Table 6.4: critical exponents by CORE simulations at Range-2 with Frustrations 0.15

| CORE Algorithm at range-2, Frustration=0.2 | | | | | | | |
|--|--------------|-----------------|----------------------------|---------------------|--------------|--------------------|--------------------|
| Energy Stabilization | | | | Singlet-Triplet Gap | | | |
| Itr.No. | Micro. Sites | Scaling Co-eff. | Scaling Expt. Energy Stab. | Itr.No. | Micro. Sites | pre-Factor Co-eff. | Critical Expt. Gap |
| 1 | 48 | 0.555914 | 1.46868 | 1 | 24 | 2.0167 | 0.660474 |
| 2 | 192 | 0.479212 | 1.39028 | 1 | 32 | 2.28722 | 0.740671 |
| 3 | 768 | 0.462469 | 1.37141 | 1 | 40 | 2.47988 | 0.789822 |
| 4 | 3072 | 0.458404 | 1.36672 | 1 | 48 | 2.61316 | 0.82089 |
| 5 | 12288 | 0.457385 | 1.36554 | 2 | 64 | 2.77172 | 0.855307 |

Table 6.5: critical exponents by CORE simulations at Range-2 with Frustrations=0.2

| CORE Algorithm at range-2, Frustration=0.2411 | | | | | | | |
|---|--------------|-----------------|----------------------------|---------------------|--------------|--------------------|--------------------|
| Energy Stabilization | | | | Singlet-Triplet Gap | | | |
| Itr.No. | Micro. Sites | Scaling Co-eff. | Scaling Expt. Energy Stab. | Itr.No. | Micro. Sites | pre-Factor Co-eff. | Critical Expt. Gap |
| 1 | 48 | 0.456211 | 1.31089 | 1 | 24 | 2.0932 | 0.658131 |
| 2 | 192 | 0.417072 | 1.26325 | 1 | 32 | 2.35003 | 0.731053 |
| 3 | 768 | 0.408055 | 1.2516 | 1 | 40 | 2.52218 | 0.773895 |
| 4 | 3072 | 0.40584 | 1.2487 | 1 | 48 | 2.63602 | 0.80016 |
| 5 | 12288 | 0.405284 | 1.24797 | 2 | 64 | 2.76612 | 0.828498 |

Table 6.6: critical exponents by CORE simulations at Range-2 with Frustrations=0.2411

6.4 CORE Simulations at range-3 for AHC with Frustration

The main advantage of going to range-3 simulations is the minimization of CORE approximation errors giving better results. One of the draw-back of going to range-3 simulations is the smaller size single blocks used during these simulations. For going to the thermodynamic limits, an increasing number of CORE iterations are needed. For example, there is only 576 micro-sites equivalent for six renormalized sites after the CORE 5th iteration. At these number of lattice sites, critical exponents are converged [64], showing the infinite lattice behaviour. The results from range-3 simulations can also be compared with other numerical studies, which describe the lattice chains upto 300 microscopic sites [64].

6.4.1 Critical Exponent of the Energy Stabilization at Range-3

The range-3 simulations give the flexibility to have good results at higher number of CORE iterations resulting in a lattice of greater number of microscopic sites. The correlation length is the minimum of the lattice length L , at which the infinite behaviour of the lattice sets in. For small alternations, this infinite lattice behaviour sets in for more than 200 sites [64]. This makes CORE 4th iteration with six renormalized sites, corresponding to upto 288 microscopic sites, a very appropriate choice for the study of critical behaviour of alternating Heisenberg chain with frustration. The plots for the energy stabilization (6.6,6.7,6.8) are made from 3^r and 4th CORE iteration with corresponding microscopic sites as indicated in the plots. It will also serve

as reference point for comparing the results.

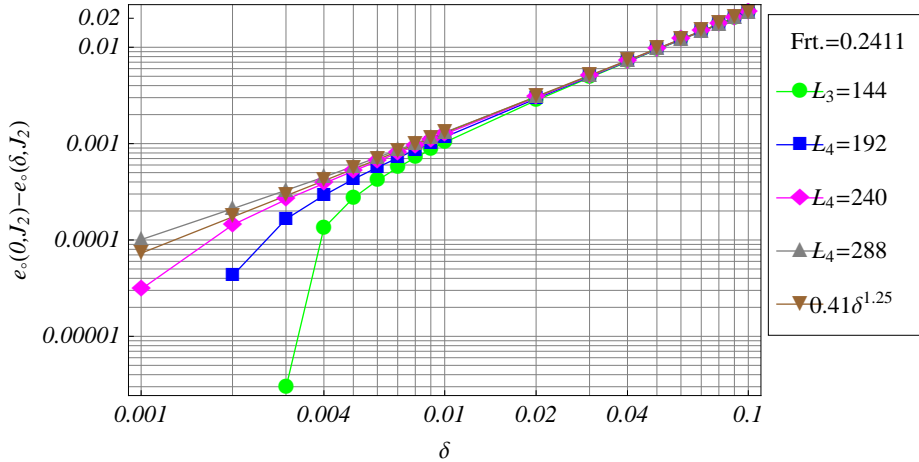


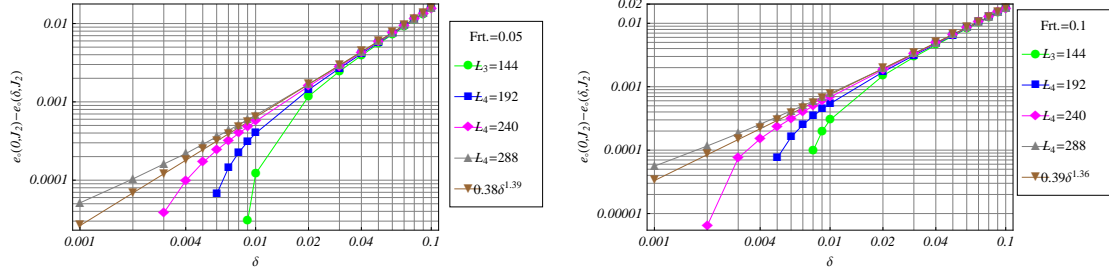
Figure 6.6: log-log plot of Energy Stabilization with alternation parameters. Hamiltonians are made from CORE 3rd and 4th iteration at range-3. The frustration is 0.2411

These plots (6.6,6.7a,6.7b,6.8a,6.8b) for the energy stabilization are made with frustrations $\{0.2411, 0.05, 0.1, 0.15, 0.2\}$ respectively. In the plot (6.6), at the frustration 0.2411, the hamiltonian (6.1) is scale invariant and there will be no corrections. The energy stabilization seems to obey the power law in the alternation span from 0.007 to 0.1. Even for the alternation span from 0.001 to 0.007, the energy stabilization and the power law with critical exponent 1.25 plots seem to nearly overlap.

For all other frustrations, the hamiltonian (6.1) does not remain scale invariant. In the plot (6.7a), the curves overlap for the alternation span from 0.007 to 0.1. Then there is maximum deviation of the energy stabilization from that of power law with critical exponent approximation of 1.39. This is consistent as the hamiltonian (6.1) with frustration 0.05 having the largest deviation from scale invariance.

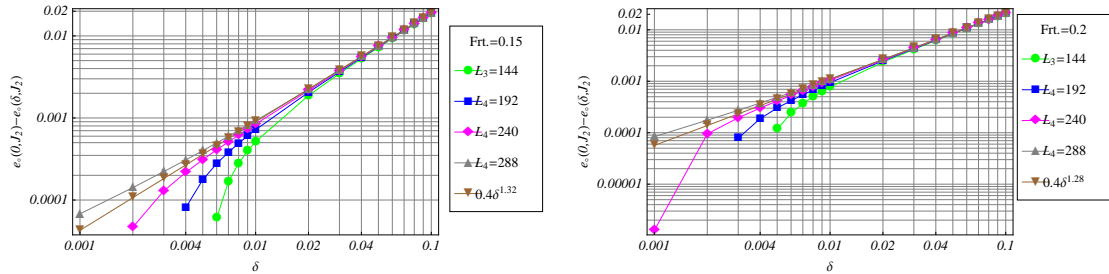
The remaining plots (6.7b, 6.8a,6.8b) also overlap for the alternation span from 0.007 to 0.1 with increasing frustrations reducing the distance between energy stabilization and power law curves.

It has also been seen as the case with range-2 simulations that increasing frustrations reduces the critical exponents. The critical exponent of the energy stabilization reduces from 1.39 for the frustration 0.05 to 1.25 for the frustration 0.2411.



(a) log-log plot of Energy Stabilization with alternation parameters. J_2 is 0.05 (b) log-log plot of Energy Stabilization with alternation parameters. J_2 is 0.1

Figure 6.7: log-log plot of Energy Stabilization with alternation parameters. Hamiltonians are made from CORE 3rd and 4th iterations at range-3.



(a) log-log plot of Energy Stabilization with alternation parameters. The frustration is 0.15 (b) log-log plot of Energy Stabilization with alternation parameters. The frustration is 0.2

Figure 6.8: log-log plot of Energy Stabilization with alternation parameters. The CORE simulations are done at range-3, Hamiltonians are made from CORE 3rd and 4th iterations.

6.4.2 Critical Exponent of the Gap at Range-3

The calculation of the singlet-triplet gap exponent are the main reason for switching to the range-3 simulations. Infinite chain behaviour sets in for the lattice of more than 200 sites [64]. CORE range-2 simulations never allowed to go for the gap at these microscopic sites. CORE range-3 simulations give good results for the gap for the same microscopic lattice sizes as used for energy stabilization. So the plots for the singlet-triplet gap are made from CORE 3rd and 4th iterations equivalent to upto 288 microscopic sites.

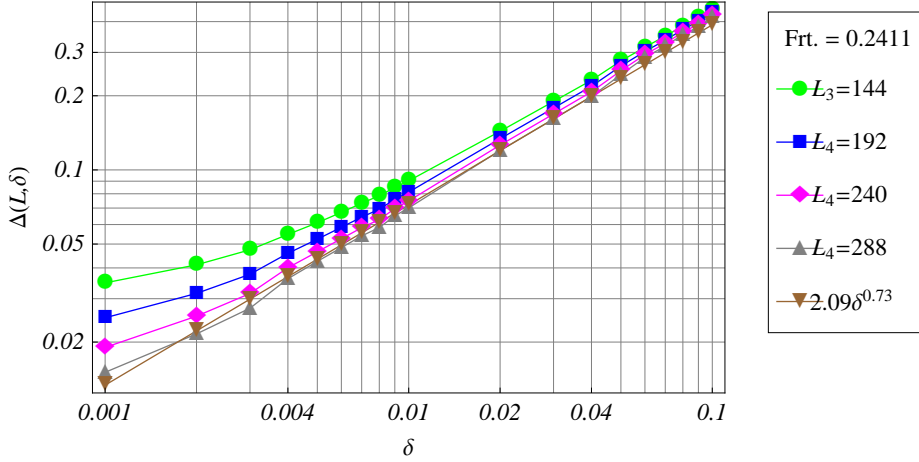
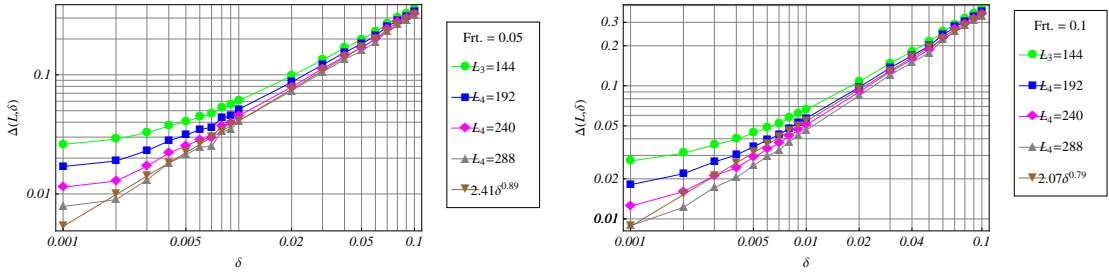


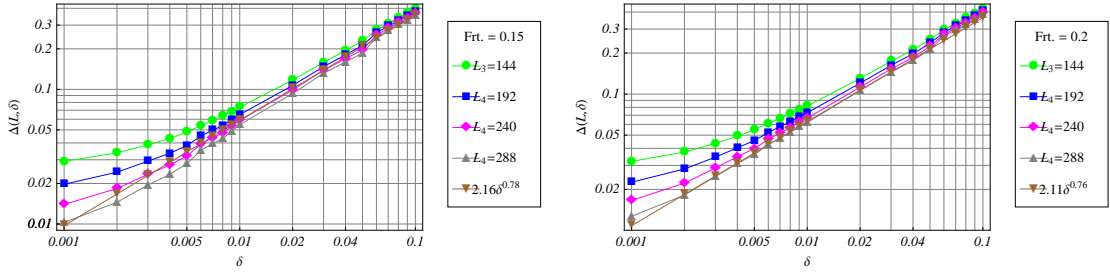
Figure 6.9: log-log plot for singlet-triplet gap with alternation parameters using CORE 3rd and 4th iteration. The frustration is 0.2411



(a) log-log plot for singlet-triplet gap with alternation parameters using CORE 2nd and 3rd iteration. J_2 is 0.05. (b) log-log plot for singlet-triplet gap with alternation parameters using CORE 3rd and 4th iteration. J_2 is 0.1.

Figure 6.10: log-log plot for singlet-triplet gap with alternations.

The critical exponents of the gap also decrease with the increasing frustrations. The critical exponent decreases from 0.89 for the frustration 0.05 to 0.73 for the frustration 0.2411.



(a) log-log plot for singlet-triplet gap with alternation parameters using CORE 3rd and 4th CORE iteration. The frustration is 0.15
 (b) log-log plot for singlet-triplet gap with alternation parameters using CORE 3rd and 4th CORE iteration. The frustration is 0.2

Figure 6.11: log-log plot for singlet-triplet gap with alternations.

6.4.3 Critical Exponents with CORE range-3 : tabulated results

To look at the lattice sizes at which the infinite lattice behaviour sets in, results from first five CORE iterations are shown in tables. This is very important information as one can design simulations for finding the renormalized hamiltonian for the lattice sizes, where the thermodynamic limit behaviour can be seen.

By observing the tables, it can be seen that for upto CORE 4th iteration, the critical exponents keep on changing. At CORE 4th and 5th iteration, the convergence of the critical exponents can be seen. The small change in the critical exponents can be attributed to approximation and numerical errors. So from using CORE algorithm, it is seen that to reach to thermodynamic limits, the alternating Heisenberg model should be solved for upto at least 288 microscopic sites.

| CORE Algorithm at range-3, Frustration = 0.05 | | | | | |
|---|--------------|----------------------|-----------------------------|---------------------|----------------------|
| | | Energy Stabilization | | Singlet-Triplet Gap | |
| Itr.No. | Micro. Sites | Critical Co-eff. | Critical Expt. Energy Stab. | Critical Co-eff. | Critical Expt. (Gap) |
| 1 | 36 | 0.694126 | 1.7107 | 1.79155 | 0.6552266 |
| 2 | 72 | 0.47988 | 1.51449 | 2.04561 | 0.734252 |
| 3 | 144 | 0.408758 | 1.42778 | 2.31861 | 0.814229 |
| 4 | 288 | 0.378833 | 1.38637 | 2.41438 | 0.885019 |
| 5 | 576 | 0.364672 | 1.36557 | 2.27463 | 0.95654 |

Table 6.7: Critical Exponents of energy stabilization and gap at range-3 with frustration 0.05

6.4. CORE SIMULATIONS AT RANGE-3 FOR AHC WITH FRUSTRATION

| CORE Algorithm at range-3, Frustration = 0.1 | | | | | |
|--|--------------|----------------------|-----------------------------|---------------------|----------------------|
| | | Energy Stabilization | | Singlet-Triplet Gap | |
| Itr.No. | Micro. Sites | Critical Co-eff. | Critical Expt. Energy Stab. | Critical Co-eff. | Critical Expt. (Gap) |
| 1 | 36 | 0.600645 | 1.58986 | 1.87781 | 0.657198 |
| 2 | 72 | 0.463205 | 1.45118 | 2.07554 | 0.718819 |
| 3 | 144 | 0.411741 | 1.38757 | 2.17724 | 0.762383 |
| 4 | 288 | 0.389036 | 1.35675 | 2.07044 | 0.790704 |
| 5 | 576 | 0.378086 | 1.34121 | 1.95147 | 0.856531 |

Table 6.8: Critical Exponents of energy stabilization and gap at range-3 with frustration 0.1

| CORE Algorithm at range-3, Frustration = 0.15 | | | | | |
|---|--------------|----------------------|-----------------------------|---------------------|----------------------|
| | | Energy Stabilization | | Singlet-Triplet Gap | |
| Itr.No. | Micro. Sites | Critical Co-eff. | Critical Expt. Energy Stab. | Critical Co-eff. | Critical Expt. (Gap) |
| 1 | 36 | 0.538473 | 1.48554 | 1.95779 | 0.655182 |
| 2 | 72 | 0.450567 | 1.39029 | 2.14828 | 0.710844 |
| 3 | 144 | 0.414457 | 1.34528 | 2.25975 | 0.754 |
| 4 | 288 | 0.397845 | 1.32315 | 2.15643 | 0.782167 |
| 5 | 576 | 0.389702 | 1.31195 | 1.64448 | 0.763111 |

Table 6.9: Critical Exponents of energy stabilization and gap at range-3 with frustration 0.15

| CORE Algorithm at range-3, Frustration = 0.2 | | | | | |
|--|--------------|----------------------|-----------------------------|---------------------|----------------------|
| | | Energy Stabilization | | Singlet-Triplet Gap | |
| Itr.No. | Micro. Sites | Critical Co-eff. | Critical Expt. Energy Stab. | Critical Co-eff. | Critical Expt. (Gap) |
| 1 | 36 | 0.495196 | 1.39299 | 2.02203 | 0.647103 |
| 2 | 72 | 0.440166 | 1.33017 | 2.17633 | 0.692176 |
| 3 | 144 | 0.415828 | 1.2997 | 2.46225 | 0.763833 |
| 4 | 288 | 0.404182 | 1.28448 | 2.10602 | 0.762948 |
| 5 | 576 | 0.398242 | 1.27658 | 1.75751 | 0.797237 |

Table 6.10: Critical Exponents of energy stabilization and gap at range-3 with frustration 0.2

| CORE Algorithm at range-3, Frustration = 0.05 | | | | | |
|---|--------------|----------------------|-----------------------------|---------------------|----------------------|
| | | Energy Stabilization | | Singlet-Triplet Gap | |
| Itr.No. | Micro. Sites | Critical Co-eff. | Critical Expt. Energy Stab. | Critical Co-eff. | Critical Expt. (Gap) |
| 1 | 36 | 0.468473 | 1.32302 | 2.06821 | 0.636977 |
| 2 | 72 | 0.432503 | 1.28058 | 2.1737 | 0.670809 |
| 3 | 144 | 0.415913 | 1.25975 | 2.27047 | 0.706276 |
| 4 | 288 | 0.40777 | 1.24924 | 2.09181 | 0.731438 |
| 5 | 576 | 0.403587 | 1.24379 | 1.97768 | 0.801918 |

Table 6.11: Critical Exponents of energy stabilization and gap at range-3 with frustration 0.2411

6.5 Conclusion

The key properties of spin- $\frac{1}{2}$ Heisenberg model both with alternations and frustrations, like energy density (ground state energy per site) and excitation gap are calculated by using CORE algorithm both at range-2 and range-3.

First of all the critical coupling point for the competing interaction model was studied. There were constraints which allow only two states to be retained for the CORE simulations. Despite of the constraint excluding many configurations for getting good results of the frustrating Heisenberg model, CORE gives a good estimate of critical coupling as 0.25. Then the evolution of the infinite lattice behaviour of the renormalization flow of the competing interactions are discussed. Making use of the plots of this infinite behaviour, a more precise estimate of the critical coupling is found which is 0.240 ± 0.001 having only 0.5% error from the actual value. The plots of energy stabilization and excitation gap (singlet-triplet gap) scale with the alternation parameter δ (Cross-Fisher power law). These plots follow the Cross-Fisher power laws as given by $A\delta^\alpha$ and $B\delta^\beta$, where α is the critical exponent of the gap and β is the critical exponent of the energy density, A and B are the coefficients of the power law respectively. These power laws are valid in the regime ($J_2 \leq J_{2c}$), where $J_{2c} = 0.2411 \pm 0.0001$ [52]. The CORE simulations will only focus on this regime and the proposed values of the increasing frustrations are $\{0.05, 0.1, 0.15, 0.2, 0.2411\}$.

For alternations close to zero, there is deviations between energy stabilization and gap with that of the power laws. The reason of these deviations is the $H(\delta, J_2)$ of not being scale invariant. This nature of $H(\delta, J_2)$ decreases with the increasing frustration and vanishes at ($J_2 = J_{2c}$). Another aspect of the study is to find the span of alternations for which there is an overlap between the plots of energy stabilization and gap with that of the power laws with exponents as found by CORE simulations. So it will interesting to see the plots in terms of overlaps and deviations.

Another important parameter needed for the calculation of energy stabilization is the bulk limit energy density for the spin- $\frac{1}{2}$ Heisenberg model with frustration $e_o(\delta = 0, J_2)$. This parameter is also found by using CORE algorithm

The range-2 simulations gives good results for critical exponents of energy stabilization but the same is not true for the singlet-triplet gap beyond 2^{nd} CORE iteration. For studying the critical behaviour, it is necessary to go for lattice sizes to be of more than 200 microscopic lattice sites [64]. For the range-2 simulations, one can go for big lattice sizes, which reaches upto 12288 microscopic sites for the six renormalized sites after only five CORE iterations. This results in the convergence of the critical exponent for the energy stabilization. The same is not true for the gap exponents with the range-2 simulations. One gets good results even for gap exponents for CORE 1^{st} and 2^{nd} iterations by using only a few renormalized sites. The convergence is not

achieved so the range-2 results for the gap at thermodynamics limits are not reliable.

| critical exponents at range-2 | | | | | | | |
|-------------------------------|-----------------|---------------------|--------------------------------|---------------------|-----------------|---------------------|-------------------------|
| Energy Stabilization | | | | Singlet-Triplet Gap | | | |
| Frust. J_2 | Micro. Sites | Critical Co-eff. | Critical Expt. Energy Stab. | Frust. J_2 | Micro. Sites | Critical Co-eff. | Critical Expt. (Gap) |
| 0.05 | 192 | 0.42 | 1.46 | 0.05 | 40 | 2.18 | 0.80 |
| 0.1 | 192 | 0.45 | 1.44 | 0.1 | 40 | 2.30 | 0.81 |
| 0.15 | 192 | 0.47 | 1.42 | 0.15 | 40 | 2.39 | 0.80 |
| 0.2 | 192 | 0.48 | 1.39 | 0.2 | 40 | 2.48 | 0.79 |
| 0.2411 | 192 | 0.42 | 1.26 | 0.2411 | 40 | 2.50 | 0.77 |

Table 6.12: coefficient and critical exponents for the power law describing the energy stabilization and singlet-triplet gap corresponding to different frustrations. These are found by CORE simulations at range-2.

In the table (6.12), the results from CORE range-2 simulations are shown. The critical exponents from the CORE 2nd iteration with six renormalized sites corresponds to 192 microscopic sites. The thermodynamics limit behaviour just sets in at this lattice size without incorporating numerical errors of repeating CORE iterations. This makes it also comparative with other studies like [51, 64]. The critical exponents of the singlet-triplet gap from CORE 1st iteration are shown in the table. These values are not at thermodynamics limits, therefore only symbolic in nature. The exponents show a decrease in their value with the increasing frustrations. According to the CORE range-2 simulations the critical exponent approximations for the energy stabilization decreases from 1.46 to 1.26 for the increasing frustration value from $J_2 = 0.05$ to $J_2 = 0.2411$.

| critical exponents by CORE Algorithm at range-3 | | | | | |
|---|-----------------|----------------------|--------------------------------|---------------------|-------------------------|
| | | Energy Stabilization | | Singlet-Triplet Gap | |
| Frust. J_2 | Micro. Sites | Critical Co-eff. | Critical Expt. Energy Stab. | Critical Co-eff. | Critical Expt. (Gap) |
| 0.05 | 288 | 0.38 | 1.39 | 2.41 | 0.89 |
| 0.1 | 288 | 0.39 | 1.36 | 2.07 | 0.79 |
| 0.15 | 288 | 0.40 | 1.32 | 2.16 | 0.78 |
| 0.2 | 288 | 0.40 | 1.28 | 2.11 | 0.76 |
| 0.2411 | 288 | 0.41 | 1.25 | 2.09 | 0.73 |

Table 6.13: coefficient and critical exponents for the power law describing the energy stabilization and singlet-triplet gap corresponding to different frustrations. These are found by CORE simulations at range-3.

One has to switch to range-3 simulations as the range-2 results for the critical exponents of the gap were not converging in the thermodynamics limit. This allows to find the energy density and gap from the renormalized hamiltonian made from the same CORE iteration with the same number of renormalized sites. From the table (6.13), the critical exponent for the energy stabilization decreases from $\beta = 1.43$ to $\beta = 1.26$ for the frustration value from $J_2 = 0.05$ to $J_2 = 0.2411$. Similarly the critical exponent approximations for the singlet-triplet gap decreases from $\alpha = 0.81$ to $\alpha = 0.70$ for the frustration value from $J_2 = 0.05$ to $J_2 = 0.2411$. These result are generally in agreement with that of quoted in [52].

The overlap between the plots of the energy density and singlet-triplet gap with that of the power law exists for all kinds of frustrations for the same alternation δ range from 0.007 to 0.1. There will be deviations in remaining span from 0.001 to 0.007. The deviations decreases with increasing frustrations. For the frustration value of $J_2 = 0.2411$, the deviation between the two plots is so small that these is almost a complete overlap for the whole alternation range. The gradual decrease in errors with the increasing frustrations J_2 is also verified by the correspondingly decreasing distance between the plots until one reaches the frustration $J_{2c} = 0.2411$, where no corrections are needed. When compared to the DMRG-extrapolated results for infinite behaviour [52], the CORE approximations for the critical exponents show a variation of error from 1% to 5% for energy density and from 5% to 9% for the gap.

Appendix A

Energy Re-Scaling for Renormalized Hamiltonians

A.1 CORE Iterations: Shifting and Re-Scaling

After each of the CORE iteration, the low energy renormalized hamiltonian can be seen as representing equivalent microscopic sites. For a 1-dimensional lattice, the number of the microscopic of sites can be given by

$$y = w \times b^I$$

where w is the total number of macroscopic sites after the iteration I . b is the number of sites in a single block used in CORE simulations. y is the total number of equivalent microscopic sites.

The renormalized hamiltonians are extensive in nature, so the energy of the renormalized hamiltonians increases after each of the CORE iteration. The result of this problem is that after only a few iterations, the renormalized hamiltonian will be overflowing with big numbers, which are representing the accumulated energy density and the accuracy will be lost due to these big numbers.

Another reason for shifting and re-scaling is the truncation of the energy spectrum. The higher excited states got truncated at each CORE iteration and the energy spectrum $\Delta E = E_{max} - E_{min}$ will decrease at each step. Therefore for continuation of CORE iteration process, the re-scaling of the energy spectrum is necessary.

In some cases, at high number of CORE iterations, e.g., fifteen or more without shifting and scaling, there will be imaginary part just creeping up the tolerance limits in the eigen values, but it is never seen while working with shifting and scaling. This is off-course an accumulated numerical error not like the fully legal accumulated energy density.

To avoid these problems, and maintain a consistant accuracy of the simulations, shifting and re-scaling at each CORE iteration step will be done. The process will be tracked, so that at the end, shifting and scaling can be nullified, or only the scaling can be nullified in case of quantities not averaged like energy gap etc.

The shifting and scaling data for the CORE iterations also give us vital information about the bahaviour of the hamiltonian system.

A.2 Energy Spectrum Re-Scaling for h_r

The re-scaling of the energy spectrum will be done for the longest super-block range- r contributions. Then all the remaining contributions will be re-scaled to the same amount. For example, in case of the range-3 simulations, the longest range h_3 hamiltonian contribution is re-scaled. Then all the remaining contributions, like h_1, h_2 are rescaled by the same amount. For re-scaling based on h_r hamiltonian contribution for the super-block range- r , the energy spectrum of the hamiltonian h_r can be defined as

$$\Delta E = E_{max} - E_{min} \quad (\text{A.1})$$

where E_{max} is the largest of the eigenvalue and E_{min} is the smallest of the eigenvalue of the h_r spectrum. ΔE is the energy spectrum of the hamiltonian. The re-scaling of the gap is done to some arbitrary value, so that truncation effect on the energy spectrum can be compensated by the following equation

$$sF = \frac{sG}{\Delta E} \quad (\text{A.2})$$

where sG is the arbitrary new intended rescaling gap, ΔE is the total energy spectrum of the hamiltonian matrix. sF is the re-scaling factor multiplying the hamiltonian matrix with this re-scaling factor shifts the gap to the intended value sG .

A.3 Shifting the hamiltonian contributions h_r

The background energy (total ground state energy) at each CORE iteration goes on increasing and can be shifted to some arbitrary value. The minimum eigen value of these hamiltonian matrices are subtracted from the number to which the energy is intended to be shifted. Subtracting this number diagonally from the hamiltonian matrices will make the energy of the system shifted to specific value.

$$shC = E_{min} - shV \quad (\text{A.3})$$

where E_{min} is the lowest of the eigen values of hamiltonian matrix. shV is the intended shifting of the eigenvalues e.g., zero. shC is the quantity which shifts the hamiltonian matrix to the desired value. It is to be noted that h_r hamiltonians contributions h_1, h_2 and h_3 , each has to be shifted independently.

When the hamiltonian contributions h_r are shifted and re-scaled at each of the CORE iterations, then it will make possible to find the CORE renormalization transformation iteration steps for more than first few iteration with considerable accuracy. Even after reaching the fix point, one can go on for more CORE iterations. Normally to find quantities based on averages per site like magnetization, one has to switch back the re-scaling and shifting but for other quantities like energy gap, the re-scaling back of the energy spectrum will be enough.

A.4 Nullifying Shifting and re-Scaling

The process of nullifying shifting and re-scaling at each iteration step depends on the geometry of the lattice under study, as some of the range- r contributions h_r are also to be counted for each of the CORE iterations I .

A.4.1 Nullifying Shifting and re-Scaling for h_1

There will be three relevant quantities in this case, the hamiltonian contribution after the implementation of shifting scaling $h_{1_{ss}}$, the background energy h_{1_b} and the scaling factor.

The switching back the shifting and re-scaling for h_1 can be done by following equation.

$$\begin{aligned}
h_1^I &= (h_{1_{ss}}^I + h_{1_b}^I) \times sF^I \\
&+ \sum_{j=1}^{I-1} \left(nh_1^j \times h_{1_b}^j + nh_2^j \times h_{2_b}^j + nh_3^j \times h_{3_b}^j \right) \\
&\times \prod_{k=1}^{I-1} sF^k
\end{aligned} \tag{A.4}$$

where I is the number of the CORE iteration, $h_{1_{ss}}^I$ is the hamiltonian contribution after the implementation of shifting scaling at CORE iteration step I , $h_{1_b}^I$ is the background shifted energy which has been taken out from the range-1 contributions h_1 , nh_1^j is the number of contributing h_1 's of that particular iteration step j as seen microscopically in the lattice. Similarly nh_2^j and nh_3^j is the number of contributing counts of the h_2^j and h_3^j of the CORE iteration step j as seen microscopically in the lattice. The number of contributing counts of the nh_1^j , nh_2^j and nh_3^j will depend on the lattice geometry.

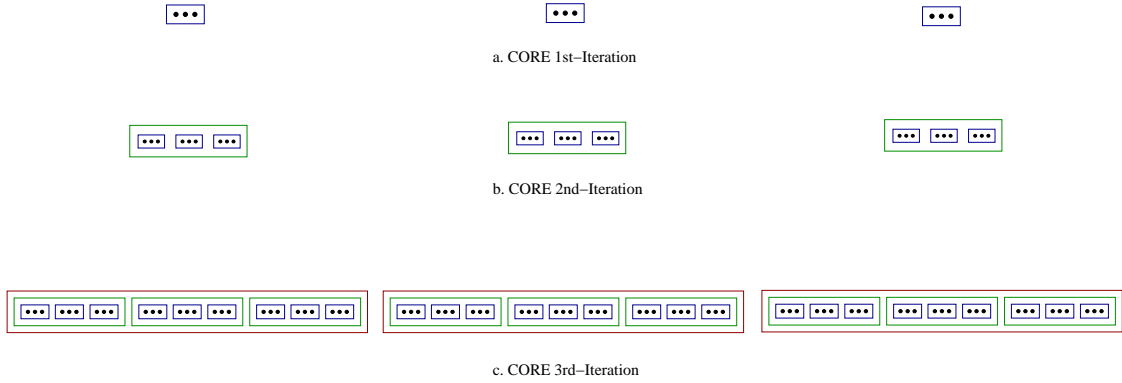


Figure A.1: Renormalized site after 1st, 2nd and 3rd-Iteration represented by blue, green and red blocks respectively

A.4.2 Nullifying Shifting and re-Scaling for h_2

The hamiltonian h_2 is the range-2 contribution that can be seen as the interaction energy between two renormalized sites. With this view, one can deduce the method of switching back its shifting and re-scaling. The situation will be made clear by the following figure (A.2).

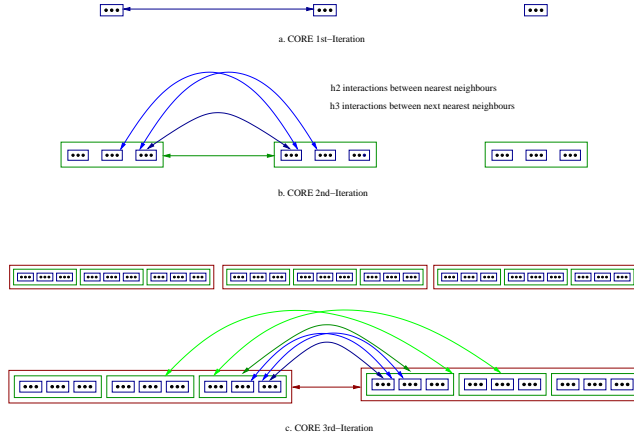


Figure A.2: After 1st, 2nd and 3rd-Iteration, interaction between two renormalized blocks is shown by arrows

$$\begin{aligned}
h_2^I &= (h_{2_{ss}}^I + h_{2_b}^I) \times sF^I \\
&+ \sum_{j=1}^{I-1} h_{2_b}^j + 2 \times h_{3_b}^j \\
&\times \prod_{k=1}^{I-1} sF^k
\end{aligned} \tag{A.5}$$

h_2^I is the range-2 contribution to the hamiltonian after the I th CORE iteration. It should be noted that there will be no missing range-1 part of the energy that is also the part of the total range-2 contributions.

so h_{1_b} from the previous renormalization steps have no contributions in the range-2 term h_2^I . But there will be missing range-2 $h_{2_b}^j$ and range-3 $h_{3_b}^j$ contributions from the previous CORE-iterations.

A.4.3 Nullifying Shifting and re-Scaling for h_3

h_3 can be defined as the hamiltonian contribution for the long range interaction between three blocks. So the missing energy of range-1 or range-2 hamiltonian contributions cannot be part of missing range-3 energy.

If one is not computing more than range-3 contributions such as range-4 or range-5, that can become part of the missing energy of the range-3 contributions in the previous CORE-iteration steps. The result is that the missing background energy of range-1 $h_{1_b}^j$ and range-2 $h_{2_b}^j$ contributions from the previous iteration steps is not included. The only missing energy will be of range-3 i.e., $h_{3_b}^j$ of the current CORE renormalized iteration.

So to find the true h_3 at some iteration step, we only have to include h_3 background energy of the current iteration step making a symbolic formula

$$h_3^I = (h_{3_{ss}}^I + h_{3_b}^I) \times sF^I \tag{A.6}$$

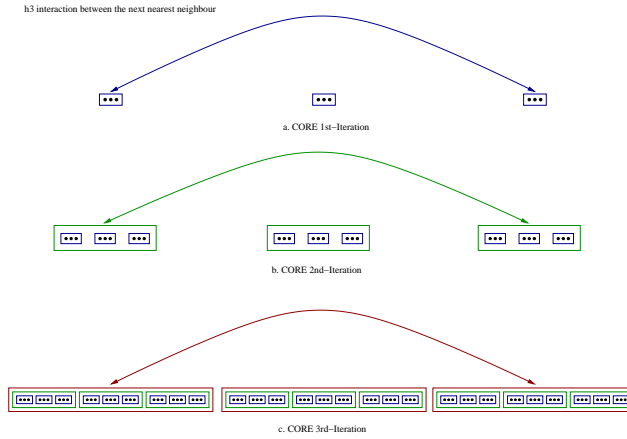


Figure A.3: Arrows show missing range-3 contributions due to shifting scaling for 1st-three CORE iterations

In the figure (A.3), for the three CORE iterations, one is not able to find a link between first and third renormalized site except the link shown by arrows.

A.5 Shifting re-Scaling for Different Lattice Geometries

These are the general ideas of how to implement shifting and re-scaling in 1-dimension and then nullifying them, when needed. One dimensional lattice was used to develop these ideas. However practically these are many types of lattices for which the formulas nullifying the shifting and re-scaling can be developed.

A.6 Conclusion

There is a major importance for shifting and re-scaling if one wants to use the CORE algorithm for more than one CORE renormalized transformation iterations. This technique not only allow to sustain the CORE iterations for considerable number of steps, but also makes the range-1, range-2 and range-3 contributions more accurate. It is better if the shifting and re-scaling is done after each of the CORE iterations. The shifting and re-scaling after the CORE simulations is nullified from the hamiltonian contributions or only the re-scaling is nullified as the problem demands.

Appendix B

CORE algorithm with Degenerate models

The conventional CORE algorithm [17] demands to know the degeneracies of the low energy states of the single block as well as of the super blocks range- r etc. For some symmetric models, for first CORE iteration, one knows the degeneracies due to some established results, so these degeneracies can be used for the implementation of CORE algorithm. On the other hand, for a given geometry, the degeneracies of some symmetric problems are not known. These degeneracies are to be decided numerically by comparing the eigen values of the hamiltonians. This method is generally successful but one should take care of some of the points.

The method of diagonalization should give low energy spectrum accurately, as the degeneracy is being decided based on the eigen values.

Then the range- r of the CORE simulations is also a very important factor. If the eigen-values of the renormalized hamiltonian is already converged at range- r simulation, then there will be no problem. For some symmetric models, if simulations is done only at range-2 and the eigen values are not converged, then there can be some very small difference like $\sim 10^{-8}$ even in the degenerate eigen-values for which tolerance limits to detect degeneracy has to be set.

If the hamiltonian system is non-degenerate, then there is no such problem as the value of the degeneracy variable D remains $D = 1$. If the spin correlated model under study is non-degenerate, like $(1+1)$ -Ising model on a one dimensional lattice then there will be no problem in implementing the CORE iterations.

But for some symmetric, one has to devise some method either to make the degeneracies correct or get rid of the degeneracies. One way of getting rid of the degeneracies is to implement the CORE algorithm for conserve- S_z sector. The super block range- r can be considered in terms of conserve- S_z basis states. Consider the CORE algorithm is applied to spin- $\frac{1}{2}$ chain in 1-dimension with three-sites single block.

B.1 Spin- $\frac{1}{2}$ Basis states for three site single block

The spin- $\frac{1}{2}$ basis for this single block is $\{\downarrow\downarrow\downarrow, \downarrow\downarrow\uparrow, \downarrow\uparrow\downarrow, \downarrow\uparrow\uparrow, \uparrow\downarrow\downarrow, \uparrow\downarrow\uparrow, \uparrow\uparrow\downarrow, \uparrow\uparrow\uparrow\}$. This spin- $\frac{1}{2}$ basis can be divided into conserve- S_z sectors as

Conserve- S_z quantum number for the single block is

$$\left\{ S_z = -\frac{3}{2}, -\frac{1}{2}, \frac{1}{2}, \frac{3}{2} \right\}$$

Conserve-Sz basis for the super block range-2 consisting of 6 sites can be written as

$$\{S_z = -3, -2, -1, 0, 1, 2, 3\}$$

Conserve-Sz basis for the super block range-3 consisting of 9 sites can be written as

$$\left\{S_z = -\frac{9}{2}, -\frac{7}{2}, -\frac{5}{2}, -\frac{3}{2}, -\frac{1}{2}, \frac{1}{2}, \frac{3}{2}, \frac{5}{2}, \frac{7}{2}, \frac{9}{2}\right\}$$

B.2 Conserve-Sz Super Block Range-2

Each of the super block sectors can be thought of as made from the single blocks of conserve-Sz sector. The super-block range-2 of the conserve-Sz sector with quantum number zero is given in terms of constituent blocks as The remaining conserve-Sz of the super block range-2 can be

| Super Block Range-2 Sz-quantum number | left block Sz-quantum number | Right block Sz-quantum number |
|--|---------------------------------|----------------------------------|
| 0 | $-\frac{1}{2}$ | $+\frac{1}{2}$ |
| 0 | $+\frac{1}{2}$ | $-\frac{1}{2}$ |
| 0 | $+\frac{3}{2}$ | $-\frac{3}{2}$ |
| 0 | $-\frac{3}{2}$ | $+\frac{3}{2}$ |

Table B.1: Conserve-Sz with Sz quantum number zero for range-2 super block

mapped similarly.

B.3 Conserve-Sz Super Block Range-3

| Super Block Range-3 Sz-quantum number | left block Sz-quantum number | Middle block Sz-quantum number | Right block Sz-quantum number |
|--|---------------------------------|-----------------------------------|----------------------------------|
| $-\frac{1}{2}$ | $-\frac{1}{2}$ | $-\frac{1}{2}$ | $+\frac{1}{2}$ |
| $-\frac{1}{2}$ | $-\frac{1}{2}$ | $+\frac{1}{2}$ | $-\frac{1}{2}$ |
| $-\frac{1}{2}$ | $+\frac{1}{2}$ | $-\frac{1}{2}$ | $-\frac{1}{2}$ |
| $-\frac{1}{2}$ | $-\frac{1}{2}$ | $+\frac{3}{2}$ | $-\frac{3}{2}$ |
| $-\frac{1}{2}$ | $-\frac{1}{2}$ | $-\frac{3}{2}$ | $+\frac{3}{2}$ |
| $-\frac{1}{2}$ | $+\frac{3}{2}$ | $-\frac{1}{2}$ | $-\frac{3}{2}$ |
| $-\frac{1}{2}$ | $-\frac{3}{2}$ | $-\frac{1}{2}$ | $+\frac{3}{2}$ |
| $-\frac{1}{2}$ | $+\frac{3}{2}$ | $-\frac{3}{2}$ | $-\frac{1}{2}$ |
| $-\frac{1}{2}$ | $-\frac{3}{2}$ | $+\frac{3}{2}$ | $-\frac{1}{2}$ |

Table B.2: Conserve-Sz for Sz quantum number $-\frac{1}{2}$ for range-3 super block

The remaining conserve- S_z of the super block range-3 can be mapped similarly. The CORE algorithm can be applied separately for each of the conserve- S_z sectors. There are many advantages of doing the CORE simulations in the conserve- S_z sector, like one is working in the reduced subspace of the full Hilbert space. Then there is always an overlap between the exact eigenstates of conserve- S_z super block and that of the tensor product of the contributing single block retained states. so no more zero columns in the projection matrix $Q(G)$. Therefore many difficulties of the CORE simulations are taken care of by applying CORE simulations in the conserve- S_z sector.

Bibliography

- [1] Michael E. Fisher, *Rev. Mod. Phys.*, Vol. 70, No. 2, April 1998
- [2] L.P.Kadanoff, Scaling laws for Ising models near T_c , *Physics* 2,263 (1966)
- [3] Kenneth G. Wilson, *Phys. Rev. B* 4, 3174–3183 (1971)
- [4] W. Lenz, *Phys. Zeitschrift* 21, 613 (1920)
- [5] E. Ising, *Z. der Physik* 31, 253 (1925).
- [6] R. Jullien and P. Pfeuty, J. N. Fields, S. Doniach *Phys. Rev. B* vol.18, issue 7, 3568–3578 (1978)
- [7] Sidney D. Drell, Marvin Weinstein and Shimon Yankielowicz, *Phys. Rev. D* vol 16, issue 6, 1769–1781 (1977)
- [8] Marvin Weinstein, *Phys. Rev. B* vol 63, issue 17 174421 (2001)
- [9] S. R. White and R. M. Noack, *Phys. Rev. Lett.* vol 68, issue 24, 3487–3490 (1992)
- [10] S. R. White, *Phys. Rev. Lett.* 69, 2863 (1992).
- [11] S. R. White, *Phys. Rev. B* 48, 10345 (1993).
- [12] U. Schollwöck, *Rev.Mod. Phy*, Vol 77, Jan 2005
- [13] Sylvain Capponi, *Theor Chem Acc* (2006), 116:524-534
- [14] Igor Herbut, *A Modern approach to Critical Phenomena*, (Cambridge University Press, The Edinburgh Building, Cambridge CB2 2RU, UK, 2007)
- [15] S. Sachdev, *Quantum Phase Transitions* (Cambridge University Press, The Edinburgh Building, Cambridge CB2 2RU, UK, 1999)
- [16] Colin J. Morningstar, Marvin Weinstein, *Phys. Rev. Lett.* 73, 1873 (1994)
- [17] Colin J. Morningstar, Marvin Weinstein, *Phys. Rev. D* 54, 4131–4151 (1996)
- [18] M. Stewart Siu, Marvin Weinstein, *Phys. Rev. B* 75, 184403 (2007)
- [19] Marvin Weinstein *Phys. Rev. D*, 1993, Jun 15;47(12):5499-5520.
- [20] C. Domb, *Adv. Phys.* 9, 149 (1960)
- [21] G. Rushbrooke, *J.Math.Phys.* 5, 1106 (1964)

- [22] L. C. Systems and G. Theory, *J.Math.Phys.* 7, 1557 (1966)
- [23] C.Domb and M.S.Green, *Phase Transitions and Critical Phenomena* edited by (Academic, London, 1974), Vol 3, p.1.
- [24] Jaegon Um , Sung-Ik Lee and Beom Jun Kim, *J. Korean Phys.Soc.* 50,285
- [25] L. Onsager, *Phys. Rev.* 65, 117 (1944)
- [26] Eduardo Fradkin and Leonard Susskind, *Phys. Rev. D* 17, 2637–2658 (1978)
- [27] J. B. Kogut, *Rev. Mod. Phys.* 51, 659 (1979)
- [28] P. Pfeuty, R.J.Elliott, *J.Phys. C:Solid St. Phys.*,2370, (1971)
- [29] Sylvain Capponi, Andreas Läuchli and Matthieu Mambrini, *Phys. Rev. B* 70, 104424 (2004)
- [30] Wim Van Saarloos, *Physica* 112A, 65-100 (1982)
- [31] Baxter, Rodney J. (1982), *Exactly solved models in statistical mechanics*, London: Academic Press Inc
- [32] J.J.Binney, N.J.Dowrick and M.Newman, *The Theory of Critical Phenomena* (Oxford University Press, Walton Street, OX@ 6DP, UK, 1995)
- [33] P.S.Bikas, K. Chaker, Amit Dutta, *Quantum Ising Phases and Transitions in Transverse Ising Model* (Springer-Verlag, Tiergartenstrasse 17,D-69121 Heidelberg, Germany, 1996)
- [34] R.J.Elliott, P.Pfeuty, *Phys. Rev. Lett.* 25, 443 (1970)
- [35] I. Vilfan, *Statistical Mechanics Notes*
- [36] Ehud Altman and Assa Auerbach, *Phys. Rev. B* 65, 104508 (2002)
- [37] Ingrid Reiweiger, *Diploma Thesis, itcp, TU-Graz* (2006)
- [38] S Mahdavifar 2007 *J. Phys.: Condens. Matter* 19 406222 doi:10.1088/0953-8984/19/40/406222
- [39] M. Siahatgar, A. Langari, *Physical Review B* 77, 054435 (2008)
- [40] A. Langari, *Physical Review B* 69, 100402(R) (2004)
- [41] M. Kenzelmann, R. Coldea, D. A. Tennant, D. Visser, M. Hofmann, P. Smeibidl and Z. Tylczynski, *Phys. Rev. B* 65, vol 14, 144432 (2002)
- [42] P. M. Duxbury and J. Oitmaa, Michael N. Barber, A. van der Bilt, K. O. Joung, and Richard L. Carlin *Phys. Rev. B* 24, 5149–5155
- [43] Kiyomi Okamoto, Hidetoshi Nishimori and Yoshihiro Taguchi *J. Phys. Soc. Jpn.* 55 (1986) pp. 1458-1465
- [44] G. Grosso and L. Martinelli, G. Pastori Parravicini, *Phys. Rev. B* vol 51, issue 19, 13033–13038
- [45] D. V. Dmitriev, V. Ya. Krivnov, and A. A. Ovchinnikov, *Phys. Rev. B* vol 65, issue 17, 172409 (2002)

- [46] D. V. Dmitriev, V. Ya. Krivnov, A. A. Ovchinnikov und A. Langari JETP 95, 538
- [47] C. N. Yang, C. P. Yang Phys. Rev. vol 150, issue 1, 321–327 (1966)
- [48] C. N. Yang, C. P. Yang Phys. Rev. vol 150, issue 1, 327–339 (1966)
- [49] Josef Kurmann, Harry Thomas, Gerhard Müller, Physica A Volume 112, Issues 1–2, May 1982, Pages 235–255
- [50] A. Fledderjohann, M. Karbach and K.-h. Mütter, Eur. Phys. J. B 5 3 (1998) 487-494
- [51] T. Papenbrock, T. Barnes D. J. Dean, M. V. Stoitsov and M. R. Strayer, Phys.Rev. B 68, 024416 (2003)
- [52] Manoranjan Kumar, S. Ramasesha, Diptiman Sen, Z. G. Soos Phys. Rev. B 75, 052404 (2007)
- [53] T. Barnes, J. Riera and D.A. Tennant, Phys. Rev B 59, 11 384 (1999)
- [54] W. Yu and S. Haas, Phys. Rev. B 62, 344 (2000)
- [55] M.C. Cross and D.S. Fisher, Phys. Rev. B 19, 402 (1979)
- [56] E. Orignac, Eur Phys. J.B. 39, 335 (2004)
- [57] I. Affleck, D. Gepner, H.J. Schulz and T. Ziman, J. Phys. A 22, 511 (1989)
- [58] J.L.Black and V.J.Emery Phys. Rev. B 23, 429–432 (1981)
- [59] K. Okamoto and K. Nomura, Phys. Lett. A 169, 433 (1992)
- [60] P.M. van den Broek, Phys. Lett. A 77 (1980) 261
- [61] B.S.Shastry and B. Sutherland, Phys. Rev. Lett. 47 (1981) 964
- [62] I.Affleck, T.Kennedy, E.H. Lieb and H. Tasaki, Commun. Math. Phys. 115 (1988) 477.
- [63] Steven R. White and Ian Affleck, Phys. Rev. B 54, 9862–9869 (1996)
- [64] R.Chitra, S.Pati, H.R. Krishnamurthy, D. Sen and Ramasesha, Phys. Rev. B 52, 6581 (1995)
- [65] M.A. Garcia-Bach, D.J. Klein, Physics Letters 89A, 2, 101
- [66] X.F. Jiang, H. Chen, D.Y. Xing and J.M. Dong, J.Phys. Condens Matter 13 (2001)
- [67] Jean-Paul Malrieu and Nathalie Guihery, Phys. Rev. B 63, 085110 (2001)